

DRYING CRACKS NETWORK IN SOILS: REMEDIAL SOLUTIONS AND 3-D ERT  
MONITORING

A Dissertation

by

SEOKHYUNG LEE

Submitted to the Office of Graduate and Professional Studies of  
Texas A&M University  
in partial fulfillment of the requirements for the degree of

DOCTOR OF PHILOSOPHY

Chair of Committee,	Marcelo Javier Sanchez Castilla
Committee Members,	Charles P. Aubeny
	Benchun Duan
	Robert L. Lytton
Head of Department,	Robin Autenrieth

August 2020

Major Subject: Civil Engineering

Copyright 2020 Seokhyung Lee

## ABSTRACT

Desiccation cracking in soils is a natural phenomenon associated with soil shrinkage during water evaporation under field conditions triggered by the soil-atmosphere interactions. Desiccation crack can cause many problems on the stability of geotechnical structures, such as foundations, embankment, and landfill. It can increase seepage and lead to failures in earth structures. The developing of drying cracks in soil is a quite complex phenomenon that possess several challenges. Electrical Resistivity Tomography (ERT) technique was adopted in this research to monitor the desiccation crack propagation with drying-wetting cycle. Two kinds of array method were compared and validated using clay-Styrofoam block structures within soil container. The three-dimensional visualization of the crack network was done by using VOXLER 3D program to enhance the interpretation of Electrical Resistivity Tomography (ERT) data. Mechanical and geophysical properties of the clay mixtures were evaluated to select the optimal composition of the filling materials to be used as remedial solutions for cracking area. The mixtures were made up from several components included to enhance the strength and workability of the injection material. The successful implementation of the injection material was verified by means of indirect (non-destructive) and direct methods including assessment of the mixing penetration by the direct observation during the sample dismantling.

## DEDICATION

This dissertation is dedicated to my mother and father, for their endless love and support. I also dedicate this work to my beloved wife Soha, and my son Jaejoon. Having you in my life is truly a blessing. Thank you very much for your love and encouragement during my Ph.D journey.

## ACKNOWLEDGEMENTS

First of all, I would like to express my deepest appreciation to my committee chair, Dr. Marcelo Sanchez, who guided and encouraged me every step of the way. Without his persistent help I would have felt like a lost child during my dissertation journey. I would also like to thank my committee members, Dr. Charles Aubeny, Dr. Robert Lytton, and Dr. Benchun Duan, for their precious feedback and encouragement.

Also, I would like to thank the staff at the Zachry Department of Civil & Environmental Engineering at Texas A&M University, very especially to Mrs. Laura Byrd and Mr. Chris Grunkemeyer, for all the help and support during this journey as a Ph.D student.

My gratitude also extends to my friends for making my time at Texas A&M University a great experience. I would especially like to thank Inwoo Jung, Yei-Eun Shin, Junho Lee, Jaechan Park, Sean Hyunseong Min, Junrak Son, Inok Jun, and Changjoo Nam.

Finally, I owe a huge debt of gratitude to my parents for always being there for me. I would not have finished this work without their never-ending trust and love. I also thank my wife Soha and my son Jaejoon who always encouraged and support me with endless love. I now return to you with a heart full of love, gratitude, and hope.

## CONTRIBUTORS AND FUNDING SOURCES

### **Contributors**

This research work was supervised by a dissertation committee consisting of Professor Marcelo Sanchez and Professor Charles Aubeny and Robert Lytton of the Zachry Department of Civil and Environmental engineering, and professor Benchun Duan of the Department of Geology & Geophysics.

All works conducted for the dissertation was completed by the student independently.

### **Funding sources**

Graduate study was supported by family.

## TABLE OF CONTENTS

	Page
ABSTRACT .....	ii
DEDICATION .....	iii
ACKNOWLEDGEMENTS .....	iv
CONTRIBUTORS AND FUNDING SOURCES .....	v
TABLE OF CONTENTS .....	vi
LIST OF FIGURES .....	ix
LIST OF TABLES .....	xiii
CHAPTER I INTRODUCTION .....	1
Background .....	1
Objective .....	3
Dissertation organization.....	4
Chapter 1 .....	5
Chapter 2 .....	5
Chapter 3 .....	5
Chapter 4 .....	6
Chapter 5 .....	6
Chapter 6 .....	7
Chapter 7 .....	7
CHAPTER II LITERATURE REVIEW .....	8
Introduction .....	8
Desiccation cracks in soil.....	8
Geophysical application for soil investigation .....	11
The clay mixture components .....	13
Carbon nano-composites .....	13
Biopolymer treatment for soil improvement .....	14
Superplasticizer .....	15
CHAPTER III APPARATUS, MATERIAL, AND EXPERIMENT PREPARATION ..	17

Introduction .....	17
Soil and clay mixture components .....	17
Natural soil .....	17
EPK Kaolinite.....	18
Graphite .....	19
Cement.....	19
Superplasticizer .....	20
Biopolymer .....	21
Test apparatus and setup .....	22
Desiccation soil container .....	22
Electrical Resistivity Tomography (ERT) measurement system .....	25
Drying test using electrical geophysical method.....	26
Mechanical laboratory tests.....	29
 CHAPTER IV EVALUATION OF MECHANICAL AND GEOPHYSICAL PROPERTIES OF CLAY MIXTURE .....	 35
Introduction .....	35
Mechanical test: Unconfined compression test.....	36
Sample preparation and test procedure .....	36
Test results and discussions.....	38
Mechanical test: Flow table test.....	47
Sample preparation and test procedure .....	47
Test results and discussions.....	47
Mechanical test: Free shrinkage test .....	53
Sample preparation and test procedure .....	53
Test results and discussions.....	54
Geophysical test: Four-electrode method.....	56
Sample preparation and test procedure .....	56
Test results and discussions.....	56
Summary and conclusions.....	61
 CHAPTER V DESICCATION CRACK MONITORING USING ELECTRICAL RESISTIVITY TOMOGRAPHY TECHNIQUE.....	 63
Introduction .....	63
Preliminary ERT using Styrofoam blocks .....	64
Test preparation and procedure .....	64
Array methods .....	66
Test results and discussion .....	68
Desiccation soil container setup for the natural soil .....	81
ERT results: Section A.....	82
Phase 3: Completely dried state after 2 <sup>nd</sup> re-saturation process .....	84
Phase 4: Completely dried state after 3 <sup>rd</sup> re-saturation process.....	87

Discussion of the test results from section A .....	91
ERT results: section B.....	92
Phase 1: Completely dried after initial setup.....	94
Phase 2: Completely dried after 1 <sup>st</sup> re-saturation .....	103
Phase 3: Completely dried after 2 <sup>nd</sup> re-saturation .....	104
Discussion of the test results from section B .....	108
Summary and conclusions.....	108
 CHAPTER VI APPLICATION OF THE CLAY MIXTURE AS FILLING MATERIAL FOR SUBSURFACE CRACKING AREA .....	 111
Introduction .....	111
Preliminary injection test using small-scale container .....	112
Electrical Resistivity Tomography (ERT) measurements for the mixture injected area .....	115
The clay mixture injection within desiccation cracking area .....	115
ERT result of the soil with clay mixture injection within crack networks.....	115
Permeability test with the phase of drying-wetting cycle .....	123
Permeability test setup and procedure .....	123
Permeability test result of section A.....	124
Permeability test result of section B .....	127
Discussion of the permeability test results .....	130
Direct shear test for soil-clay mixture structure .....	131
Test setup and procedure .....	131
Direct shear test results.....	132
Soil structure exploration with dismantlement .....	133
Summary and conclusions.....	136
 CHAPTER VII CONCLUSIONS .....	 139
Evaluation of mechanical and geophysical properties of clay mixture as filling material.....	140
Electrical Resistivity Tomography (ERT) technique for mapping of desiccation crack network within subsurface crack area .....	142
Applicability of the clay mixture as filling material for subsurface crack area .....	144
Future works.....	146
 REFERENCES .....	 147
 APPENDIX A THREE DIMENSIONAL VISUALIZATION OF ERT RESULTS USING VOXLER 3D (SECTION B3) .....	 158
A1. 3-D ERT results (section B3, phase 2) .....	158
A2. 3-D ERT results (section B3, phase 3) .....	165



## LIST OF FIGURES

	Page
Figure III-1 Desiccation soil container setup (Front view) .....	22
Figure III-2 Water content probe installation for desiccation soil container .....	23
Figure III-3 Water content probe calibration using small-scale soil container .....	24
Figure III-4 Water content probe calibration results .....	24
Figure III-5 ARES earth meter equipment .....	25
Figure III-6 Electrode arrangement (12 by 8) .....	26
Figure III-7 Scheme of the four-electrode method (Pozdnyakova, 1999) .....	27
Figure III-8 Experimental setup for four-electrode method.....	28
Figure III-9 Unconfined compression test setup .....	29
Figure III-10 Flow table test (a) preparation of mortar (b) measurement of the flow .....	31
Figure III-11 Direct shear test apparatus.....	33
Figure IV-1 Unconfined compression test results with variation of graphite proportion	40
Figure IV-2 Unconfined compression test results with variation of beta-glucan proportion .....	41
Figure IV-3 Unconfined compression test results with variation of xanthan gum proportion .....	42
Figure IV-4 Unconfined compression test results with variation of cement proportion..	44
Figure IV-5 Unconfined compression test results with variation of xanthan gum and cement proportion .....	46
Figure IV-6 Flow of the clay mixture with superplasticizer concentration (%) .....	50
Figure IV-7 Flow of the clay mixture with various components (cement and biopolymers) .....	51
Figure IV-8 Flow of the clay with graphite composition.....	52

Figure IV-9 Flow of the clay mixture with xanthan gum proportion.....	53
Figure IV-10 Electrical resistivity with graphite concentration.....	58
Figure IV-11 Electrical resistivity with beta-glucan biopolymer proportion.....	59
Figure IV-12 Electrical resistivity with xanthan gum biopolymer proportion.....	60
Figure IV-13 Electrical resistivity with cement concentration .....	60
Figure V-1 Electrode installation for the preliminary ERT measurements.....	65
Figure V-2 Schlumberger and Dipole-Dipole array configurations.....	67
Figure V-3 Schlumberger array results for the clay with three block structure (d=30cm).....	69
Figure V-4 Dipole-Dipole array results for the clay with three block structure (d=30cm).....	70
Figure V-5 Stereoscopic view for the result of Schlumberger array (d=30cm).....	71
Figure V-6 Stereoscopic view for the result of Dipole-Dipole array (d=30cm) .....	72
Figure V-7 Schlumberger array results for the clay with two block structure (d=20cm)	73
Figure V-8 Stereoscopic view for the result of Schlumberger array (d=20cm).....	74
Figure V-9 Dipole-Dipole array results for the clay with two block structure (d=20cm).....	75
Figure V-10 Stereoscopic view for the result of Dipole-Dipole array (d=20cm) .....	76
Figure V-11 Schlumberger array results for the clay with one block structure (d=10cm).....	77
Figure V-12 Stereoscopic view for the result of Schlumberger array (d=10cm).....	78
Figure V-13 Dipole-Dipole array results for the clay with one block structure (d=10cm).....	79
Figure V-14 Stereoscopic view for the result of Dipole-Dipole array (d=10cm) .....	80
Figure V-15 Desiccation crack propagation with drying-wetting cycle on section A .....	83
Figure V-16 Three area selection for the ERT measurements (Section A, phase 3) .....	84

Figure V-17 ERT result (A1, phase 3) .....	85
Figure V-18 ERT result (A2, phase 3) .....	86
Figure V-19 ERT result (A3, phase 3) .....	87
Figure V-20 Three area selection for the ERT measurements (Section A, phase 4) .....	88
Figure V-21 ERT result (A1, phase 4) .....	89
Figure V-22 ERT result (A2, phase 4) .....	90
Figure V-23 ERT result (A3, phase 4) .....	91
Figure V-24 Desiccation crack propagation with drying-wetting cycle on section B .....	93
Figure V-25 Area selection for the ERT measurement (Section B, phase 1) .....	94
Figure V-26 ERT result (B3, phase 1) .....	95
Figure V-27 3-D image of the ERT measured subsurface area (B3, phase 1) .....	96
Figure V-28 Horizontal sliced cut of ERT measured subsurface area (Top view, B3, phase 1) .....	97
Figure V-29 Horizontal sliced cut of ERT measured subsurface area (Front view, B3, phase 1) .....	98
Figure V-30 Horizontal sliced cut of ERT measured subsurface area (3-D view, B3, phase 1) .....	99
Figure V-31 Vertical sliced cut of ERT measured subsurface area (Top view, B3, phase 1) .....	100
Figure V-32 Vertical sliced cut of ERT measured subsurface area (Side view, B3, phase 1) .....	101
Figure V-33 Vertical sliced cut of ERT measured subsurface area (3-D view, B3, phase 1) .....	102
Figure V-34 Area selection for the ERT measurement (Section B, phase 2) .....	103
Figure V-35 ERT result (B3, phase 2) .....	104
Figure V-36 Three area selection for the ERT measurements (Section B, phase 3) .....	105

Figure V-37 ERT result (B1, phase 3) .....	105
Figure V-38 ERT result (B2, phase 3) .....	106
Figure V-39 ERT result (B3, phase 3) .....	107
Figure VI-1 Preliminary injection test procedure .....	113
Figure VI-2 Surface image of section B after the clay mixture injection and area selection .....	116
Figure VI-3 ERT result of mixture injected area (B1) .....	117
Figure VI-4 ERT result of mixture injected area (B2) .....	118
Figure VI-5 ERT result of mixture injected area (B3) .....	119
Figure VI-6 Surface image of section B after permeability test .....	120
Figure VI-7 ERT result of mixture injected area after saturation (B1) .....	120
Figure VI-8 ERT result of mixture injected area after saturation (B2) .....	121
Figure VI-9 ERT result of mixture injected area after saturation (B3) .....	122
Figure VI-10 Constant head test setup .....	124
Figure VI-11 Test specimen preparation for the direct shear test .....	132
Figure VI-12 Direct shear test results .....	132
Figure VI-13 Surface image of section B after completely dried .....	133
Figure VI-14 Boundary of the natural soil and the clay mixture (B2) .....	134
Figure VI-15 Boundary of the natural soil and the clay mixture (B3) .....	135
Figure VI-16 Injected clay mixture structure (B3).....	135

## LIST OF TABLES

	Page
Table III-1 Physical properties of natural soil.....	18
Table III-2 #5339 Graphite (Superior Graphite Company).....	20
Table IV-1 Specimen description for unconfined compression test .....	37
Table IV-2 Unconfined compression test results .....	39
Table IV-3 Flow table test specimen profile and test results .....	48
Table IV-4 Free shrinkage test specimen profile and test results .....	55
Table IV-5 Four-electrode test specimen profile and test results.....	57
Table VI-1 The clay mixture description for preliminary injection test .....	112
Table VI-2 The clay mixture component and additive composition.....	115
Table VI-3 Permeability test for section A at the initial phase (Falling head test) .....	125
Table VI-4 Permeability test result for section A at the phase 4 (Constant head test)...	126
Table VI-5 Permeability test for section B at the initial phase (Falling head test) .....	127
Table VI-6 Permeability test result for section B at the phase 2 (Constant head test)...	128
Table VI-7 Permeability test result for section B at the phase 3 (Constant head test)...	129
Table VI-8 Permeability test result for section B after injection (Constant head test) ..	130
Table VI-9 Overall permeability test results .....	131

# CHAPTER I

## INTRODUCTION

### **Background**

Desiccation cracking in soils is a natural phenomenon associated with soil shrinkage during water evaporation under field conditions triggered by the soil-atmosphere interactions. The presence of desiccation crack in soils are very detrimental and significantly affect several physical properties of soils. For example, soil compressibility and strength are strongly impacted by the presence of drying cracks. Also, permeability of soils can increase significantly because of desiccation cracking (Tay et al., 2001; Dyer et al., 2009).

The stability of the geotechnical structures, such as foundation, earth embankment, and landfill can be affected by the occurrence of desiccation cracks. The landfill covers and clay liners can be damaged by desiccation cracking (Daniel and Wu, 1993; Melchior, 1997; Yesiller et al., 2000; Philip et al., 2002; Southen and Rowe, 2005; Albright et al., 2006; Jones et al., 2012) and desiccation crack can also increase seepage and lead to failures in embankment (Marsland, 1957).

The phenomena associated with the formation of desiccation crack in soil are quite complex and therefore it possesses several challenges for study in the lab. The initiation and propagation of desiccation cracks in soils is a strongly coupled hydro-mechanical problem (Sanchez et al., 2013). Many research efforts have been conducted involving qualitative and quantitative studies to progress the current understanding

behind the formation and propagation of desiccation cracks in soils, however more research is necessary in this very relevant area.

The interest in subsurface investigation using geophysical electrical techniques has steadily increased. The study of the desiccation cracks network in the soil mass using geophysical methods is a new area of research. Electrical conductance in soils as in other materials is due to the movement of anions and cations (Reynolds, 1997). The Electrical Resistivity Tomography (ERT) technique was utilized to draw desiccation crack network in two-dimensions (i.e. in a plane) from a laboratory scale soil container (Sentenac et al., 2009; Jones et al., 2012). In this study, the verification of miniature arrays and desiccation crack monitoring under drying-wetting cycle is conducted. Furthermore, three-dimensional visualization process is suggested using inversion data.

In addition, study on injection material is emerged to stabilize the soil structure with filling of defected area and trace easily with electrical conductive elements (Sentenac et al., 2009). The electrical conductive particles (e.g. carbon nanotube, graphite) can freely organize and reduce the space available between them to form conductive networks under drying condition (Gong et al., 2000; Landi et al., 2009). Also, combination of clay and electrical conductive components improve dispersion without damage mechanical properties (Liu and Grunlan, 2007).

The biopolymers, such as  $\beta$ -glucan and xanthan gum are studied recently for soil improvement with effect on significant permeability reduction and soil strength increment. In addition, superplasticizer is highly recommended property to reduce the cohesion of soil-cement structure and to enhance the workability of material (Perrot et

al., 2013). Based on these characteristics, the evaluation of the mechanical and geophysical properties of clay mixture as filling material is conducted. Also, applicability of clay mixture as filling material is investigated by injection and laboratory experiments.

### **Objective**

The main objectives of this dissertation are:

- (1) enhance Electrical Resistivity Tomography (ERT) technique for exploration cracked soils area with crack network;
- (2) investigate, in the laboratory, possible remedial solutions for cracked soils based on different soil-mixtures involving several components including clays, graphite, and cement to inject them in desiccation cracks in soils;
- (3) verify the performance of the suggested clay mixtures as filling material after injecting in scaled (medium size) tests; and
- (4) assess the suitability of the ERT to evaluate cracked soils treated with soil mixtures and monitored them.

For the first objective, the preliminary measurement will be conducted to compare two kind of arrays (Dipole-Dipole and Schlumberger). Desiccation soil container will be prepared with two different initial conditions and the electrical resistivity will be measured under various condition with drying-wetting cycle. In addition, collected ERT data will be analyzed using post processing programs. Two-



dimensional mapping data will be drawn using RES3DINV program and three-dimensional visualization will be conducted using VOXLER 3D program.

For the second objective, experimental research will be performed using various kind of mechanical and geophysical tests. The primary outcome of this task is to determine the clay mixture for filling material within crack area as (1) relatively higher strength, (2) lower shrinkage and cracking potential, (3) higher electrically conductive, and (4) material with suitable liquidity.

For the third objective, the preliminary clay mixture injection will be conducted using various type of mixture components. By this procedure, washing out problem will be prevented prior to the primary mixture injection. Also, the direct shear test using soil and clay mixture structure will be carried out to verify the strengthening effect of mixture injection within crack in soils.

For the fourth objective, the clay mixture will be injected to desiccation cracking area and monitored using ERT measurements. In addition, permeability test will be conducted to verify the hydraulic conductivity reduction effect by the mixture injection.

### **Dissertation organization**

This dissertation focuses on the enhancement of the Electrical Resistivity Tomography (ERT) for monitoring the desiccation crack network and suggestion of three-dimensional visualization technique, and the clay mixture as remedial solution for crack in soils. This dissertation consists of seven chapters:

## *Chapter 1*

Research background and objective are presented, and the dissertation organization is explained.

## *Chapter 2*

In this chapter, a searching investigation of published literature concerning the desiccation crack in soil is presented. A comprehensive literature review of desiccation crack initiation and propagation, Electrical Resistivity Tomography (ERT) technique for mapping subsurface area, geophysical and mechanical method for soil investigation, image analysis technique for quantification of factors relating to desiccation crack, biopolymer application for reinforcement of clay mixture, and superplasticizer for soil-cement mixture is introduced for clarification of research background. The main objective of this chapter is the establishment of research methodology for the behavior of soil subjected to drying and evaluation of clay mixture as filling material for crack area. It is also important to review other experimental and analytical studies of desiccation crack to support the development of present knowledge. In addition, the interpretation of current studies of desiccation crack problems is accomplished by this literature review.

## *Chapter 3*

Test apparatus such as desiccation soil container, Electrical Resistivity Tomography (ERT) measurement system, and mechanical and geophysical experiment

instruments are introduced, and physical properties of soil and mixture are explained. The procedure for experiment preparation of desiccation soil container with installation of water content probe and drainage system for permeability test is presented.

#### *Chapter 4*

The aim for this chapter is characterization of mechanical and geophysical properties of clay mixture with carbon nanoparticle, cement with superplasticizer, and biopolymers. Three kind of mechanical tests and one of geophysical method are applied to evaluate the applicability of clay mixture as remedial solution for crack area. Unconfined strength, liquidity, shrinkage characteristics, and electrical conductivity are compared with various mixture profile to determine appropriate clay mixture composition for filling material.

#### *Chapter 5*

The aim of this chapter is enhancement of an experimental technique to monitor the desiccation crack propagation in soils using high resolution miniature arrays with three-dimensional survey methods. For the verification of the arrays, the preliminary measurements is carried out to compare Dipole-Dipole and Schlumberger arrays. The Electrical Resistivity Tomography (ERT) measurements are conducted for the desiccation soil container with two different initial condition under drying-wetting cycle. Post processing is conducted and compared using two programs for two-dimensional and three-dimensional visualization of the results.

## *Chapter 6*

The applicability of the clay mixture as remedial solution is investigated by various laboratory experiments. The preliminary injection using small-scale soil container is conducted to explore washing out problem for each factors in the clay mixture. To evaluate the shear strength of soil with clay mixture structure, the direct shear test is conducted. The permeability test is conducted for each drying-wetting cycle to compare the hydraulic conductivity at the various condition and to evaluate the reduction effect by filling material. The Electrical Resistivity Tomography (ERT) measurement is also conducted to compare the soil structure with injected clay mixture.

## *Chapter 7*

Conclusions from the study are summarized.

## CHAPTER II

### LITERATURE REVIEW

#### **Introduction**

Enhancing of the Electrical Resistivity Tomography (ERT) technique and the development of the clay mixture as filling material within the desiccation cracking area are the main purpose of this dissertation. Thus, understanding of background theories and research trend related to these topics are significant factor of this research. In this chapter, the background theories and research trend of desiccation crack in soil is introduced, and geophysical application for soil investigation including ERT and four-electrode measurement is investigated by reviewing the research articles. The principle of electrical resistivity measurement and some case studies of equipment application and result analysis are introduced. In addition, the previous studies on the clay mixture components including graphite-cement mixture, biopolymers, and superplasticizer is also reviewed, especially focused on the function of each factor on soil improvement.

#### **Desiccation cracks in soil**

Desiccation crack in soil is natural occurrence which is caused by dramatic climate change. The initiation and propagation of desiccation crack is a highly complex phenomenon because of the strong connection between mechanical and hydraulic properties of soils (Sanchez et al., 2013). The stability and integrity of landfill structures can be affected by desiccation crack formation in accordance with rapid and direct flow

of water and solutes from the surface to the deeper area of soil (Armstrong et al., 1994; Rounsevell et al., 1999; Yesiller et al., 2000). Due to the development of crack in soil, permeability can be increased and it can cause the failure of waste containment system (Tay et al., 2001; Li et al., 2011). Also, the increase of hydraulic conductivity of soils can accelerate the infiltration of water to the underground and the shear strength of soil can be weakened. Furthermore, desiccation cracks can affect shrinkage-swelling potential of the soil, and it can cause serious damage to the geotechnical foundation structures (Marsland, 1968).

Desiccation crack occurs from dehydration of soil which leads to increase the capillary force and exceed strength of soil by evaporation. Water transport in porous media of soil is basically controlled by the hydraulic properties of the soil mass, which in turn affects the mechanical behavior, because soil tends to contract under the suction (Rodriguez, 2007). Rayhani et al. (2007) presented that the dimension of desiccation cracks propagate with increase of plasticity index and drying-wetting processes. Nahlawi and Kodikara (2006) performed several experiments of crack generation under restrained laboratory condition. The length of the molds were relatively longer than widths, so parallel cracking was generated in thin layers. The increase of negative pore pressure (suction) due to an air-water interface enters into the saturated medium makes the desiccation crack (Shin and Santamarina, 2011). Desiccation crack in soil is developed as soil is restrained against the volume change resulting from the soil suction generated with a desiccation of soil mass (Nahrawi and Kodikara, 2002). During the desiccation,

some cracks initiate at the bottom and develop vertically upward to the free surface and laterally outward to adjacent cracks adjacent cracks (Weinberger. 1999).

Crack pattern characterization is widely used in the different fields of geo-science and engineering. Techniques for quantification of the crack patterns have been developed in recent years from direct measurement to sophisticated method, such as digital image processing. The study of crack formation in unsaturated soils of alluvial plants was generated by empirical method related to measurement of crack network determined from conventional surveys (Yassoglou et al., 1994). Direct measurement methods were developed by several researchers, but these methods required manual measurement of crack pattern in the field. Another method of two- and three-dimensional measurement of crack pattern is in terms of geometrical and topological descriptors based on integral geometry. The result of this approach is an objective numerical characterization of a given pattern of cracks (Michielsen and de Raedt, 2001). A number of researchers have used image processing techniques in various geotechnical problems for direct and indirect measurement of soil properties, including characterization of desiccation crack patterns, crack detection and monitoring (Sarmah et al., 1996; Preston et al., 1997; Horgan 1998; Velde, 1999; Puppala et al., 2004; Vogel et al., 2005). Lecocq and Vandewalle (2002, 2003) utilized a digital camera to investigate the crack and dynamics of crack initiation in one-dimensional desiccation experiments. Digital image processing was used to study unsaturated soil behavior (Gachet et al., 2003) and to monitor the change of drying bentonite-sand mixtures (Önal et al., 2008). Costa and Kodikara (2008) utilized the time-lapse photography to investigate the crack

pattern of soils in the form of video clips. Particle image velocimetry has been used to explore the soil's crack pattern and it is proved to be a useful technique for analysis of strain and stress distribution of soil subjected to drying (White et al., 2003; Thusyanthan et al., 2007; Costa et al., 2008). Lakshmikantha (2009) utilized the image processing to characterize the two-dimensional desiccation crack network developed on the soil surface. Also, quantification of many researchers which characterize the crack pattern were conducted. Atique and Sanchez (2009) also utilized the digital image processing technique to analyze the result form desiccation plate tests.

### **Geophysical application for soil investigation**

Geophysical investigation is based on the response of the earth to the electrical current flow. An electrical current is passing through the ground and two potential electrodes allow to record the resultant potential difference between them with direct measurement of the electrical impedance of the soil area. Electrical resistivity measurement is associated with varying depths relative to the distance between the current and potential electrodes in a survey, and it can be interpreted qualitatively and quantitatively in terms of geo-hydraulic model of subsurface area (Cardimona, 2002). The interest in site investigation using electrical resistivity technique has gradually increased. Electrical conductivity is related to the particle size by the electrical charge density at the particle surface. In addition, the pore geometry including void distribution and formation determines the proportion of a number of soil properties, such as the nature of solid constituents (particle size distribution, mineralogy), arrangement of voids



(porosity, pore size distribution, connectivity), degree of saturation, electrical resistivity of the fluid and temperature (Samouelian et al., 2004). Electrical resistivity measurement was conducted to figure out the relationship between the electrical resistivity and soil characteristics. Robain et al. (1996) linked resistivity values with macro- and meso-porosity. Samouelian et al. (2003) presented that crack opening investigation in centimetric scale.

Furthermore, electrical resistivity measurement improved with respect to measurement time. The modification of computer-controlled multi-channel resistivity measurement using multi-electrode arrays led to a significant development of electrical resistivity investigation. Electrical Resistivity Tomography (ERT) technique is widely used to analyze the mapping of underground targets. Electrical conductance through the soil media occurs due to the movement of anions and cations during electrical field application (Reynolds, 1997). Geophysical methods based on miniature arrays are solution for the small desiccation cracks as proved to be reliable to monitor contaminant transport in soil models in centrifuge tests (Depountis et al., 1999). This technique improves the measurement accuracy with reduction of soil disturbance, because it is non-invasive technique. ERT technique is widely used recently to detect crack formation in clayey soil by laboratory and field experiments (Sentenac and Zielinski, 2009; Jones et al., 2009). Sentenac and Zielinski (2009) showed that change in electrical resistivity associated with crack propagation is monitored as a function of time.

In addition, it is proved that Schlumberger array is sensitive to both vertical and horizontal crack formation in the clayey soil. Sentenac et al. (2012) conducted a field

study using complementary electromagnetic and low resolution resistivity surveys. It is showed that ERT technique is practical to explore desiccation cracking area in the cross-section of an embankment. Jones et al. (2014) examined the application of miniature and field scale ERT measurements on a fissured flood embankment.

### **The clay mixture components**

#### *Carbon nano-composites*

Nanotechnology is a rapidly expanding research area where novel properties of materials manufactured on the nano-scale can be used for the benefit of civil engineering and construction materials. In addition, a number of developments can potentially improve the time and life cycle cost of civil engineering projects. Nanotechnology is the use of tiny particles of the material to generate new large-scale materials. A nanoparticle is a microscopic particle measured in nanometers (nm). It is defined as a particle with at least one dimension less than 200nm. The size of the particle is very important, because the length and properties of material can be affected (Mann, 2006). The field of nanotechnology is a broad and interdisciplinary area of worldwide research activity that has been grown significantly in the past few years (Siegel, 2006). Taha (2009) conducted laboratory tests to analyze the fundamental properties of soil mixture and product from ball milling operation. Fang et al. (2009) presented that nanoparticles are stable in soil suspensions. Polymer composites containing carbon-based filler become applicable due to unique combination of electrical conductivity and polymer flexibility. Drying or cooling of a melt-based system, the nanotubes can freely organize themselves, resulting

in a relatively homogenous conductivity network (Gong, 2000; Landi, 2009). Liu and Grunlan (2007) conducted electrical conductivity test to investigate that clay composite with carbon nanoparticles improves dispersion without damaging electrical conductivity and mechanical performance. Clay is mechanically strong and known as good dispersion transfer characteristics in polymer composites (Giannelis, 1996; Wang et al., 2005). The combination of clay and carbon nanoparticle allows electrical conductivity to be enhanced without damage on mechanical properties of mixture.

#### *Biopolymer treatment for soil improvement*

Soil improvement and stabilization is a significant consideration all over the history of human civilization. Cement, petrochemicals, and bacteria are recently being progressively applied in an effort to improve soil in the aspects of mechanical and chemical properties (van Elsas and Heijnen, 1990; Tungittiplakorn et al., 1981). Especially, cement is the most widely used element for soil improvement in soil strengthening, ground water control, and contaminant storage (Winograd, 1981; Xanthakos et al., 1994; Nataraja et al., 2008; Yoon and Abu-Farsakh, 2009). Meanwhile, several alternatives including geopolymers, alkali-activated cement, geocement, and inorganic polymer concrete have been investigated to reduce or replace cement (Davidovits, 2008; Alonso and Palomo, 2001; Krivenko and Kovachuk, 2007; Sofi and van Deventer, 2007). Biopolymer was applied as stabilizers for soil to control or reduce the soil erosion (Orts et al., 2007; Sposito, 1989). In addition, biopolymer was used for drilling mud and temporary excavation supports (Mitchell and Santamarina, 2005).

Chang and Cho (2014) conducted experimental research on residual soil mixture with  $\beta$ -glucan biopolymer to examine the strengthening effect. It was proved that  $\beta$ -glucan biopolymer is effective to increase the tensile strength of the soil mixture and improve the compressibility by ionic bonding between biopolymer and soil particles. Chang et al. (2015) performed experimental research on the soil mixture with Xanthan gum biopolymer, and it was shown that the strengthening effect of Xanthan gum is significant within fine-grained soil. In addition, it was proved that Xanthan gum interacts with cations of the clay particles to generate chemically stronger ionic bonds added to hydrogen bonds (Chang et al., 2015). Gallipoli et al. (2017) presented that significant improvements on the mechanical properties of soil by guar gum and xanthan gum based biopolymers.

### *Superplasticizer*

Superplasticizer (Polycarboxylate Ether) is improved chemical admixtures over plasticizers with highly effective plasticizing effects on wet cement material. The advantage of using superplasticizer is avoiding particle segregation, such as gravel, coarse and fine sands and improvement of the flow characteristics of suspensions. This material is self-leveling and self-compacting material with high strength and performance of cement. Cement mixture tends to clump together in water due to dissimilar surface electrical charges and trap mixing water. In addition, it behaves like larger and rougher particles and increasing mixture viscosity. To solve these problems, superplasticizer can be applied to neutralize the attractive charge and free up trapped

water. Furthermore, superplasticizer causes the mixture particles to repel each other. Kanema et al. (2016) evaluated the effect of the superplasticizer on reducing macro cracks desiccation using two-dimensional samples. It was also shown that the superplasticizer doesn't affect significantly the drying process of mixture. Also, it reduces the crack appearance and enhances the workability of mixture. Perrot et al. (2013) conducted the study on superplasticizer treated grouting material into soil. It was presented that the superplasticizer reduce the cohesion of cement based grout and the strength and workability of grouting material was developed.

## CHAPTER III

### APPARATUS, MATERIAL, AND EXPERIMENT PREPARATION

#### **Introduction**

In this dissertation, various kind of experimental research for soil and clay mixture was conducted. First one is mechanical tests on natural soil and clay mixture components. Basic laboratory tests such as Atterberg limit and compaction test were performed to figure out physical properties of natural soil related to hydraulic characteristics. Also, free shrinkage, unconfined compression, flow table test, permeability test, and direct shear test were carried out to investigate clay mixture components for filling material. Second one is geophysical methods using electrical resistivity. Four-electrode test and Electrical Resistivity Tomography (ERT) measurements were applied to investigate the geophysical aspects of soil and clay mixtures. In this chapter, soil and clay mixture components, experiment apparatus and procedures are introduced.

#### **Soil and clay mixture components**

##### *Natural soil*

The natural soil chosen for this experiments was collected from the field experiment site in RELIS campus of Texas A&M University. Gravels and organic components (leaves, twigs, and bugs) were removed by hand and the soil was air-dried under the controlled laboratory environment. After completely dried, soil was crushed

using the batching machine in the concrete laboratory. In addition, crushed soil was separated using No. 20 (0.85mm) sieve to collect fine-grained elements. A series of tests have been conducted to investigate the physical properties of natural soil, such as modified proctor test and Atterberg limits. The maximum dry unit weight for natural soil is  $20.4\text{kN/m}^3$  at an optimum water content of 10.6%. Liquid limit and plastic limit for tested soil was 41.27% and 10.44%, respectively (Table III-1). This soil has low plasticity with the plasticity index of 30.83%. The natural soil was classified as silty soil with low plasticity (ML) following USCS soil classification.

**Table III-1 Physical properties of natural soil**

<b>Physical properties</b>	<b>Values</b>
<b>Liquid limit, LL (%)</b>	41.27
<b>Plastic limit, PL (%)</b>	10.44
<b>Plasticity index, PI (%)</b>	30.83
<b>Maximum dry unit weight, <math>\gamma_{d,\text{Max}}</math> (<math>\text{kN/m}^3</math>)</b>	20.40
<b>Optimum water content, <math>w_{\text{opt}}</math> (%)</b>	10.60

#### *EPK Kaolinite*

EPK (Edgar Plastic Kaolin) Kaolinite is a secondary water-washed kaolin that is mined in Florida. This material is popular because of its plasticity and it was selected as base material for the clay mixture considering its excellent casting properties. Liquid

limit and plastic limit for EPK was 61.0% and 36.0%, respectively. The plasticity index was 25.0%.

### *Graphite*

Graphite is a crystalline form of the element carbon with its atoms arranged in a hexagonal structure. This material is commonly used in pencils and lubricants and it is a good conductor of electricity and heat. This characteristic allows it can be widely used in electronic products. In this research, graphite is chosen for the electrical conductivity, so it is possible to trace the clay mixture within defected area using Electrical Resistivity Tomography (ERT) measurements. The detailed profile provided by Superior Graphite Company is shown in Table III-2.

### *Cement*

Cement is a substantial material used for construction that sets, hardens, and adheres to other materials to bind them together. This material is usually used to bind aggregates (sand and gravel) together for producing of concrete or it can also create mortar mixed with fine aggregates. In the previous research by Kim, some portion of cement was applied in clay mixture to prevent washing out problem of filling material within cracked area. This material was also used as main components in this research, but the amount reduction was suggested without loss of strength and workability.



### *Superplasticizer*

Superplasticizer is improved chemical admixtures over plasticizers with highly effective plasticizing effects on wet concrete. It can avoid aggregate segregation and improve the liquidity of suspensions. In this research, the one of the most important factor was decrease of water content without loss of workability. To enhance the fluidity and minimize the shrinkage of the clay mixture, the superplasticizer was applied for these purposes. ADVA Cast 575 was used in this research.

**Table III-2 #5339 Graphite (Superior Graphite Company)**

<b>Appearance</b>	<b>Powder or pellet</b>
<b>Color</b>	Black
<b>Carbon, min</b>	99.9%
<b>Ash, max</b>	0.1%
<b>Moisture, max</b>	0.1%
<b>Surface area, min</b>	7.18m <sup>2</sup> /g
<b>Scott volume</b>	0.100g/cc
<b>Density</b>	2.231g/cm <sup>3</sup>
<b>Passing %</b>	<b>Particle size</b>
<b>90% (&lt; 20 microns)</b>	20.24 µm
<b>50%</b>	9.57 µm
<b>10%</b>	3.10 µm

## *Biopolymer*

### **$\beta$ -glucan**

$\beta$ -glucan comprise a group of  *$\beta$ -D-glucose polysaccharides* naturally occurring in the cell walls of cereals, bacteria, and fungi, with significantly differing physicochemical properties dependent on source material. In the field, this material can be applied as water reducing agents in concrete and additive in superplasticizers. In this research,  $\beta$ -glucan was investigated the strengthening effect and shrinkage reduction of clay mixture.

### **Xanthan gum**

Xanthan gum is a polysaccharide produced by fermentation of glucose or sucrose by the *Xanthamonas campestris bacterium* and commonly used as a food additive and rheology modifier (Davidson, 1980; Rosalam and England, 2006). The popular characteristics of this material is pseudo-plasticity (Casas et al., 2000). Xanthan gum can induce a dramatic increase in the viscosity of a fluid with a small amount. This material is also used in the oil industry as a drilling mud thickener to provide consistent rheology through the hole (Comba and Sethi, 2009). Also, it can be applied as an additive in concrete to increase viscosity and prevent wash-outs (Plank, 2004). In this research, Xanthan gum was applied to reinforce the strength with decrease of cement portion and to prevent washing out problem of clay mixture under saturation.

## Test apparatus and setup

### *Desiccation soil container*

The acrylic rectangular container with dimensions of  $0.63\text{m} \times 0.44\text{m} \times 0.32\text{m}$  was manufactured for desiccation of natural soil. This box was divided into two sections with same dimension ( $0.63\text{m} \times 0.22\text{m} \times 0.32\text{m}$ ) by acrylic barrier for the two experiments with different initial water content. To allow drainage through the soil, the drainage holes were drilled with regular spacing. The granular soil layer for the drainage was placed at the bottom of the container with thickness of 5cm and non-woven fabric was placed at the top and the bottom of granular soil layer to prevent loss of soil particles and mixing with natural soil. The natural soil was prepared for two sections with 15cm depth. Figure III-1 shows the desiccation soil container setup in front view.



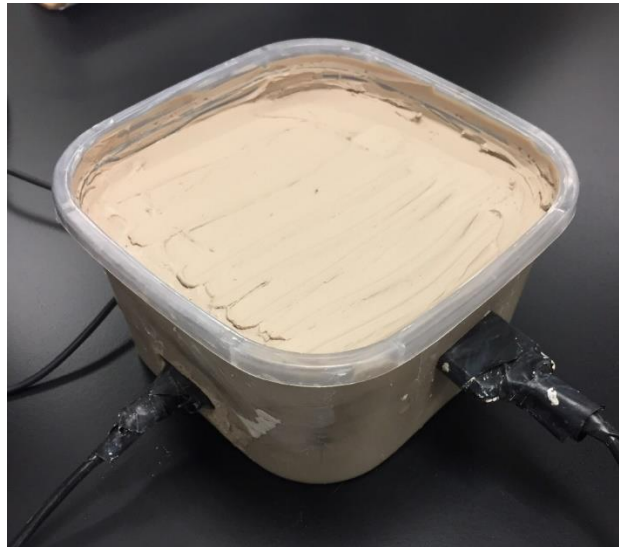
**Figure III-1 Desiccation soil container setup (Front view)**

On section A, the chosen value of water content was 10% corresponding to the dry side water content for 90% of relative compaction. For the soil preparation, each 5cm depth of soil layer was compacted. On section B, the water content of 60% was selected for the natural soil. This value of water content was within the range for 150% of liquid limit. Soil was prepared using soil mixing machine and poured into desiccation container.

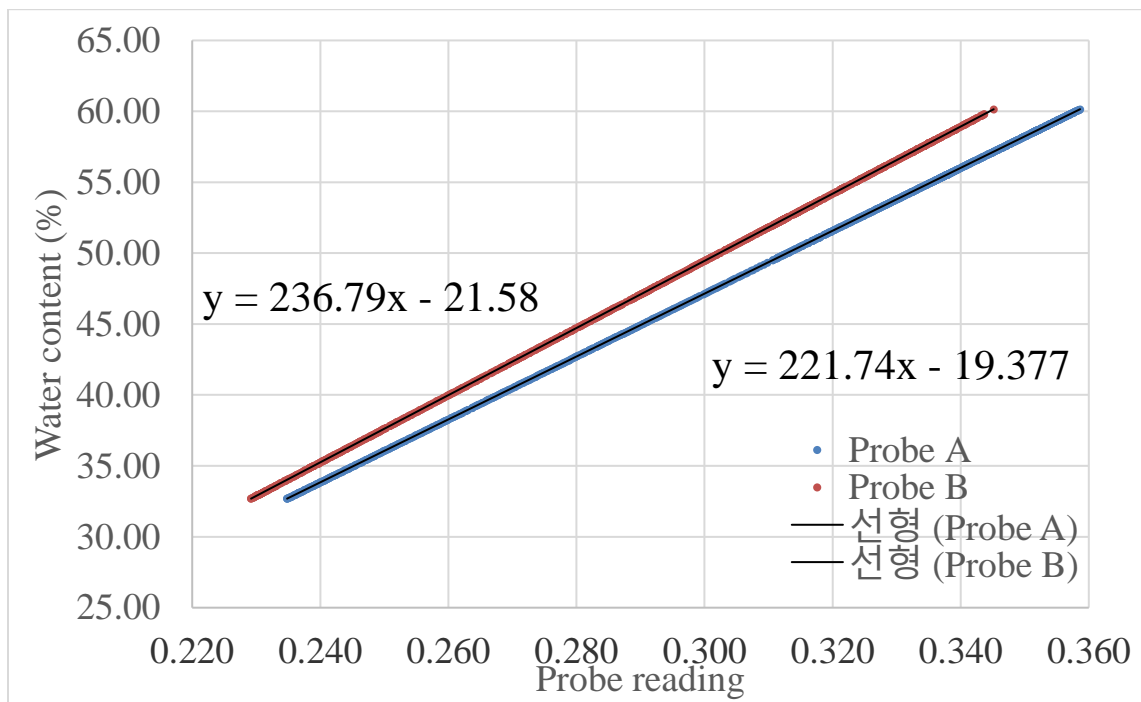
Water content probes were installed to measure the moisture content with time at the various depth at each section (Figure III-2). Prior to installation in the container, the probes were calibrated using small-scale container. EPK Kaolinite was mixed with 60% of water content and placed into small container. Two water content probes for each section were installed at the middle of the soil layer (Figure III-3). The water content probe reading was collected with regular time interval under drying condition. Figure III-4 shows the calibration results from two probes. These formulas were applied to calculate the water content evolution within desiccation soil container.



**Figure III-2 Water content probe installation for desiccation soil container**



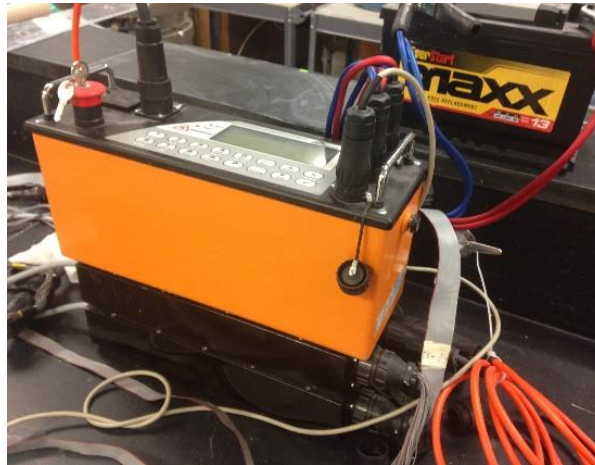
**Figure III-3 Water content probe calibration using small-scale soil container**



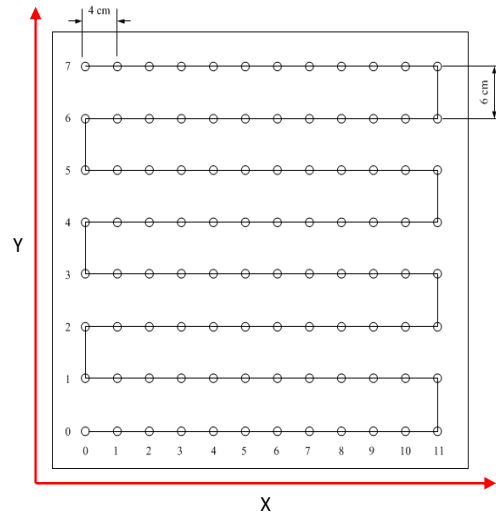
**Figure III-4 Water content probe calibration results**

### *Electrical Resistivity Tomography (ERT) measurement system*

Electrical Resistivity Tomography (ERT) technique using miniature electrodes array in a clay model to monitor the propagation of desiccation crack in two-dimensional and three-dimensional models was used by several researchers (Sentenac and Zielinski, 2009; Jones et al., 2012). Miniature geo-electrical method using resistivity arrays could be used as non-invasive method for the desiccation crack monitoring. In this research, a miniature resistivity array was adjusted to connect with ARES earth meter equipment (Figure III-5) manufactured by GF instruments. 96 electrodes was placed in a 12 by 8 (Figure III-6), and the distance between each electrodes is 2cm and 3cm in x- and y-direction, respectively. Desiccation cracks in soil was recorded and displayed as ERT using RES3DINV program. In addition, the scale factor of x-, y-, and z-direction acquired from the inversion process of this program was visualized as three-dimensional stereoscopic view of soil structure using VOXLER 3D program.



**Figure III-5 ARES earth meter equipment**



**Figure III-6 Electrode arrangement (12 by 8)**

*Drying test using electrical geophysical method*

The electrical exploration method became progressively popular in geo-environmental aspects. Electrical geophysical methods allow fast and stable measurement of electrical properties of soil, such as electrical conductivity, electrical resistivity, and potential at the subsurface area of undisturbed soil. The geophysical measurement device LandMapper ERM-02 was used for this research. This device was connected with four-electrode to measure the electrical resistivity (or electrical conductivity) (Figure III-7(b)). Four-electrode method was employed for many decades to evaluate soil moisture content and salinity under field environment. Electrode principle was proposed by Pozdnyakova (1999) (Figure III-7(a)). When the electrical current ((I) is applied to two electrodes located at the outside (A and B), the potential difference ( $\Delta\phi$ ) prompted between the two inside electrodes (M and N) will be measured. In this theory, the electrical resistivity is defined as follows:

$$ER = \frac{A\Delta\phi}{LI} = K \frac{\Delta\phi}{I} \quad (1)$$

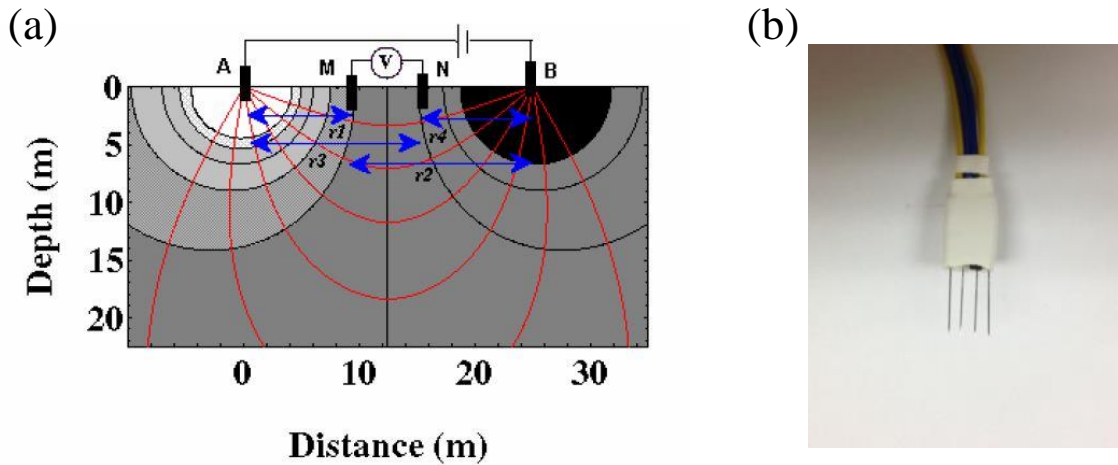
The electrical conductivity is the reciprocal of the measured resistivity:

$$EC = \frac{1}{ER} \quad (2)$$

The geometrical factor (coefficient  $K$ ) in Eq. (3) depends on the distance between the electrodes A, M, N, and B. The distance between each neighboring electrodes is the same value as 2mm (0.002m) in this study. The coefficient  $K$  is calculated with the following formula:

$$K = \pi \frac{[AM] \cdot [AN]}{[MN]} \quad (3)$$

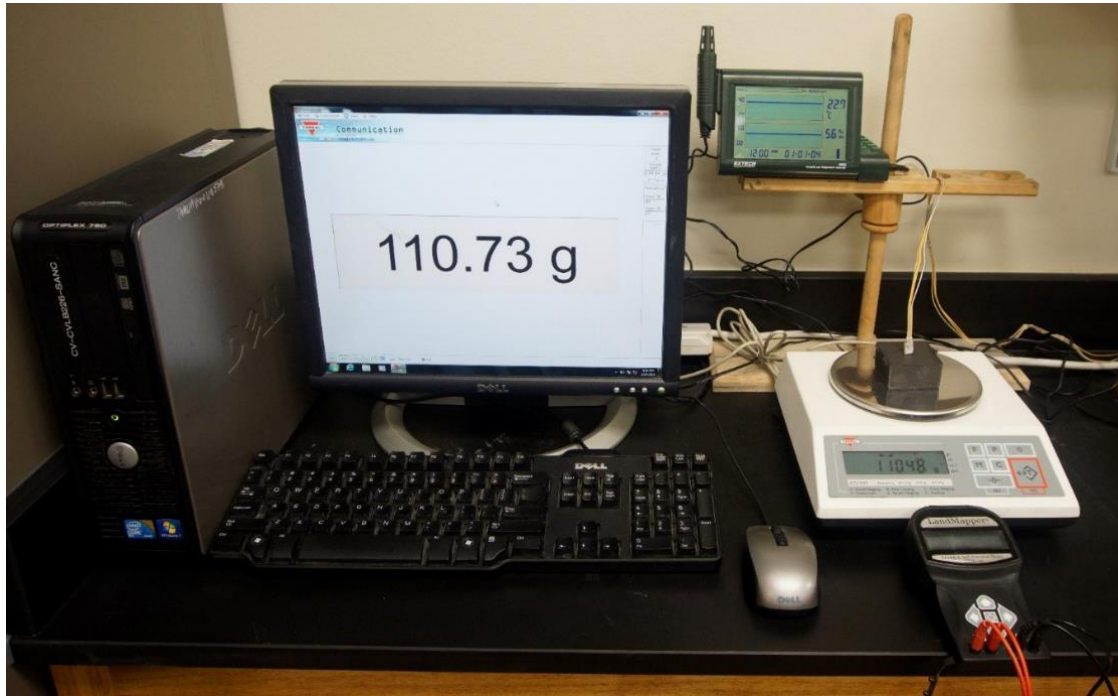
where, AM, AN, and MN are distances between electrodes measured in meters.



**Figure III-7 Scheme of the four-electrode method (Pozdnyakova, 1999)**



Experimental setup for four-electrode method is shown in figure III-8. As shown in this figure, the soil specimen was placed at the top of the balance connected to the computer system to record water content evolution during the measurement of the electrical resistivity/conductivity under drying condition. This experiment was conducted under controlled laboratory condition. The comparison analysis for time-dependent electrical resistivity/conductivity of the various kind of clay mixture specimens was performed to investigate geophysical characteristics of each components.

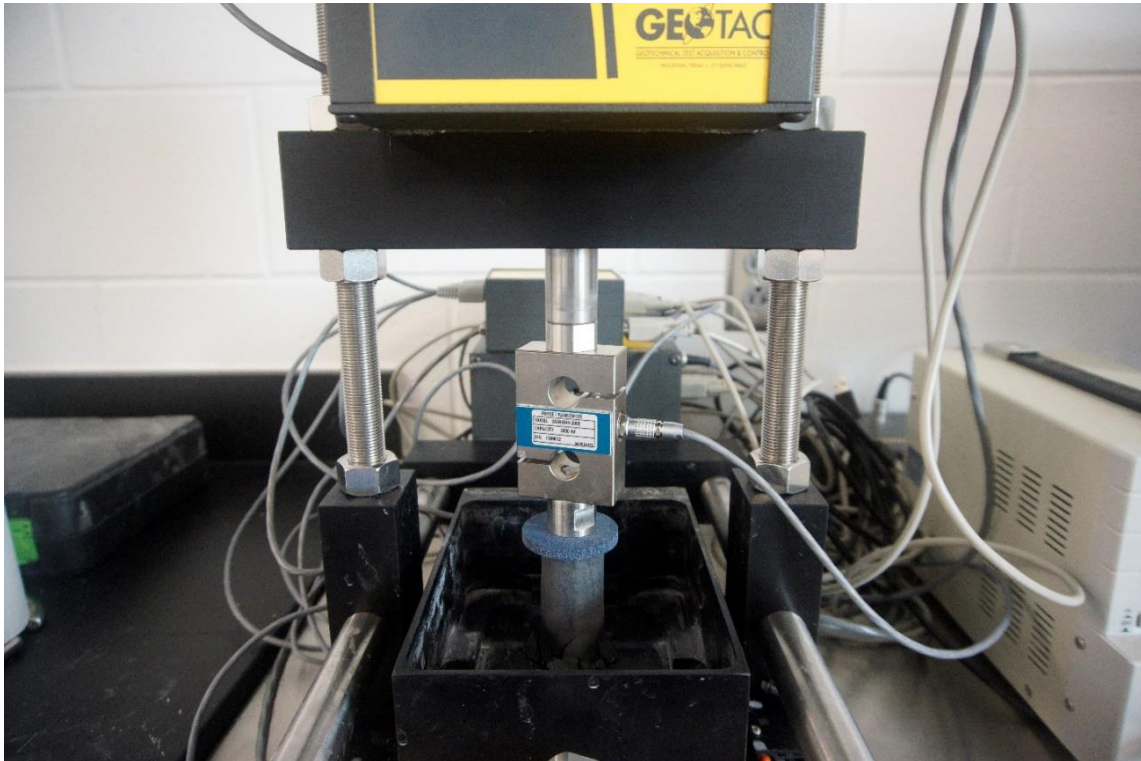


**Figure III-8 Experimental setup for four-electrode method**

## *Mechanical laboratory tests*

### **Unconfined compression test**

The unconfined compression test is one of the most popular laboratory test to investigate the soil strength with simple and economic procedure. This test was conducted following the standard procedure of ASTM D 2166. The specimens were prepared for the test with various portion profile of each components. The main objective of this experiment was to figure out the reinforcement effect of each clay mixture components. Figure III-9 shows the experimental setup for unconfined compression test.



**Figure III-9 Unconfined compression test setup**

The unconfined compressive strength can be calculated using the following formula.

$$q_{uc} = \frac{Q_{ult}}{A} \quad (4)$$

Where,  $q_{uc}$  = unconfined compressive strength

$Q_{ult}$  = ultimate compressive load at failure

$A$  = surface area of specimen

### **Flow table test**

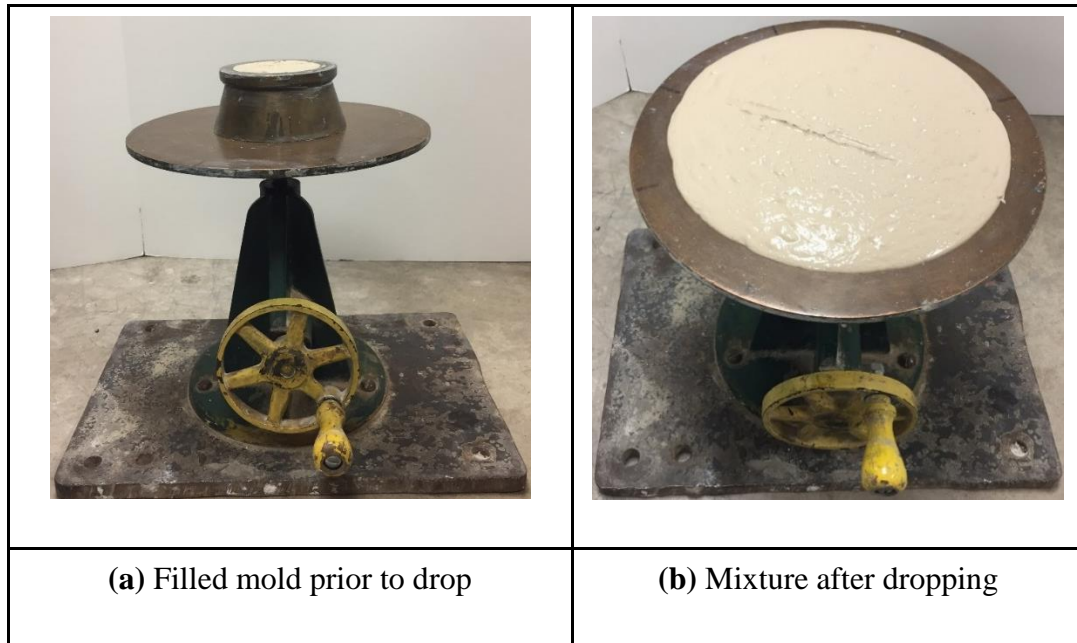
In the previous research conducted by Kim, the clay-graphite mixture injected crack area was completely washed out under saturated condition. To prevent washing out of mixture from injected area, some portion of cement was applied for the mixture in the previous research. In this research, especially on clay mixture components, various components were suggested in the aspect of reduction of cement portion and water content without loss of workability and strength. Figure III-10 shows the procedure of flow table test briefly.

The flow table test was usually conducted to measure the workability of mortar or wet cement. The aim of this experiment is to figure out the effect of superplasticizer on enhancing workability of clay mixture and to determine the optimum mixture ratio considering other components, such as biopolymer and graphite. The test was carried out following the standard procedure of ASTM C1437-15. Flow can be calculated using the following formula.

$$\text{flow (\%)} = \frac{d_{\text{avg}} - d_{\text{inner}}}{d_{\text{inner}}} \times 100 \quad (5)$$

Where,  $d_{\text{avg}}$  = average diameter of the tested specimen

$d_{\text{inner}}$  = inner diameter of the mold



**Figure III-10 Flow table test (a) preparation of mortar (b) measurement of the flow**

### Free shrinkage test

Free shrinkage test is simple method to quantify the shrinkage characteristics of the soil under controlled conditions. The main purpose of this experiment is to evaluate the impact of biopolymer, graphite, and cement on preventing shrinkage of clay mixture. PVC material circular plate with smooth base was used for this test. The specimen was placed on the balance to measure the mass change corresponding to water evaporation,

and automatic digital camera equipment was installed to collect images with regular time interval. The volumetric strain can be calculated using following formula.

$$\epsilon_{vol.}(\%) = \left(1 - \frac{V_{final}}{V_{initial}}\right) \times 100 \quad (6)$$

Where,  $\epsilon_{vol.}$  = volumetric strain (%)

$V_{final}$  = final volume of specimen

$V_{initial}$  = initial volume of specimen

### **Direct shear test**

In the direct shear test, horizontal stress was applied until failure to figure out the shear strength of soil specimen under controlled vertical stress. This test was conducted following the standard procedure of ASTM D3080. The aim of this experiment is to evaluate and compare the shear strength of natural soil and soil-clay mixture structure. Figure III-11 shows the experimental setup of the direct shear test. The horizontal stress and the vertical stress can be calculated using these formulae.

$$\sigma_h = \frac{F_h}{A} \quad (7)$$

$$\sigma_v = \frac{F_v}{A} \quad (8)$$

Where,  $\sigma_h$  = horizontal stress

$\sigma_v$  = vertical stress

$F_h$  = horizontal force

$F_v$  = vertical force

$A$  = cross-sectional area of the specimen



**Figure III-11 Direct shear test apparatus**

### **Permeability test**

Permeability test was conducted to evaluate the hydraulic conductivity evolution under drying-wetting cycle and effect of clay mixture as filling material. There were two types of laboratory permeability test applied in this research; (1) the constant head test and (2) the falling head test. These tests were conducted following the standard procedure of ASTM D2434 and ASTM D5084. The hydraulic conductivity can be estimated using this formula in constant head test.

$$k = \frac{QL}{Ath} \quad (9)$$

Where, k = permeability (cm/sec)

Q = total discharge volume (cm<sup>3</sup>)

L = flow length (cm)

A = cross-sectional area of the soil container (cm<sup>2</sup>)

t = elapsed time (sec)

h = the loss of total head (cm)

For the falling head test, the calculation of the permeability is as follows.

$$k = \frac{aL}{At} \ln \left( \frac{h_0}{h_1} \right) \quad (10)$$

Where, a = cross-sectional area of pipet (cm<sup>2</sup>)

h<sub>0</sub> = initial head (cm)

h<sub>1</sub> = final head (cm)

## CHAPTER IV

### EVALUATION OF MECHANICAL AND GEOPHYSICAL PROPERTIES OF CLAY MIXTURE

#### **Introduction**

The aim of this chapter is to determine the profile for the clay mixture as remedial solution for desiccation cracking area. In the previous research, the injection technique was suggested with the clay mixture including graphite and cement. Graphite is an electric conductive material allowing to trace the clay mixture profile using Electrical Resistivity Tomography (ERT) technique. The clay-graphite mixture was washed out during the saturation of the soil, so cement application was suggested to solve this problem. However, due to relatively high water content for workability of the mixture, several cracks were generated at the surface of injected area, and this obstacle should be modified.

In this research, to develop the performance of clay mixture, some additional components were investigated using several mechanical tests and geophysical test. Biopolymers are recently spotlighted for soil improvement and ground fertilization in the aspect of soil environment. Also, superplasticizer is widely applied to enhance the workability of the cement material. These materials were applied as additives for the clay mixture and tested in many directions. The final goal is the suggestion of the clay mixture with good workability under relatively low water content and minimize the crack generation and propagation which weaken the strength of soil-mixture structure.



## **Mechanical test: Unconfined compression test**

### *Sample preparation and test procedure*

The unconfined compression test was conducted to investigate the axial strength and peak strain for various combination of clay mixture components. The specimens were prepared using PVC tubes, they were chosen for this research because they are easier to test in numerous mixing cases in terms of specimen preparation and test performance. The clay mixture was placed into a cylindrical mold and air dried at room temperature (22.7°C), forming a firm clay mixture. 17 specimens were prepared with various combination of mixture components. The main components are EPK kaolinite, graphite, and cement, and the additives are biopolymers ( $\beta$ -glucan, Xanthan gum) and superplasticizers. Firstly, the main components were dry-mixed with specified combination following test plan. After mixing of main components, the additives were added with proportion of dry mass of the main components. The water content of specimens were standardized as 90%. The description of specimens are shown in table IV-1.

The unconfined compressive strength of cylindrical specimens was measured using a GEOTAC triaxial testing device. The compression speed was 1%/min. All geometric dimensions of each specimen were measured, as was mass, while the top and bottom surfaces were slightly trimmed using sandpaper to prevent an irregular stress distribution during the loading. In addition, in order to avoid stress localization, porous stone was placed above and below the samples during the experiment. All specimens were loaded until failure and the residual compressive strength was monitored.

**Table IV-1 Specimen description for unconfined compression test**

No.	Label	Main components (%)			Additives (%)			Mass (g)	d (mm)	h (mm)	V (cm <sup>3</sup> )	Y <sub>d</sub> (g/cm <sup>3</sup> )
		Kaolinite	Graphite	Cement	β-glucan	Xanthan gum	SP					
1	K1	100.00	0.00	0.00			1.50	78.91	35.50	75.00	74.23	1.06
2	G1	90.00	10.00	0.00			1.50	76.78	32.00	71.00	57.10	1.34
3	G2	80.00	20.00	0.00			1.50	89.72	35.88	69.19	69.96	1.28
4	G3	70.00	30.00	0.00			1.50	85.91	34.88	68.21	65.16	1.32
5	B1	70.00	30.00	0.00	0.50		1.50	88.52	35.05	70.58	68.10	1.30
6	B2	70.00	30.00	0.00	1.00		1.50	80.97	34.26	65.50	60.38	1.34
7	B3	70.00	30.00	0.00	1.50		1.50	87.65	35.37	68.85	67.65	1.30
8	X1	70.00	30.00	0.00		0.50	1.50	80.57	35.00	81.00	77.93	1.03
9	X2	70.00	30.00	0.00		1.00	1.50	88.65	34.92	70.91	67.89	1.31
10	X3	70.00	30.00	0.00		1.50	1.50	93.59	36.00	85.00	86.52	1.08
11	C1	60.00	30.00	10.00			1.50	83.02	33.52	63.00	55.58	1.49
12	C2	55.00	30.00	15.00			1.50	161.52	36.83	81.28	86.59	1.87
13	C3	50.00	30.00	20.00			1.50	146.66	31.75	62.23	49.27	2.98
14	CX1	60.00	30.00	10.00		0.30	1.50	138.25	33.53	60.96	53.82	2.57
15	CX2	60.00	30.00	10.00		0.70	1.50	153.92	33.53	71.12	62.79	2.45
16	CX3	60.00	30.00	10.00		1.50	1.50	155.14	31.75	67.31	53.29	2.91
17	N1	NATURAL SOIL						118.74	36.00	69.00	70.23	1.69

The elastic modulus was estimated by measuring the slope of straight line (in most cases, between 1-2% strain) of the stress-strain plot during compression.

### *Test results and discussions*

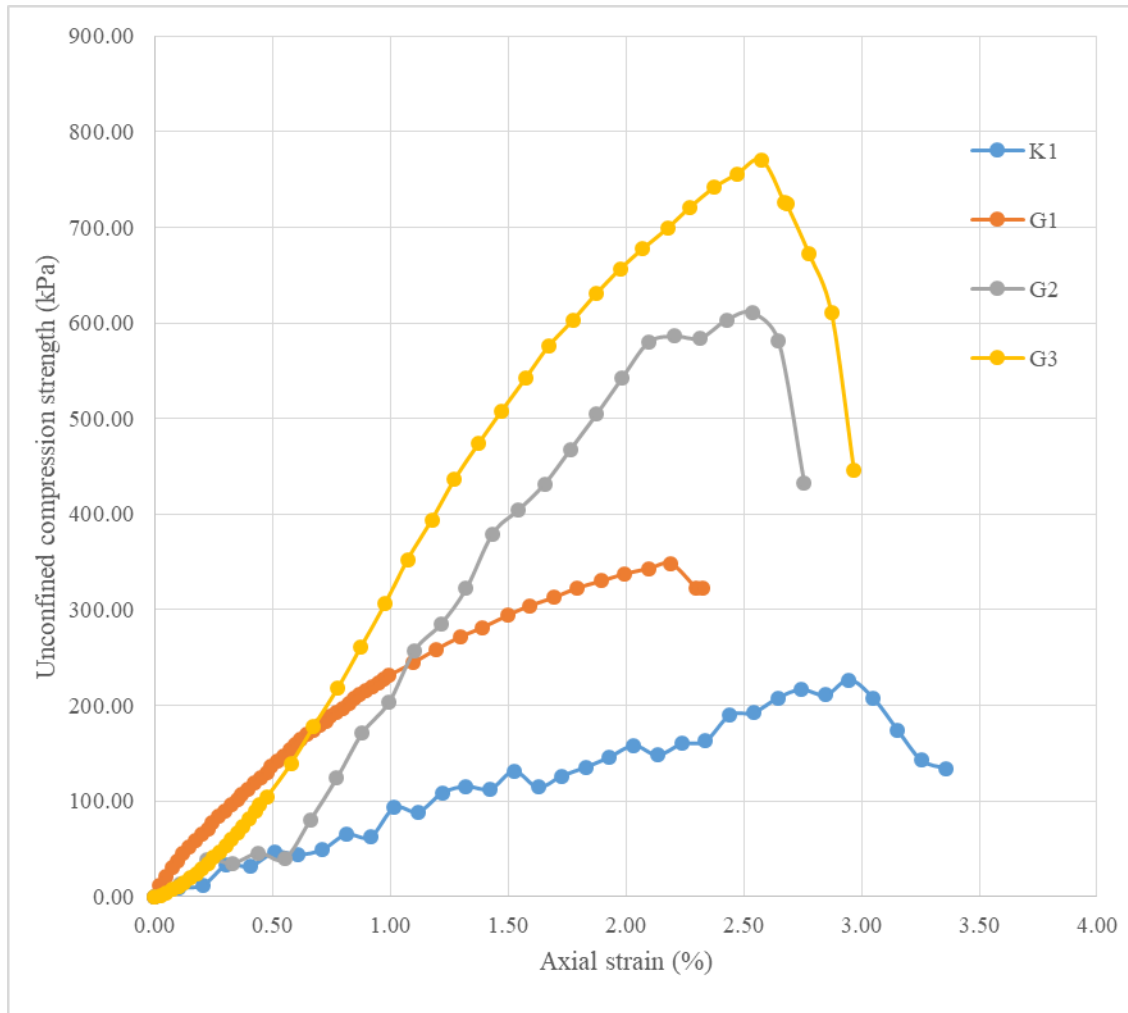
The profile of various clay mixtures at 28 days are shown in table IV-1. All specimens were completely dried, and thus effect of moisture on soil and clay mixture can be negligible in strengthening explanations. Test results is shown in table IV-2.

Generally, the clay mixture with various components shown in table IV-2 exhibited significant increases in compressive strength and elastic modulus. Figure IV-1 shows the test results of clay mixture with variation of graphite proportion. As shown in this figure, the unconfined compression strength and the Young's modulus were gradually increased with graphite proportion increment. Axial strength of clay mixture was approximately doubled with 10% increment of graphite proportion.

The compressive strength of the  $\beta$ -glucan polymer treated clay mixture was shown in figure IV-2. The main component of these specimens are clay (70%) and graphite (30%) and  $\beta$ -glucan is only applied as additive. As shown in this figure, the axial strength and elastic modulus of clay mixture were increased geometrically corresponding to the increment of  $\beta$ -glucan concentration. The effect of  $\beta$ -glucan biopolymer were insignificant when the concentration of polymer is less than 0.5%, but the uniaxial strength was increased drastically with the larger portion of polymers.

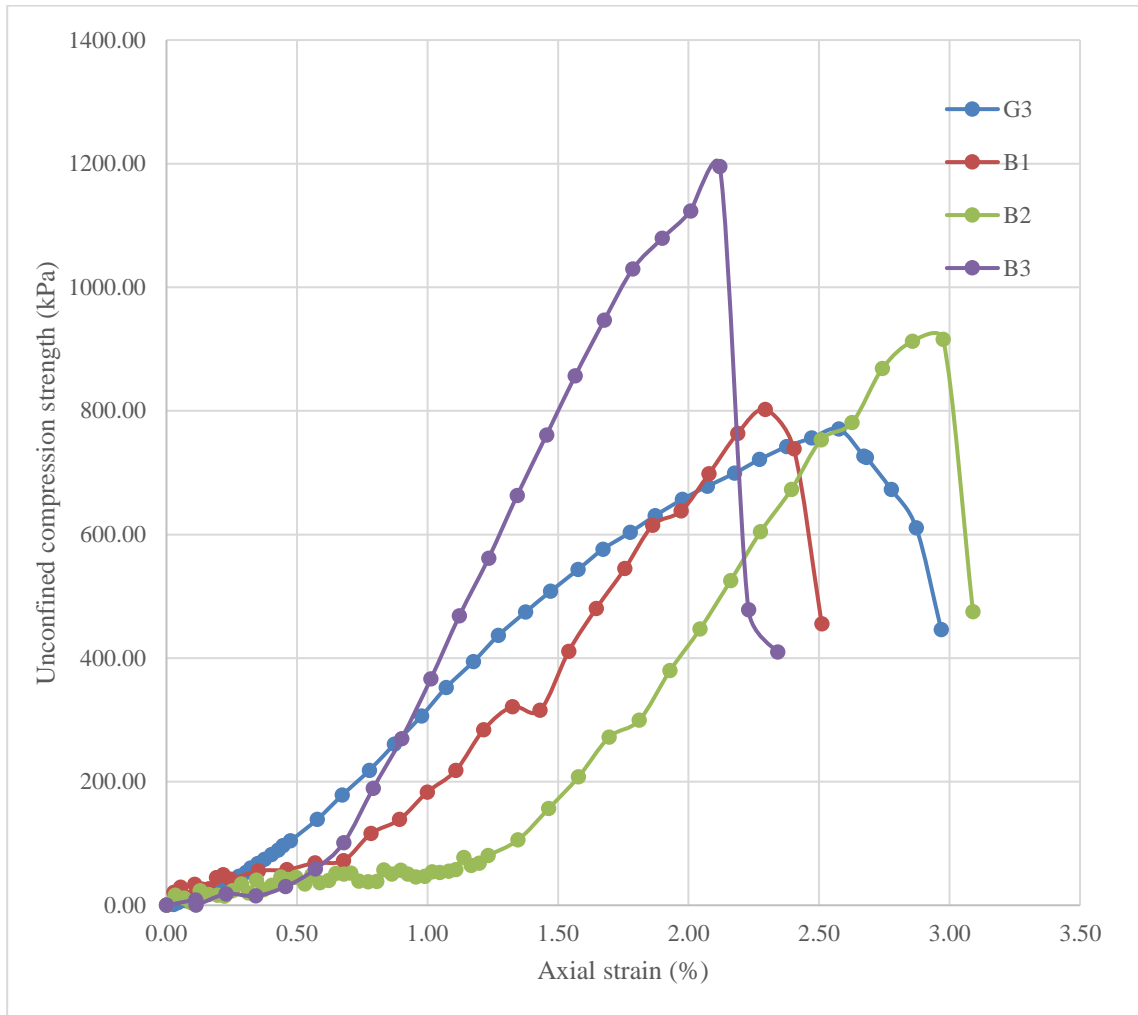
**Table IV-2 Unconfined compression test results**

<b>No.</b>	<b>Name</b>	<b>q<sub>uc</sub> (kPa)</b>	<b>ε<sub>peak</sub> (%)</b>	<b>E (MPa)</b>
1	K1	226.88	2.95	7.79
2	G1	348.27	2.19	36.00
3	G2	610.85	2.54	43.63
4	G3	770.65	2.58	51.11
5	B1	802.24	3.14	74.44
6	B2	915.48	2.98	86.36
7	B3	1195.12	2.12	84.55
8	X1	911.42	2.26	66.00
9	X2	941.84	2.26	77.27
10	X3	1477.13	7.89	25.56
11	C1	804.53	1.00	80.00
12	C2	1055.85	2.25	71.00
13	C3	2139.73	5.36	100.00
14	CX1	1839.20	6.55	902.00
15	CX2	2127.18	6.60	1200.00
16	CX3	4380.21	8.42	2655.00
17	N1	539.87	1.90	66.36



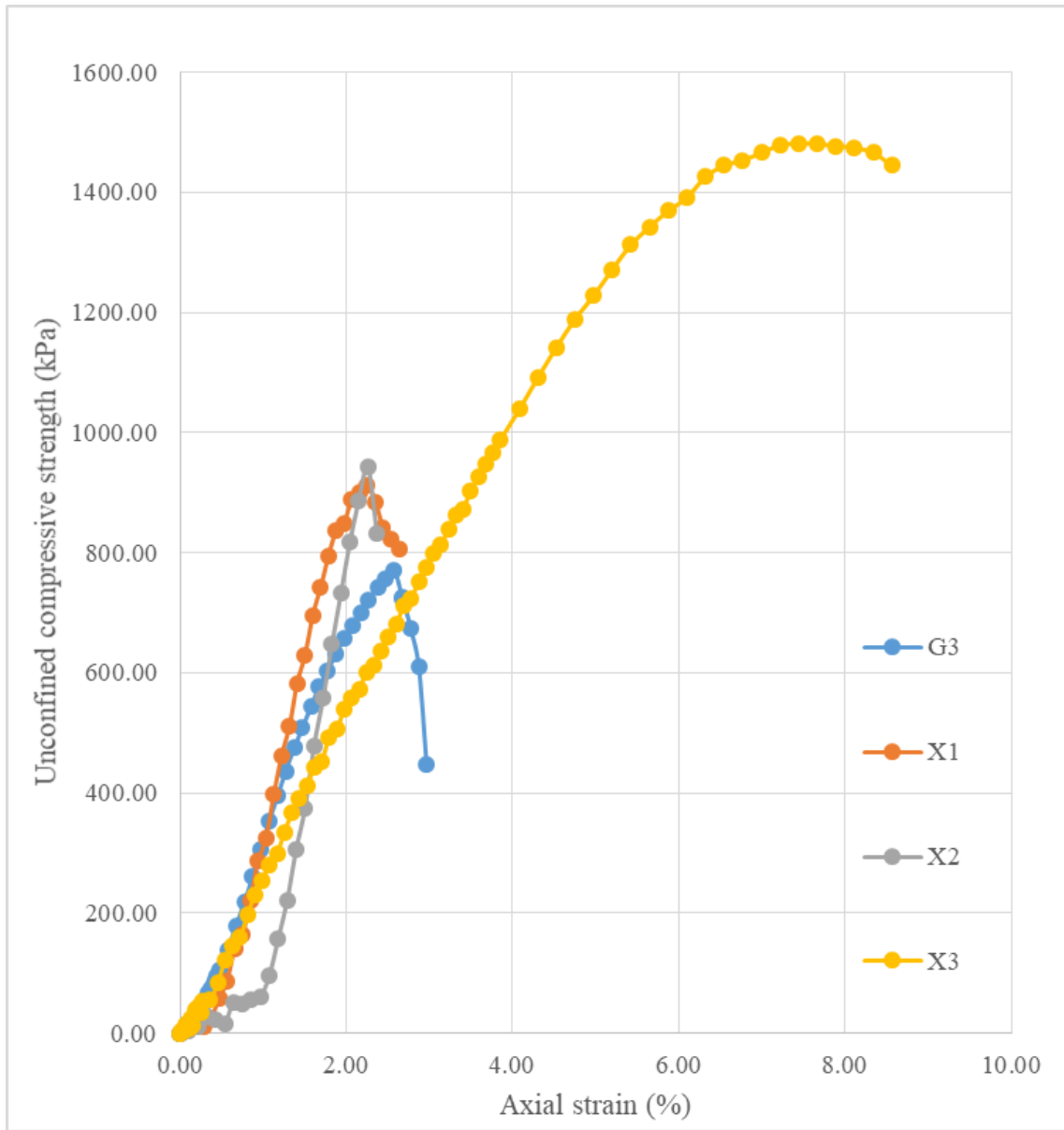
**Figure IV-1 Unconfined compression test results with variation of graphite proportion**

The portion of  $\beta$ -glucan biopolymer enhances the ionic bonding between the  $\beta$ -glucan polymer chains and clay mixture particles (Change and Cho, 2012).



**Figure IV-2 Unconfined compression test results with variation of beta-glucan proportion**

Xanthan gum treated clay mixture shown in figure IV-3 showed significant increases in compressive strength. The main component of these specimens are clay (70%) and graphite (30%) and xanthan gum is only applied as additive. Xanthan gum biopolymer enhances the inter-particle bonding of clay mixture exhibiting dramatically compressive strength improvement. The uniaxial strength of xanthan gum treated composites are relatively higher than  $\beta$ -glucan treated clay mixture.

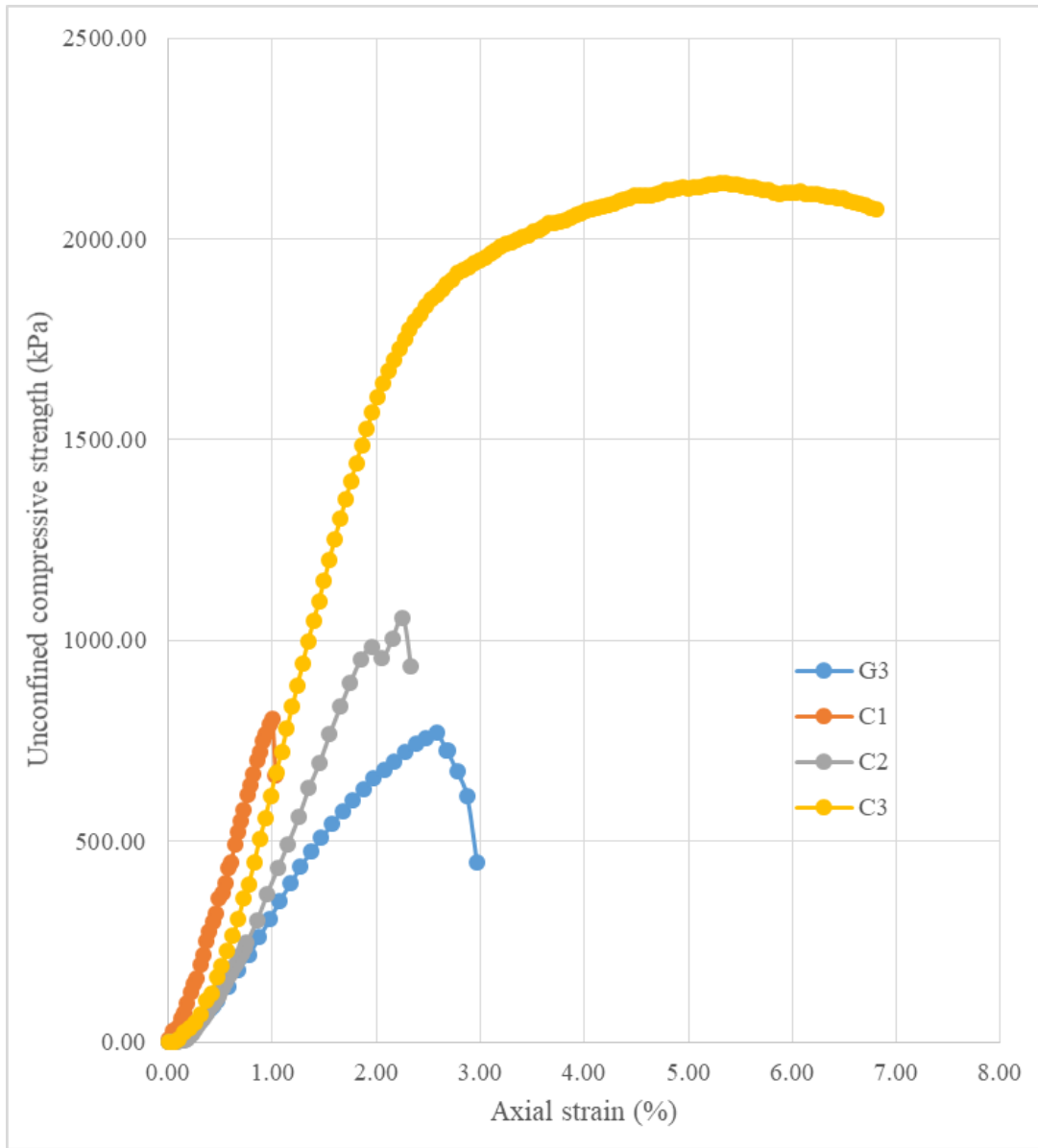


**Figure IV-3 Unconfined compression test results with variation of xanthan gum proportion**

The effect of cement is also experimented by variation of concentration. The graphite proportions are maintained as 30% and the quantity of EPK kaolinite is changed corresponding to increment of cement ratio. As expected, the increase of cement

proportion shows dramatic increment of unconfined compressive strength of clay mixture (Figure IV-4). Also, the elastic modulus is increased with proportion of cement in clay mixture. From the viewpoint of strength, the biopolymer ( $\beta$ -glucan and xanthan gum) treated clay mixture with 1.5% concentration has similar compressive strength value range comparing to the clay mixture with 15% of cement ratio.

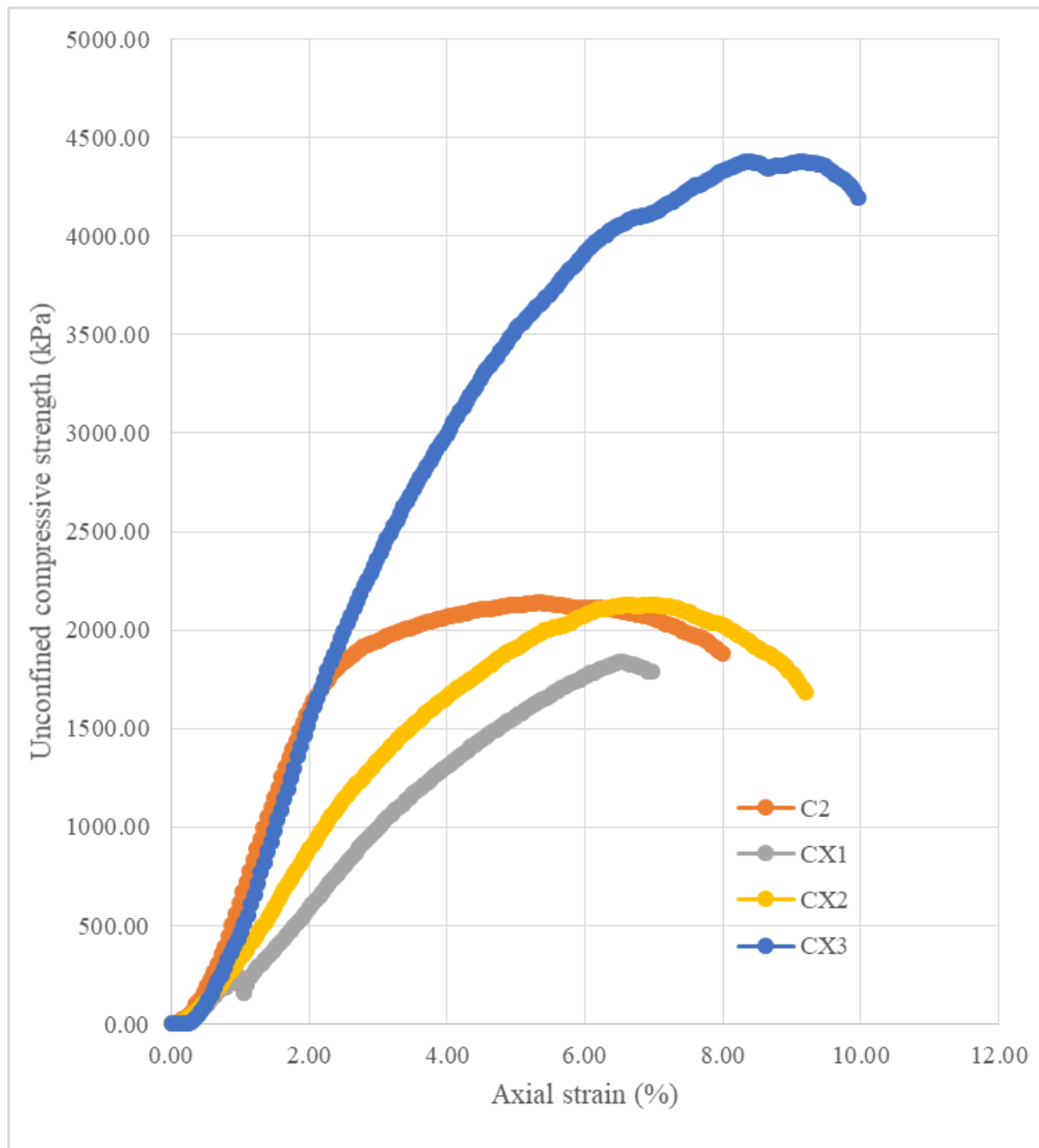




**Figure IV-4 Unconfined compression test results with variation of cement proportion**

In the previous research by Kim, the suggested clay mixture component was 50% of clay, 30% of graphite, and 20% of cement for filling material within defected soil area. Cement was added to prevent wash-out problem of clay mixture, but the proportion

was estimated as excessive for the mixture considering the strength and economical aspects. In this research, the combination of cement and xanthan gum biopolymer is also investigated to figure out the strength compensate effect of xanthan gum corresponding to decrement in the cement proportion. The clay mixture component ratio was maintained as 60%, 30%, and 10% for EPK kaolinite, graphite, and cement, respectively. Considering the workability of clay mixture with various xanthan gum concentration, 0.3%, 0.7%, and 1.5% of xanthan gum were applied for this investigation. Figure IV-5 shows the unconfined compression strength with axial strain of xanthan gum biopolymer treated clay mixture. The clay mixture with 20% of cement is also drawn in this figure for the comparison. As shown in this figure, the uniaxial strength and elastic modulus of Xanthan gum treated clay mixture is increased with Xanthan gum ratio. 0.7% of Xanthan gum treated mixture shows the similar value of compressive strength to 20% of cement mixture, but the elastic modulus was much smaller. The compressive strength was increased twice with Xanthan gum proportion as 1.5%. In the aspect of compressive strength, the Xanthan gum proportion can be less than 1.0% when the clay mixture is consisted with 10% of cement mixture.



**Figure IV-5 Unconfined compression test results with variation of xanthan gum and cement proportion**

## **Mechanical test: Flow table test**

### *Sample preparation and test procedure*

The flow table test was carried out to evaluate the workability of the clay mixture with various components and additives ratio. The target value of the flow is  $110 \pm 5\%$  which is corresponding to the flow value for mortar using at the construction site. In this experiment, the variation of superplasticizer, graphite, cement, and biopolymers are examined with various ratio profile. The clay mixture was prepared within the mixing bowl following the proportions and casted into the flow mold right after mixing. The flow table test was conducted immediately and the length of diameter was measured in four different directions. The average value was evaluated and the flow was calculated based on this value.

### *Test results and discussions*

The flow table test specimen profiles and results are shown in table IV-3. 29 cases of experiment was conducted with various combination of the components. Generally, the increase of the concentration of superplasticizer enhances the workability of the clay mixture especially interacting with cement, but the graphite and biopolymers disrupt the workability of the mixture.

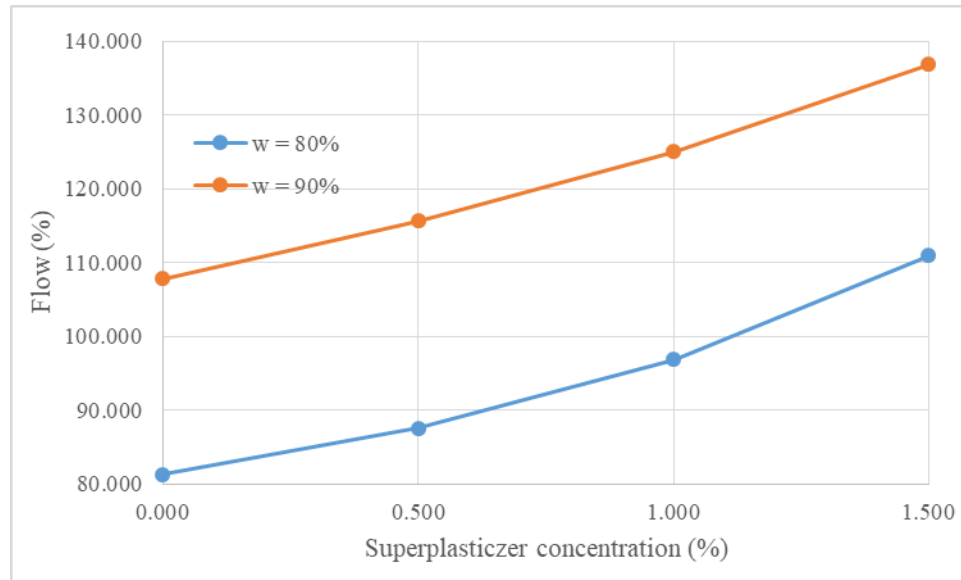
Figure IV-6 shows the flow of the clay mixture under different water contents with the variation of superplasticizer concentration. The clay mixture is consist of 80% of kaolinite and 20% of cement in this case. As shown in this figure, the superplasticizer enhances the workability of the clay mixture significantly.

**Table IV-3 Flow table test specimen profile and test results**

No.	Main components (%)			Additives (%)			W/C (%)	d <sub>1</sub> (in)	d <sub>2</sub> (in)	d <sub>3</sub> (in)	d <sub>4</sub> (in)	d <sub>avg</sub> (in)	flow (%)
	Kaolinite	Graphite	Cement	β-glucan	Xanthan-gum	SP							
1	80.00		20.00			0.00	80.00	7.250	7.250	7.250	7.250	7.250	81.250
2	80.00		20.00			0.50	80.00	7.500	7.500	7.500	7.500	7.500	87.500
3	80.00		20.00			1.00	80.00	7.750	7.750	8.000	8.000	7.875	96.875
4	80.00		20.00			1.50	80.00	8.750	8.250	8.250	8.500	8.438	110.938
5	80.00		20.00			0.00	90.00	8.750	8.250	8.250	8.000	8.313	107.813
6	80.00		20.00			0.50	90.00	8.750	8.500	8.500	8.750	8.625	115.625
7	80.00		20.00			1.00	90.00	9.000	8.750	9.000	9.250	9.000	125.000
8	80.00		20.00			1.50	90.00	9.500	9.450	9.500	9.450	9.475	136.875
9	50.00	30.00	20.00			0.00	90.00	6.750	6.750	6.750	6.750	6.750	68.750
10	50.00	30.00	20.00			0.50	90.00	7.375	7.375	7.250	7.375	7.344	83.594
11	50.00	30.00	20.00			1.00	90.00	7.500	7.500	7.500	7.750	7.563	89.063
12	50.00	30.00	20.00			1.50	90.00	8.750	8.750	8.750	8.750	8.750	118.750
13	70.00	30.00		1.50		0.00	90.00	5.500	5.500	5.500	5.500	5.500	37.500
14	70.00	30.00		1.50		0.50	90.00	5.750	5.750	5.750	6.000	5.813	45.313
15	70.00	30.00		1.50		1.00	90.00	6.250	6.250	6.250	6.250	6.250	56.250
16	70.00	30.00		1.50		1.50	90.00	7.000	7.000	6.750	6.750	6.875	71.875
17	70.00	30.00			1.50	0.00	90.00	4.125	4.000	4.000	4.125	4.063	1.563
18	70.00	30.00			1.50	0.50	90.00	4.250	4.250	4.250	4.250	4.250	6.250
19	70.00	30.00			1.50	1.00	90.00	4.250	4.375	4.375	4.250	4.313	7.813

20	70.00	30.00			1.50	1.50	90.00	4.500	4.500	4.500	4.625	4.531	13.281
21	60.00	30.00	10.00		0.00	0.00	90.00	7.000	7.250	7.250	7.375	7.219	80.469
22	60.00	30.00	10.00		0.00	0.50	90.00	7.500	7.500	7.500	7.250	7.438	85.938
23	60.00	30.00	10.00		0.00	1.00	90.00	8.250	8.500	8.500	8.500	8.438	110.938
24	60.00	30.00	10.00		0.00	1.50	90.00	9.000	9.250	9.250	9.250	9.188	129.688
25	60.00	30.00	10.00		0.10	1.50	90.00	9.000	9.000	8.875	8.875	8.938	123.438
26	60.00	30.00	10.00		0.30	1.50	90.00	8.250	8.250	8.250	8.250	8.500	112.500
27	60.00	30.00	10.00		0.50	1.50	90.00	7.250	7.250	7.250	7.250	7.250	81.250
28	60.00	30.00	10.00		0.70	1.50	90.00	6.500	6.500	6.500	6.500	6.500	62.500
29	60.00	30.00	10.00		0.90	1.50	90.00	6.250	6.500	6.250	6.125	6.281	57.031

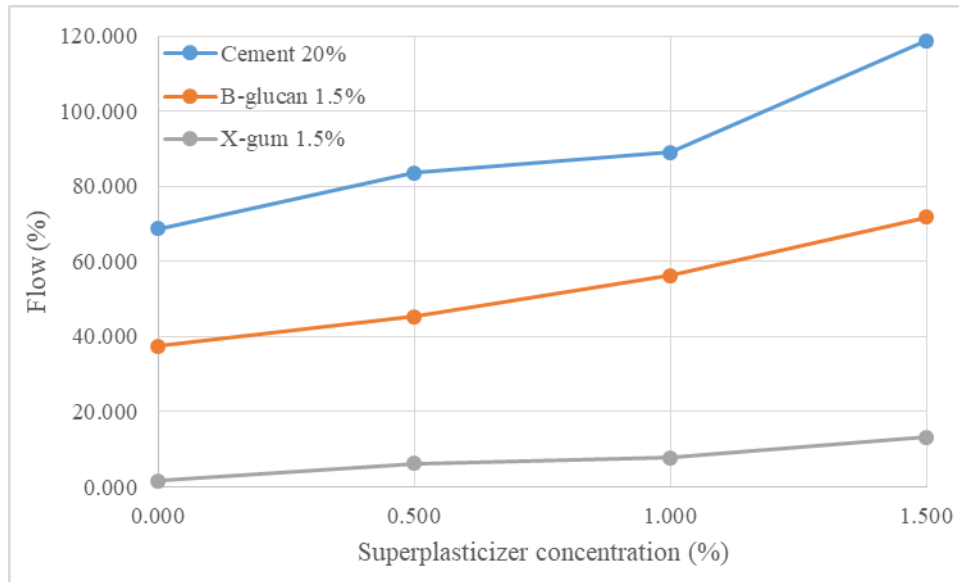
The clay mixture with water content of 80% reaches to the flow as 110% with 1.5% of superplasticizer and it corresponds to the mixture with 90% of water contents.



**Figure IV-6 Flow of the clay mixture with superplasticizer concentration (%)**

Figure IV-7 shows the flow of the clay mixture with various components profile. In this case, every specimen contains 30% of graphite component and cement is not applied to the mixture with biopolymers ( $\beta$ -glucan and xanthan gum). As shown in this figure, the workability of the clay mixture was increased with superplasticizer in general, but it was not effective enough to biopolymers, especially xanthan gum. Xanthan gum is sticky material with highly bonding effect, so it doesn't work properly with superplasticizer. The workability of the cement mixture is much higher than that of biopolymers and it implies that cement is essential component in the aspect of the workability of the clay mixture. The workability is connected to penetration ability of

the filling material directly, so some amount of cement proportion is essential for the mixture.

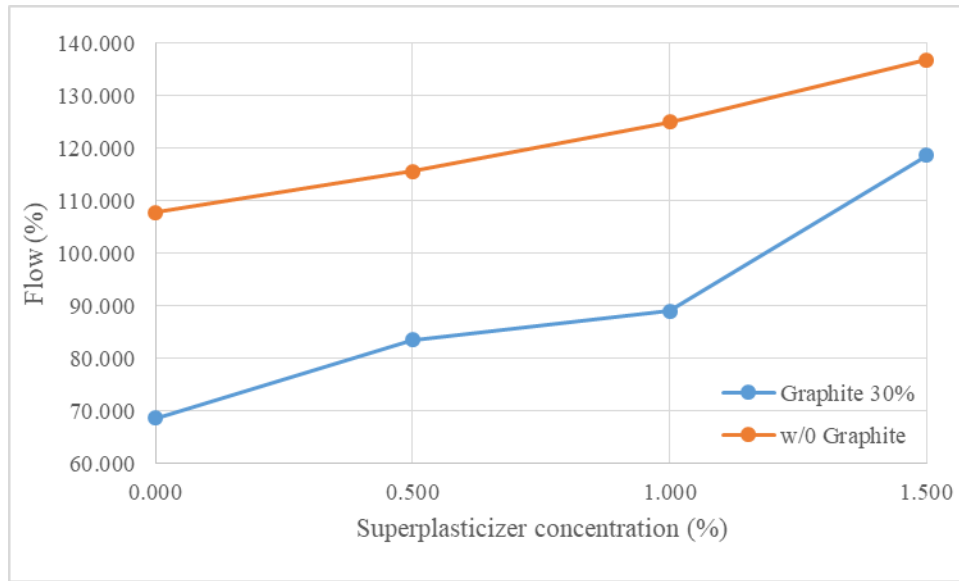


**Figure IV-7 Flow of the clay mixture with various components (cement and biopolymers)**

Graphite is also not interacting properly with superplasticizer. The increase of graphite proportion disrupts the workability of the clay mixture. Figure IV-8 shows that the workability of the clay mixture can be undermined with graphite proportion. The amount of impediment is not noticeable as much as biopolymers, but it is quite disturbing at the viewpoint of fluidity.

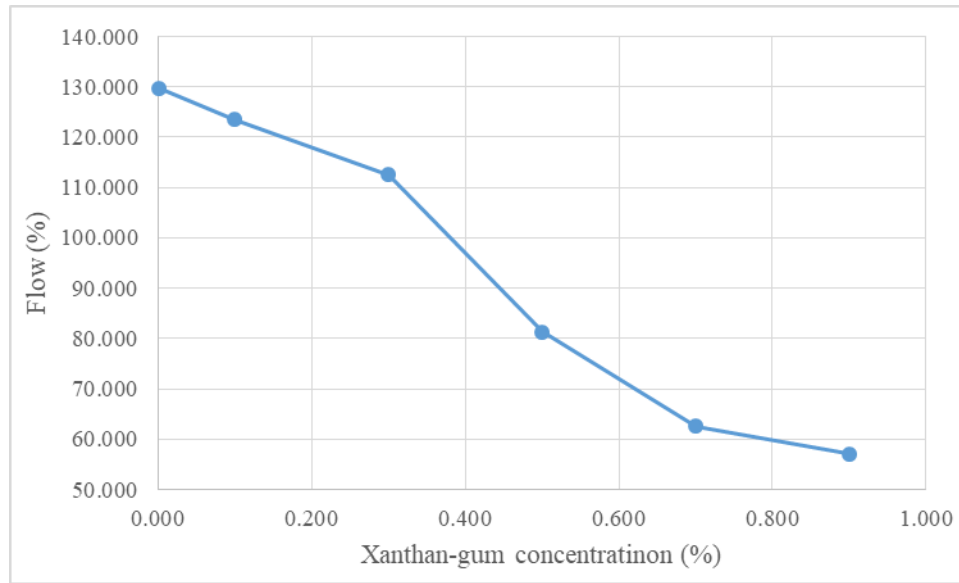
In the unconfined compression test, cement proportion was decreased to 10% with addition of xanthan gum biopolymers. The 20% of cement in the previous research is quite excessive value in the aspect of workability and economy, also the general range of cement proportion in soil-cement or mortar is approximately 10%.





**Figure IV-8 Flow of the clay with graphite composition**

Thus, the portion of cement is modified as 10% and several ratio of xanthan gum biopolymers applied to the clay mixture to figure out the appropriate portion in the aspect of the workability of the clay mixture. Figure IV-9 shows the flow evolution with xanthan gum concentration. As shown in this figure, the workability of xanthan gum mixture was decreased with increment of biopolymer proportion, this trend was accelerated passing the point of inflection at 0.3%. The workability of the clay mixture with 0.3% of xanthan gum is 112.5% which is in the range of target value. Thus, the clay mixture profile is determined with 60% of EPK Kaolinite, 30% of graphite, and 10% cement with 0.3% Xanthan gum biopolymer and 1.5% superplasticizer as additives.



**Figure IV-9 Flow of the clay mixture with xanthan gum proportion**

### **Mechanical test: Free shrinkage test**

#### *Sample preparation and test procedure*

Free shrinkage test is quantification of volumetric strain with simple procedure. In this research, several specimens were prepared to compare the shrinkage characteristics with different combination of the clay mixture. PVC circular plate was used for specimen drying, and the diameter of the plate is 10.6cm and the depth is 2cm. The inner surface of the plate was coated with Vaseline to allow the specimen shrink freely. The initial water content of all specimens were 90%. The mass of specimen was monitored to check the mass change corresponding to water content decrement until completely dried.

### *Test results and discussions*

Table IV-4 shows the description of specimens and the results of the shrinkage tests. As shown in table IV-4, the increase of cement proportion reduces the shrinkage of the clay mixture. Also, graphite proportion can diminish the volumetric strain.

Biopolymers are slightly effective on prevent the volumetric shrinkage, but this effect is not noticeable comparing to cement and graphite proportion. B-glucan biopolymer is more effective than xanthan gum on reducing of volumetric strain.

**Table IV-4 Free shrinkage test specimen profile and test results**

No.	Main components (%)			Additives (%)			d <sub>1</sub> (cm)	d <sub>2</sub> (cm)	d <sub>3</sub> (cm)	d <sub>4</sub> (cm)	d <sub>avg</sub> (in)	h (cm)	m (kg)	V (cm <sup>3</sup> )	e <sub>vol</sub> (%)
	Kaolinite	Graphite	Cement	$\beta$ -glucan	Xantan-gum	SP									
<b>1-1</b>	90.00		10.00				8.80	8.80	8.80	8.80	8.80	1.60	0.14	97.31	44.86
<b>1-2</b>	90.00		10.00			1.50	8.80	8.70	8.70	8.70	8.73	1.50	0.14	89.68	49.19
<b>1-3</b>	90.00		10.00	1.00			8.70	8.70	8.70	8.70	8.70	1.60	0.14	95.11	46.11
<b>1-4</b>	90.00		10.00	1.00		1.50	8.80	8.80	8.80	8.80	8.80	1.60	0.13	97.31	44.86
<b>2-1</b>	80.00		20.00				9.10	9.10	9.10	9.10	9.10	1.70	0.14	110.57	37.35
<b>2-2</b>	80.00		20.00			1.50	9.10	9.10	9.10	9.10	9.10	1.70	0.15	110.57	37.35
<b>2-3</b>	80.00		20.00	1.00			9.10	9.10	9.10	9.10	9.10	1.80	0.13	117.07	33.67
<b>2-4</b>	80.00		20.00	1.00		1.50	9.15	9.15	9.10	9.10	9.13	1.70	0.15	111.17	37.01
<b>3-1</b>	60.00	30.00	10.00				8.90	8.90	8.90	8.90	8.90	1.70	0.13	105.76	40.08
<b>3-2</b>	60.00	30.00	10.00			1.50	9.00	9.00	9.00	9.00	9.00	1.60	0.13	101.79	42.33
<b>3-3</b>	60.00	30.00	10.00	1.00			9.00	9.00	9.00	9.00	9.00	1.70	0.14	108.15	38.72
<b>3-4</b>	60.00	30.00	10.00	1.00		1.50	9.10	9.10	9.10	9.10	9.10	1.75	0.13	113.82	35.51
<b>4-1</b>	50.00	30.00	20.00			1.50	9.70	9.70	9.60	9.70	9.68	1.80	0.22	132.33	25.02
<b>4-2</b>	70.00	30.00		1.50		1.50	9.00	9.00	9.00	9.00	9.00	1.70	0.22	108.15	38.72
<b>4-3</b>	70.00	30.00			1.50	1.50	9.00	9.00	9.00	9.00	9.00	1.60	0.21	101.79	42.33
<b>4-4</b>	70.00	30.00			0.00	1.50	8.80	8.70	8.70	8.70	8.73	1.40	0.19	83.70	52.57

## **Geophysical test: Four-electrode method**

### *Sample preparation and test procedure*

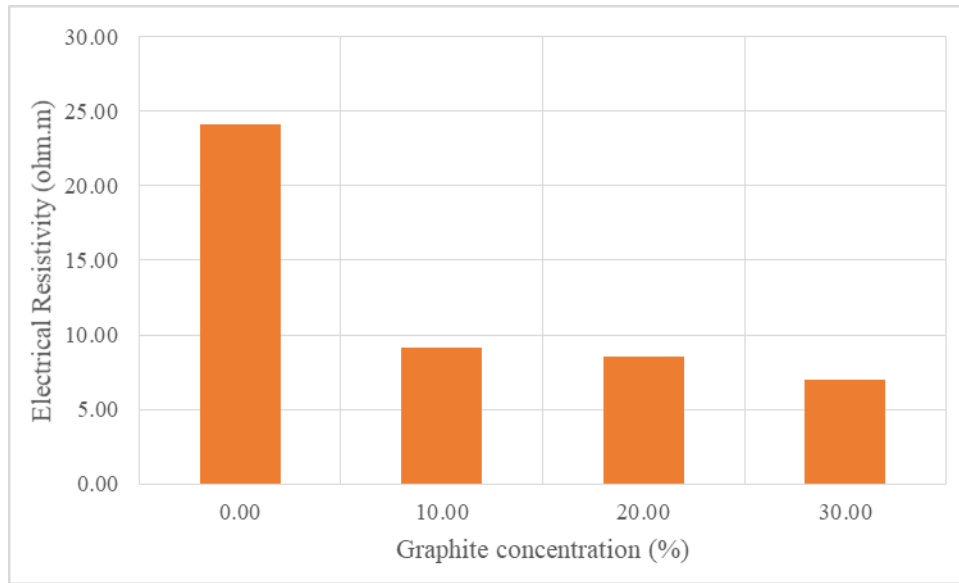
The electrical resistivity (or conductivity) measurement using four-electrode device was conducted to evaluate the electrical resistivity of the natural soil and the clay mixture with various components. Acrylic rectangular-shaped box was used for the specimen. To monitor the shrinkage and cracking behavior within frictional surfaces, any kind of agents were applied at the inner surface of the box. The initial water content of all specimen was 90%. The weight of the specimen was monitored with time corresponding to the loss of water until completely dried. Electrical resistivity was measured with regular time interval.

### *Test results and discussions*

Generally, as shown in this table, the initial value of the electrical resistivity is quite high because the clay mixture is at the slurry state with high water content value. The clay mixture is stabilized with decrease of water content, the electrical resistivity value reduces dramatically as conductive materials. This value is minimized until shrinkage limit. After the shrinkage limit, the void area is starting to be filled with air and it causes the increase of the electrical resistivity values. In this research, initial value, minimum value at the shrinkage limit, and the final value of electrical resistivity are selected to compare in table IV-5. As shown in this table, the electrical resistivity value of dried natural soil is 83 ohm  $\cdot$  m which is in the typical silty clay's ER value (20-200). Also, the electrical resistivity of dried EPK kaolinite is 24 ohm  $\cdot$  m.

**Table IV-5 Four-electrode test specimen profile and test results**

	Main components (%)			Additives (%)			EC (S/m)			ER (ohm.m)		
	Kaolinite	Graphite	Cement	beta-glucan	Xanthan-gum	SP	Initial	Maximum	Final	Initial	Minimum	Final
<b>1-C</b>	100.00	0.00					0.0871	0.7234	0.0415	11.4857	1.3823	24.1023
<b>1-1</b>	90.00	10.00					0.0853	16.1415	0.1093	11.7194	0.0620	9.1483
<b>1-2</b>	80.00	20.00					0.0858	73.0069	0.1177	11.6603	0.0137	8.4974
<b>1-3</b>	70.00	30.00	0.00	0.00	0.00		0.0908	663.1456	0.1423	11.0094	0.0015	7.0271
<b>1-4</b>	70.00	30.00		0.50			0.0855	82.8932	0.2523	11.6930	0.0121	3.9634
<b>1-5</b>	70.00	30.00		1.00			0.0819	165.7864	0.3191	12.2133	0.0060	3.1341
<b>1-6</b>	70.00	30.00		1.50			0.0940	361.7158	0.8168	10.6437	0.0028	1.2242
<b>2-C</b>	<b>NATURAL SOIL</b>						0.0310	0.6566	0.0120	32.2453	1.5230	83.0260
<b>2-1</b>	60.00	30.00	10.00				0.0565	318.3099	0.2030	17.7060	0.0031	4.9260
<b>2-2</b>	55.00	30.00	15.00				0.0658	612.1344	0.3681	15.1927	0.0016	2.7168
<b>2-3</b>	50.00	30.00	20.00				0.0661	1989.4368	0.6150	15.1173	0.0005	1.6261
<b>2-4</b>	70.00	30.00		0.50			0.0691	87.4478	0.7681	14.4639	0.0114	1.3019
<b>2-5</b>	70.00	30.00		1.00			0.0770	100.7310	0.8854	12.9936	0.0099	1.1295
<b>2-6</b>	70.00	30.00		1.50			0.0772	265.2582	1.0180	12.9559	0.0038	0.9823
<b>2-7</b>	70.00	30.00			0.50		0.0575	11.7198	0.3059	17.4044	0.0853	3.2685
<b>2-8</b>	70.00	30.00			1.00		0.0584	20.4045	0.4231	17.1280	0.0490	2.3637
<b>2-9</b>	70.00	30.00			1.50		0.0642	40.8090	0.5362	15.5823	0.0245	1.8648

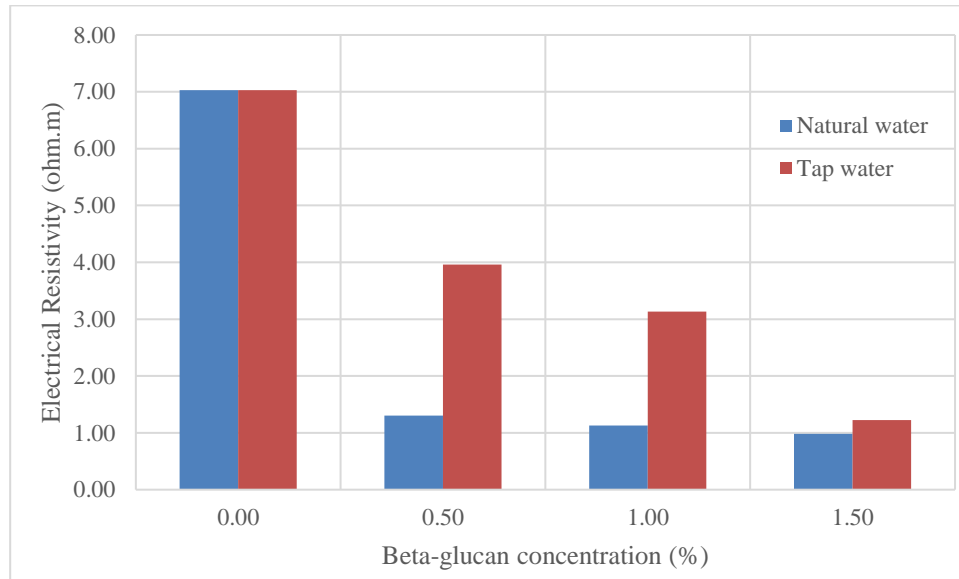


**Figure IV-10 Electrical resistivity with graphite concentration**

Figure IV-10 shows the electrical resistivity value with different proportion of graphite. EPK Kaolinite only mixture shows 24 ohm · m at the completely dried state, and this value decreased significantly with increase of graphite ratio. The amount of falling is reduced with increment of graphite proportion which means the existence of graphite is the critical influencing factor for the electrical conductivity.

Figure IV-11 shows the electrical resistivity variation with different  $\beta$ -glucan ratio under different type of water. In the field case, the water is generally collected from the natural resources. To compare the electrical resistivity value under different type of water, natural water was collected from the local lake and applied in this experiment. Due to the chemical properties of natural water, the electrical resistivity value of natural water applied mixture is much lower than that of tap water. The detailed ingredients are not tested for the natural water, but this results implies that relatively lower value of

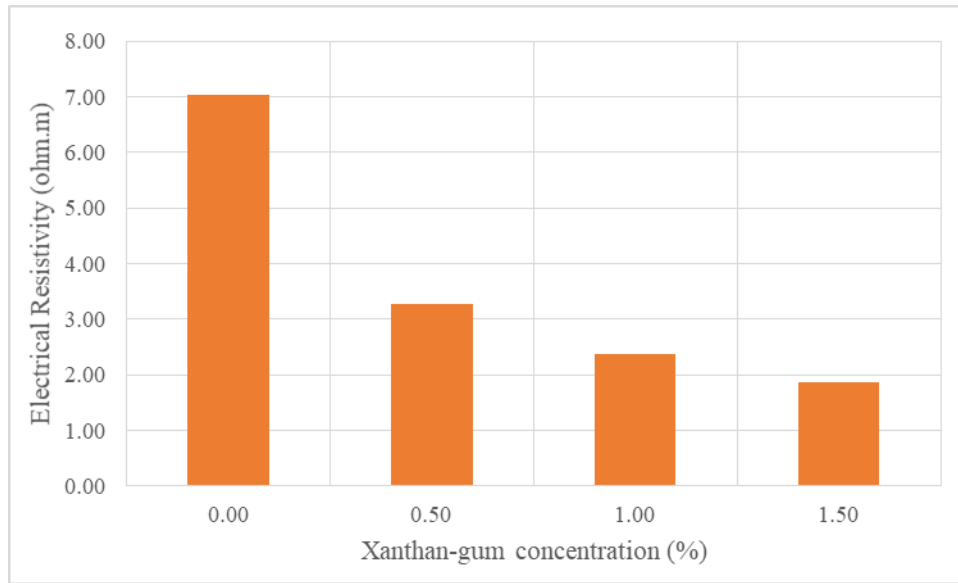
electrical resistivity is expected at the field test comparing to the laboratory based results. Also,  $\beta$ -glucan biopolymer is effective to reduce the electrical resistivity because of interaction between polymers and the cations of the clay mixture.



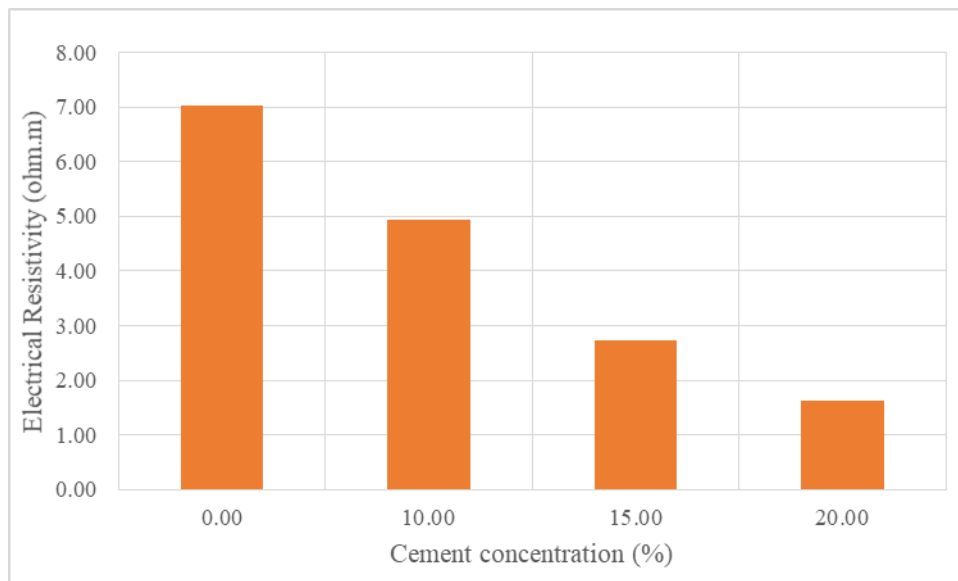
**Figure IV-11 Electrical resistivity with beta-glucan biopolymer proportion**

Xanthan gum biopolymer has also reducing effect of the electrical resistivity with chemical reaction within polymers and clay particles (Figure IV-12). In addition, the increase of cement proportion is contributing on decrease of the electrical resistivity (Figure IV-13). In the aspect of the electrical conductivity of the clay mixture, graphite is essential factor because of its electrical conductivity. In addition, cement and biopolymers are also decreasing the electrical resistivity of the clay mixture.





**Figure IV-12 Electrical resistivity with xanthan gum biopolymer proportion**



**Figure IV-13 Electrical resistivity with cement concentration**

## **Summary and conclusions**

In this study, a series of mechanical tests and geophysical test were conducted to evaluate the mechanical and geophysical properties of the clay mixture with various combination of components and additives. Unconfined compression test, flow table test, free shrinkage test, and four-electrode test were carried out, and the following results were obtained.

1. Unconfined compression test were performed to evaluate uniaxial strength, peak strain, and the elastic modulus of the clay mixture with various profile. All components and additives are effective to enhance the compressive strength of the clay mixture, especially xanthan gum biopolymer is highly efficient with small amount. Xanthan gum biopolymer can be applied as the compensating material with decrease in cement portion from 20% to 10%.
2. Flow table test were conducted to evaluate the workability of the clay mixture. Superplasticizer is chosen for the enhancement of the fluidity of the mixture and it is proved that this additive is the most effective interacting with cement. Thus, cement is required to apply the superplasticizer and maximize the workability. Biopolymers and graphite decreased the workability of the mixture, but it can be overcome by application of cement and superplasticizer. To satisfy the workability criteria, xanthan gum biopolymer proportion is suggested as 0.3% corresponding to 110% of flow.
3. Free shrinkage test was carried out to evaluate the volumetric strain with various component of the clay mixture. All of components and additives are effective on

reducing the volumetric shrinkage, but the cement is the most critical to minimize the shrinkage. Biopolymers are also working as shrinkage reducing agent, especially  $\beta$ -glucan is slightly better than xanthan gum in the aspect of volumetric shrinkage.

4. Four-electrode method was applied to evaluate the electrical resistivity (or conductivity) of the clay mixture with various component ratio. The electrical resistivity values changed with the state of the mixture related to water content. Initial, minimum, and the final values are analyzed from the different type of the clay mixtures. Graphite is the highly electrical conductive material and it is the most effective on reducing the electrical resistivity of the clay mixture. Cement and biopolymers are also efficient to enhance the electrical conductivity of the clay mixture with chemical interaction between polymers and clay particles, but this is not enough comparing to graphite. Thus, to trace the clay mixture within desiccation cracking area, graphite is the key factor with electrical conductivity.

CHAPTER V

DESICCATION CRACK MONITORING USING ELECTRICAL RESISTIVITY  
TOMOGRAPHY TECHNIQUE

**Introduction**

Electrical Resistivity Tomography (ERT) technique is a widely used geophysical application for the visualization of shallow subsurface area. Electrical resistivity equipment have been improved recently, so the quality and efficiency of complex investigation is developed. In addition, inversion program and computer techniques have been advanced on modelling of resistivity data (Jones et al., 2012).

In this research, Dipole-Dipole and Schlumberger arrays were compared for the three-dimensional investigation of the evolution of crack networks in clay subjected to drying. Polystyrene blocks were used to realize the discontinued area with high electrical resistivity. Two types of array method were applied for the clay with various depth profile of Styrofoam structures and the results were compared to determine the arrays for the ERT measurements of the desiccation crack networks within natural soil.

In addition, Electrical Resistivity Tomography (ERT) measurements were conducted for various condition of the natural soil subjected to drying. Database from the equipment was post-processed using RES3DINV program with inversion procedure and three-dimensional mapping was developed using VOXLER 3D program to stereoscopic visualization of desiccation crack network of the natural soil.

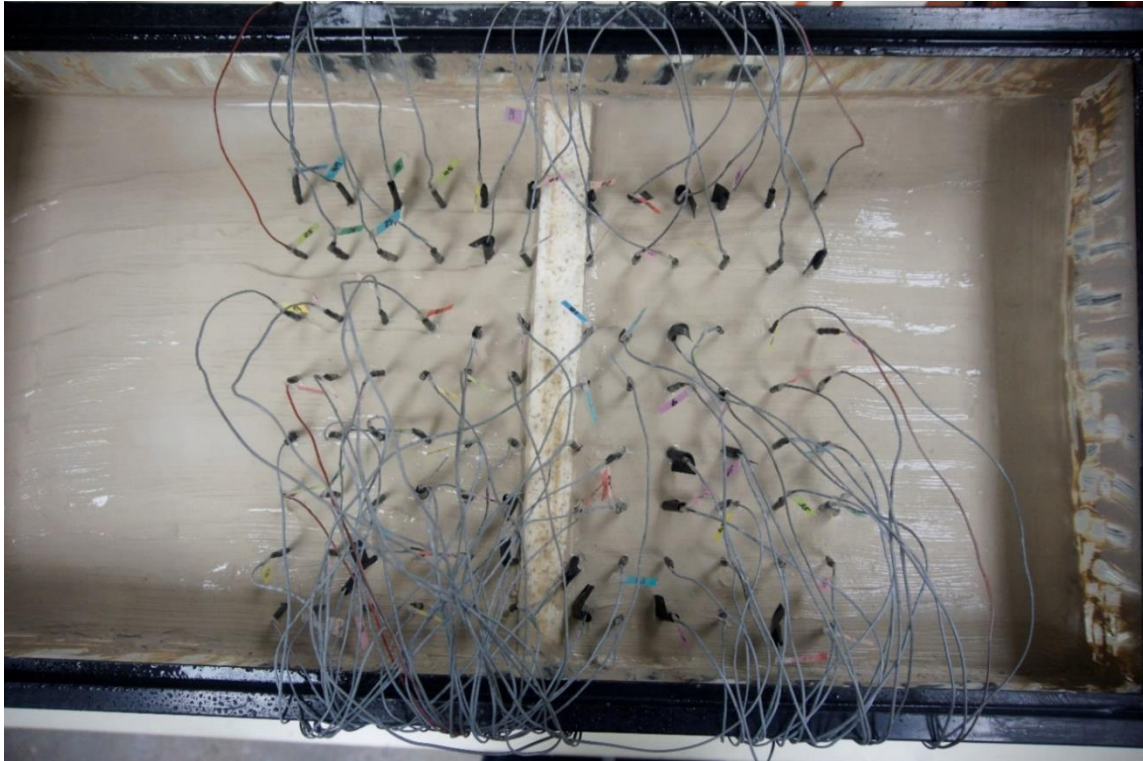
## **Preliminary ERT using Styrofoam blocks**

### *Test preparation and procedure*

Preliminary ERT measurements was conducted to verify the array methods; (1) Dipole-Dipole array and (2) Schlumberger array. Acrylic rectangular box with dimension of 60cm  $\times$  30cm  $\times$  36cm was prepared for the clay container. Three blocks of Styrofoam were used as high resistivity material to realize the discontinuity of clay network. The dimension of this block is 30cm  $\times$  10cm  $\times$  2.5cm. Figure V-1 shows the test setup of preliminary ERT measurements. Test preparation steps are as follows.

- (1) Three Styrofoam block were stacked up to create 30cm depth structure and located at the center of the container.
- (2) EPK kaolinite was mixed to reach the water content of 90%, and poured into acrylic container reaching to the depth of 30cm corresponding to the depth of styrofoam blocks structure.
- (3) For the measurement of ERT, the aluminum pins were connected with 96 electrodes and inserted at the surface of the clay. The formation of electrodes were 12 by 8 and the distance between each electrodes is 2cm and 3cm in horizontal and vertical direction, respectively.
- (4) ERT was measured using Dipole-Dipole array and Schlumberger array method.
- (5) The Styrofoam block at the bottom was removed from the container and the clay was reorganized. The depth of Styrofoam block was decreased to 20cm and the procedure (4) was repeated.

(6) The Styrofoam block at the middle was removed from the container, so the depth of block was 10cm. (4) procedure was repeated.

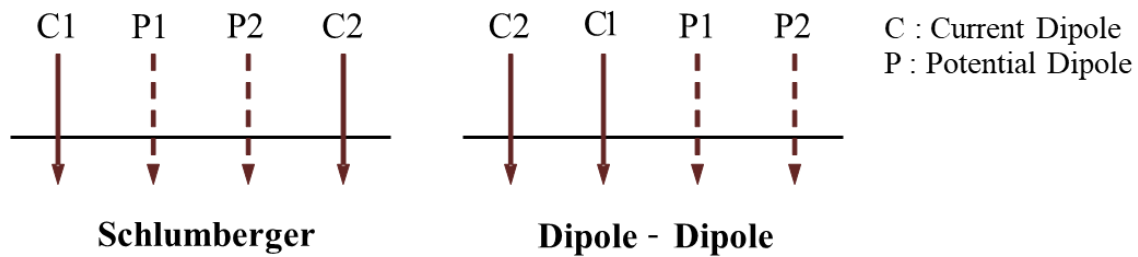


**Figure V-1 Electrode installation for the preliminary ERT measurements**

## *Array methods*

### **Dipole-Dipole array method**

In Dipole-Dipole array method, the two current and two potential electrodes making a pair of dipoles are located at opposite end of the array (Figure V-2). As with the Schlumberger array, increasing depths are measured by increasing the distance between dipoles. The highest sensitivity values are placed between the two current and potential dipoles, effecting in high sensitivity to horizontal difference in resistivity and subsequently lower sensitivities to vertical changes. In the aspect of three-dimensional exploration, the Dipole-Dipole array method has a much larger range outside the main line of measurement than any other array methods. This aspect can influence the accuracy of a two-dimensional exploration where non-aligned objects can result in interference. Nevertheless, it can cause Dipole-Dipole arrays more appropriate to three-dimensional surveys when using parallel lines of electrodes. The arrangement of the Dipole-Dipole array results in greater data coverage than the Schlumberger array over the same exploration, although the array also is affected from poor data coverage at the edges of the model in a three-dimensional grid. Another factor which should be considered in Dipole-Dipole array method is the requirement for good contact between the electrode and the soil. Dry soil would act to increase the contact resistance between electrode and soil, so resulting in larger uncertainties within the range of data.



**Figure V-2 Schlumberger and Dipole-Dipole array configurations**

### **Schlumberger array method**

Schlumberger arrays locate the current electrodes at opposite ends of the array with the potential electrodes placed in central (Figure V-2). Increasing depths are measured by expansion of the space between the current and potential electrodes by a factor of  $n$ . The arrangement generates an array which has the most value of sensitivity at the center of the array between the potential electrodes. At low values of  $n$ , the array method is most sensitive to changes in the horizontal plane, while when  $n$  increases the array is progressively sensitive to vertical changes (Barker, 1979). This allows the Schlumberger array method to be sensitive to both horizontal and vertical structures. Consideration of the three-dimensional sensitivity, the array displays a narrow range resulting in poor coverage of data outside the main survey line, leading the Schlumberger array to less proper for three-dimensional exploration when parallel lines are employed, particularly when the lines are not closely spaced. In addition, the Schlumberger array has unsatisfactory data coverage at the edges of the exploration when deliberating a three-dimensional grid and this problem is extended as greater depths are investigated.

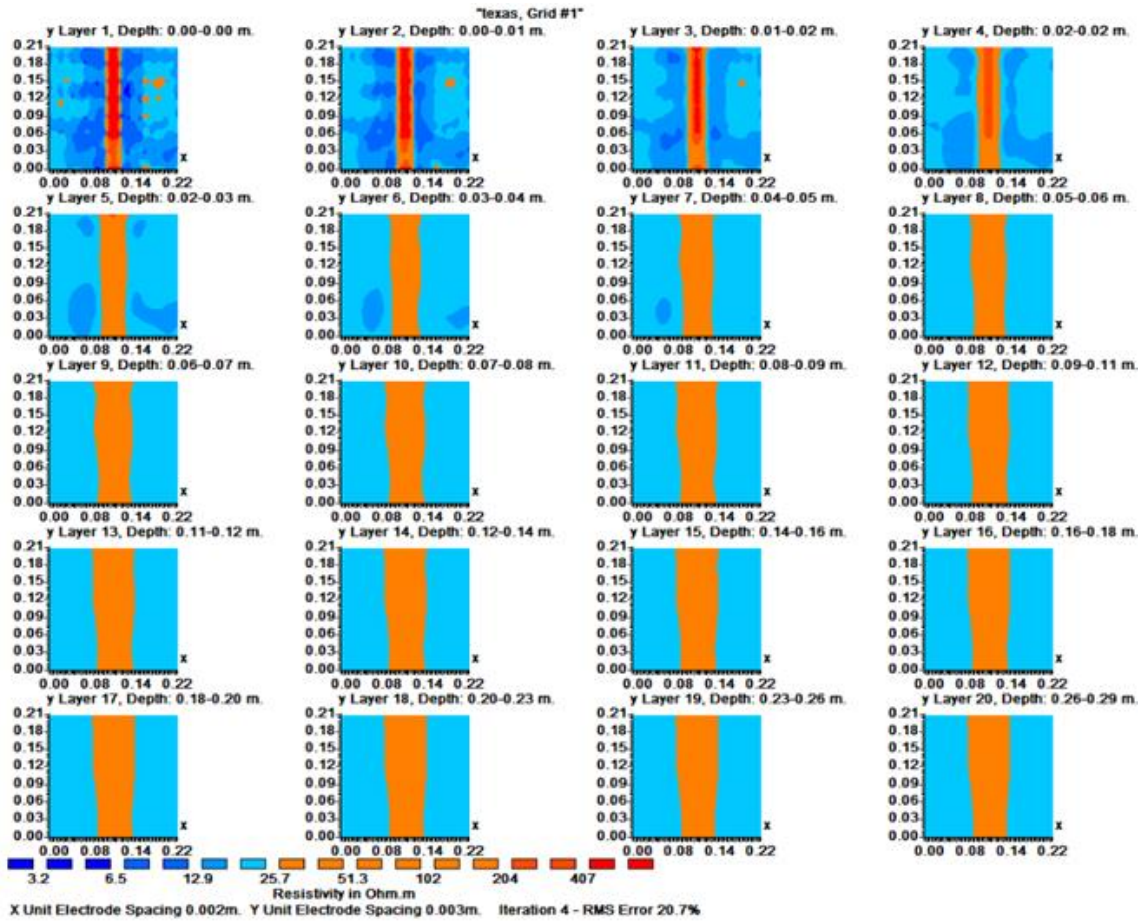


### *Test results and discussion*

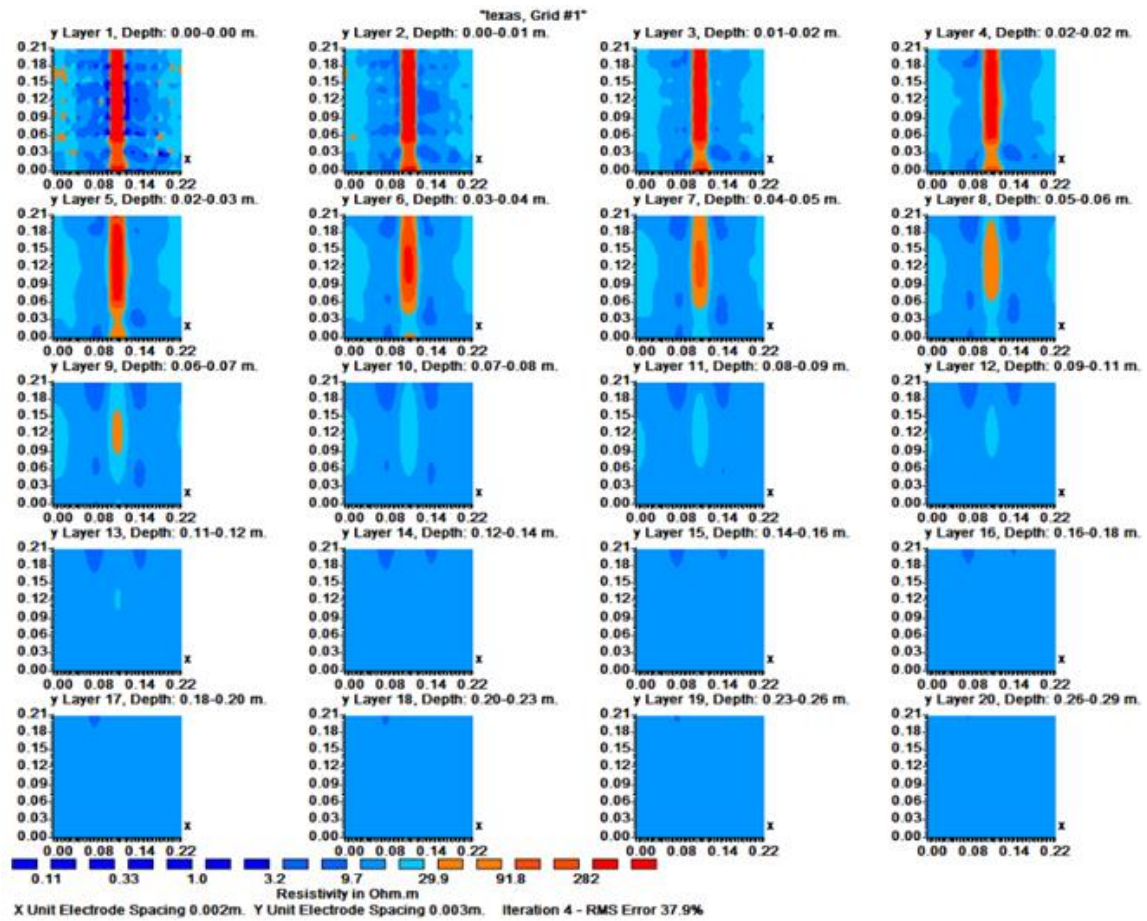
#### **Three Styrofoam blocks structure (depth = 30cm)**

The preliminary Electrical Resistivity Tomography (ERT) measurements was conducted for the clay container with three Styrofoam blocks. Total depth of block structure was 30cm. The measured data was processed using the inversion program RES3DINV. The electrical resistivity value of Styrofoam was explored as larger than  $250\text{ohm} \cdot \text{m}$  corresponding to the shape of the structure at the center. Figure V-3 shows two-dimensional plane view with depth for the Schlumberger array method. As shown in this figure, the Schlumberger array detected the shape of Styrofoam blocks structure accurately with entire depth, but the width of structure was overestimated with increase of depth to the bottom of the container.

Meanwhile, the Dipole-Dipole array was not effective to detect the vertical shape of the block structure with depth (Figure V-4). The entire depth of structure was 30cm in this case, but the Dipole-Dipole array discovered only 7cm from the surface. This array method shows the high sensitivity at the horizontal plane of surface which is detecting the detailed location of the electrodes with difference of resistivity value. There was not an overestimation of block structure's width.

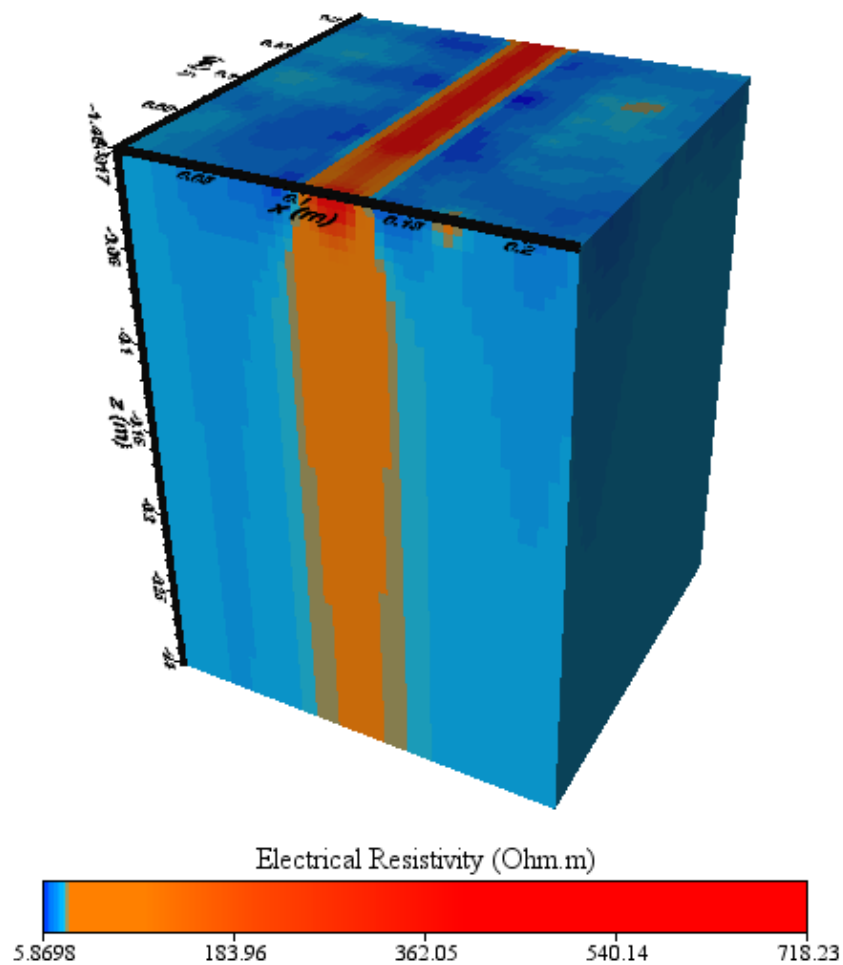


**Figure V-3 Schlumberger array results for the clay with three block structure (d=30cm)**



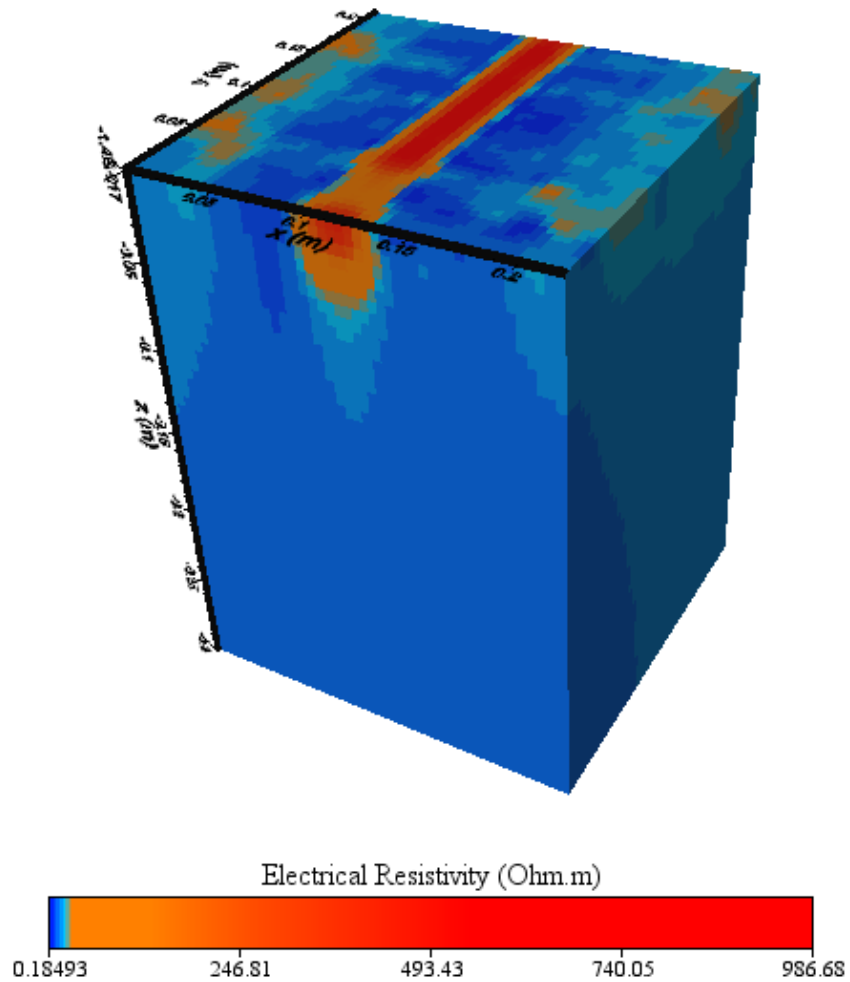
**Figure V-4 Dipole-Dipole array results for the clay with three block structure (d=30cm)**

The electrical resistivity results with x-, y-, and z- coordinates were extracted from the inversion program. Three-dimensional visualization was developed with this data using VOXLER 3D program. Entire contour color profile was matched with RES3DINV program, so color profile was identified for every results. Figure V-5 shows three-dimensional profile of Schlumberger array.



**Figure V-5 Stereoscopic view for the result of Schlumberger array (d=30cm)**

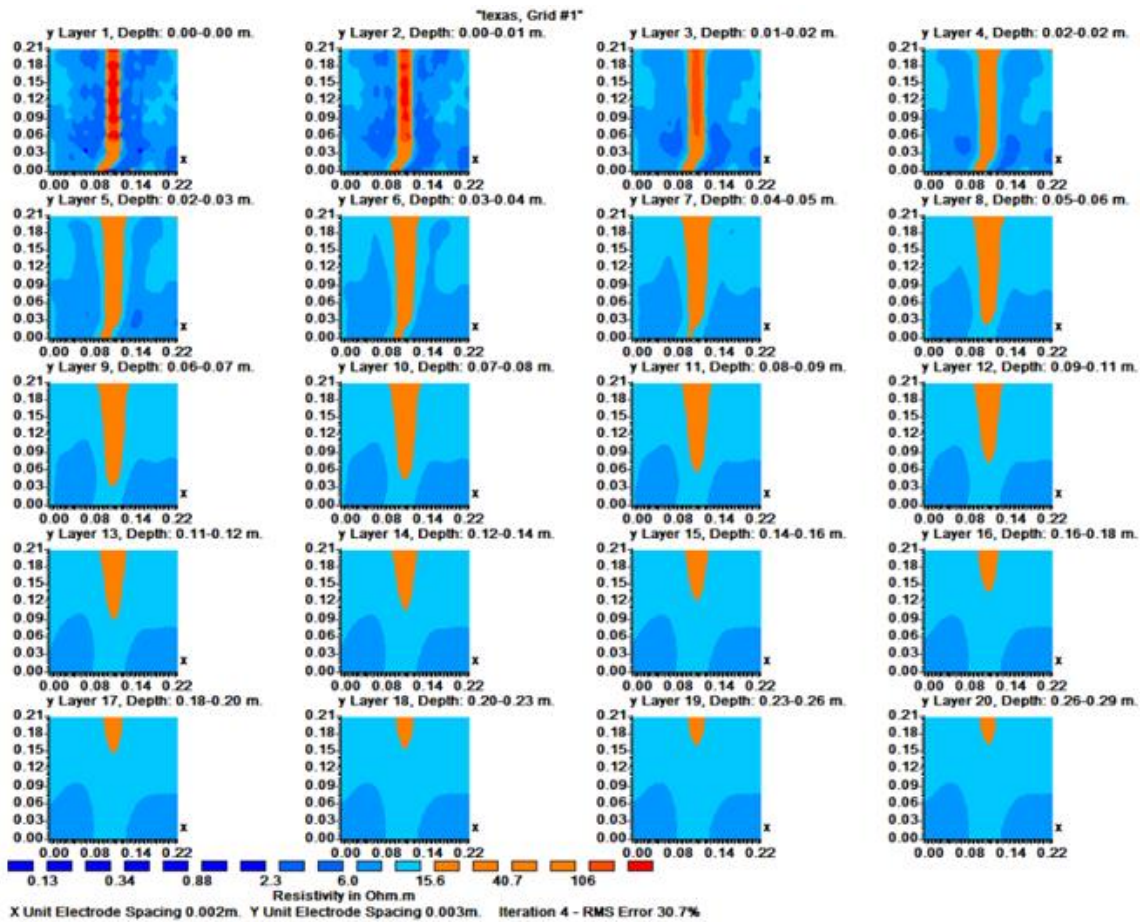
As shown in this figure, the entire grid of measurement is expressed as stereoscopic figure with three-dimensional profile. The Dipole-Dipole array method result was also visualized using same procedure (Figure V-6).



**Figure V-6 Stereoscopic view for the result of Dipole-Dipole array (d=30cm)**

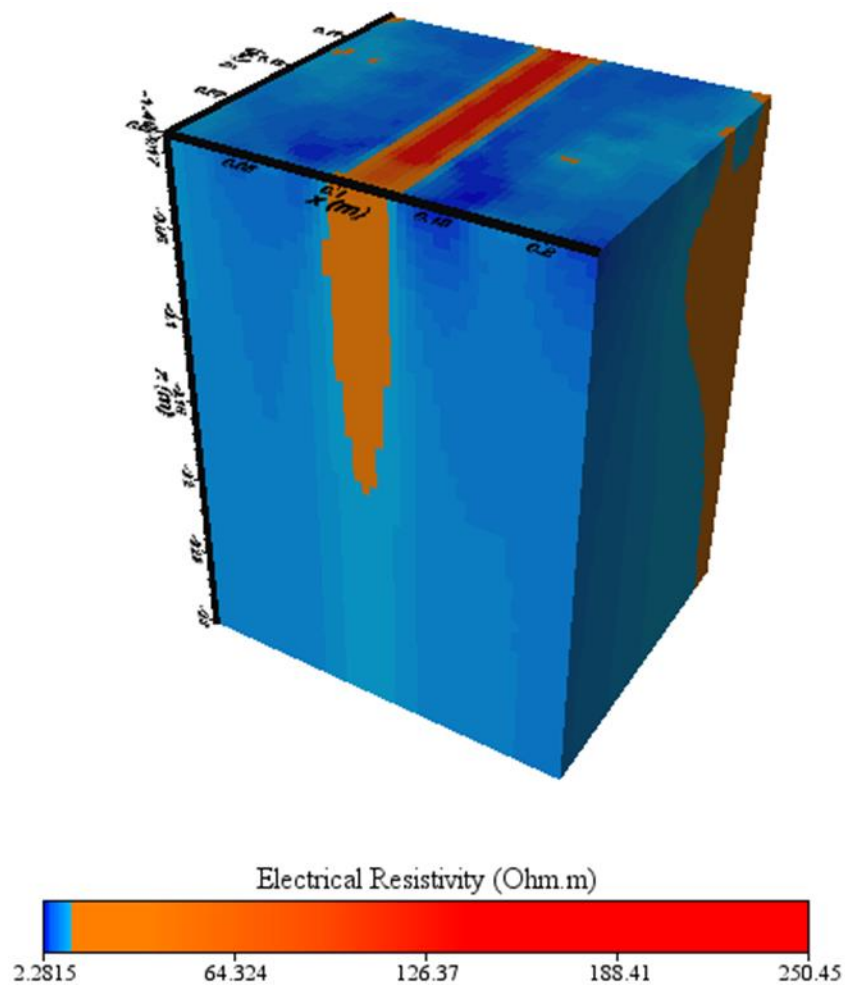
## Two Styrofoam blocks structure (depth = 20cm)

The Styrofoam block at the bottom was pulled out from the container and the clay was reorganized and stabilized for the further measurements. In this case, total depth of block structure was 20cm from the surface. Entire processing of data acquisition is as same as previous exploration. Figure V-7 shows two-dimensional plane view with depth for the Schlumberger array.



**Figure V-7 Schlumberger array results for the clay with two block structure (d=20cm)**

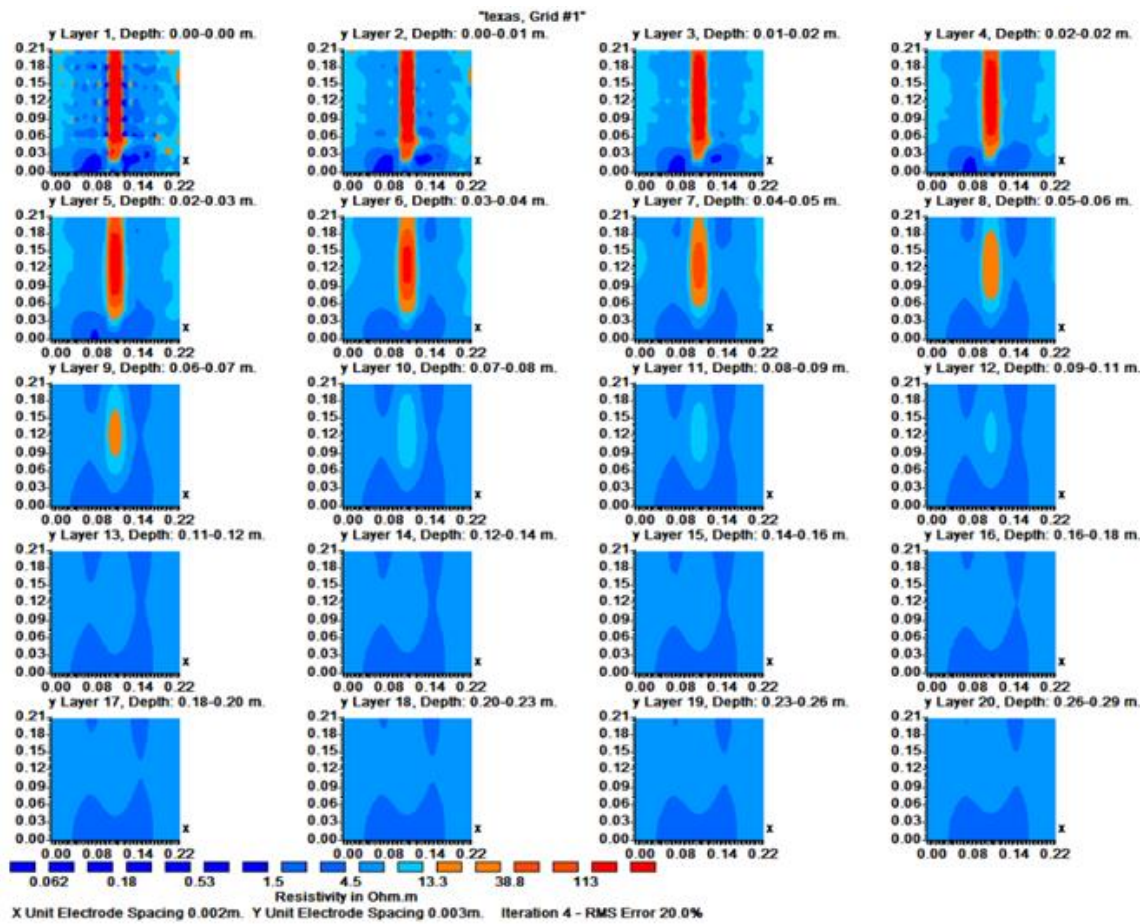
As shown in this figure, the Schlumberger array figured out the depth of Styrofoam blocks structure properly, but the shape of the block was not accurate. In this inversion program, the contour values was arbitrarily determined and it could not be edited. Thus, the problem was caused when the exact value should be selected for the visualization.



**Figure V-8 Stereoscopic view for the result of Schlumberger array (d=20cm)**



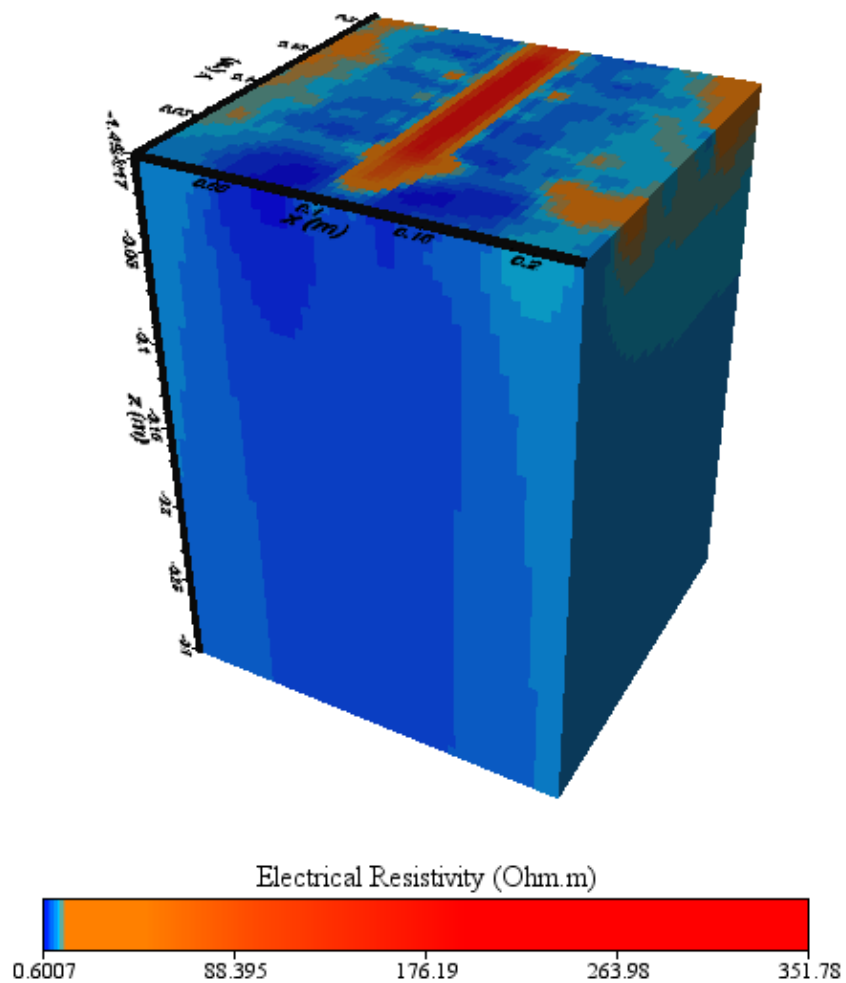
Whereas, using VOXLER 3D program, the contour values could be changed and standardized following the circumstances of resistivity profile. Figure V-8 shows three-dimensional figure processed by visualization program with modified contour value profile. As shown in this figure, the Schlumberger array detects the shape of Styrofoam block structure with both depth and width.



**Figure V-9 Dipole-Dipole array results for the clay with two block structure (d=20cm)**



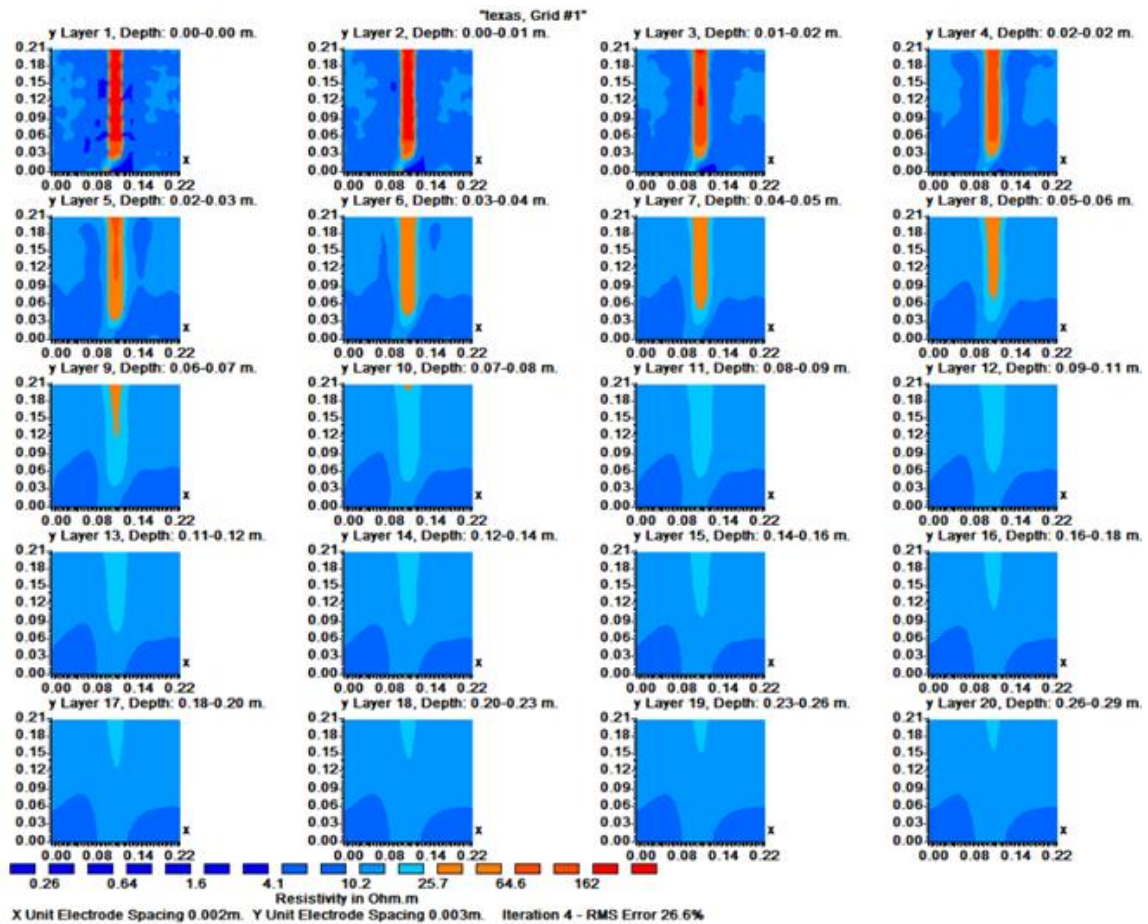
However, the Dipole-Dipole array could not detect the vertical depth of Styrofoam block structure with depth, either (Figure V-9). In the previous case, this array figured out only 7cm depth from the surface, and this value was also same within this case. The entire depth of block structure was decreased as 20cm, but the Dipole-Dipole array kept detecting maximum value of 7cm. Three-dimensional images was also processed (Figure V-10).



**Figure V-10 Stereoscopic view for the result of Dipole-Dipole array (d=20cm)**

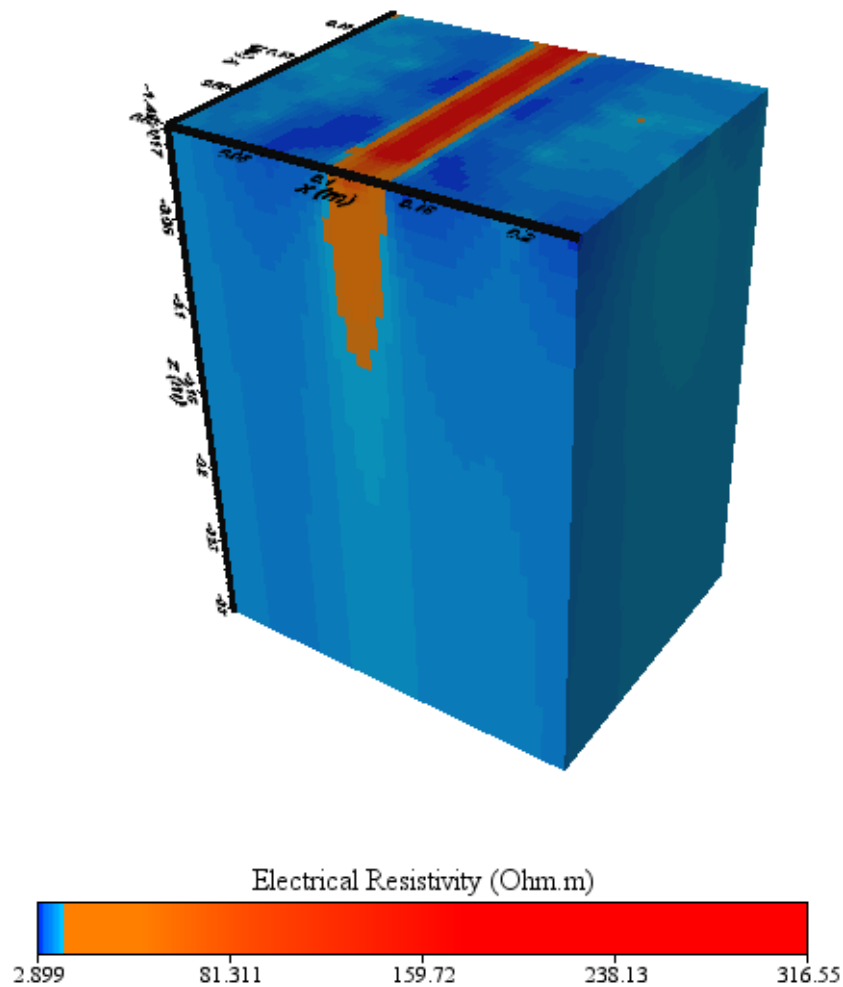
### One Styrofoam block structure (depth = 10cm)

The Styrofoam block at the middle was pulled out from the container and the clay was reorganized and stabilized again for the measurements. Total depth of block structure was 10cm from the surface. Entire post processing is same with previous investigation. Figure V-11 shows two-dimensional plane view with depth for the Schlumberger array.



**Figure V-11 Schlumberger array results for the clay with one block structure (d=10cm)**

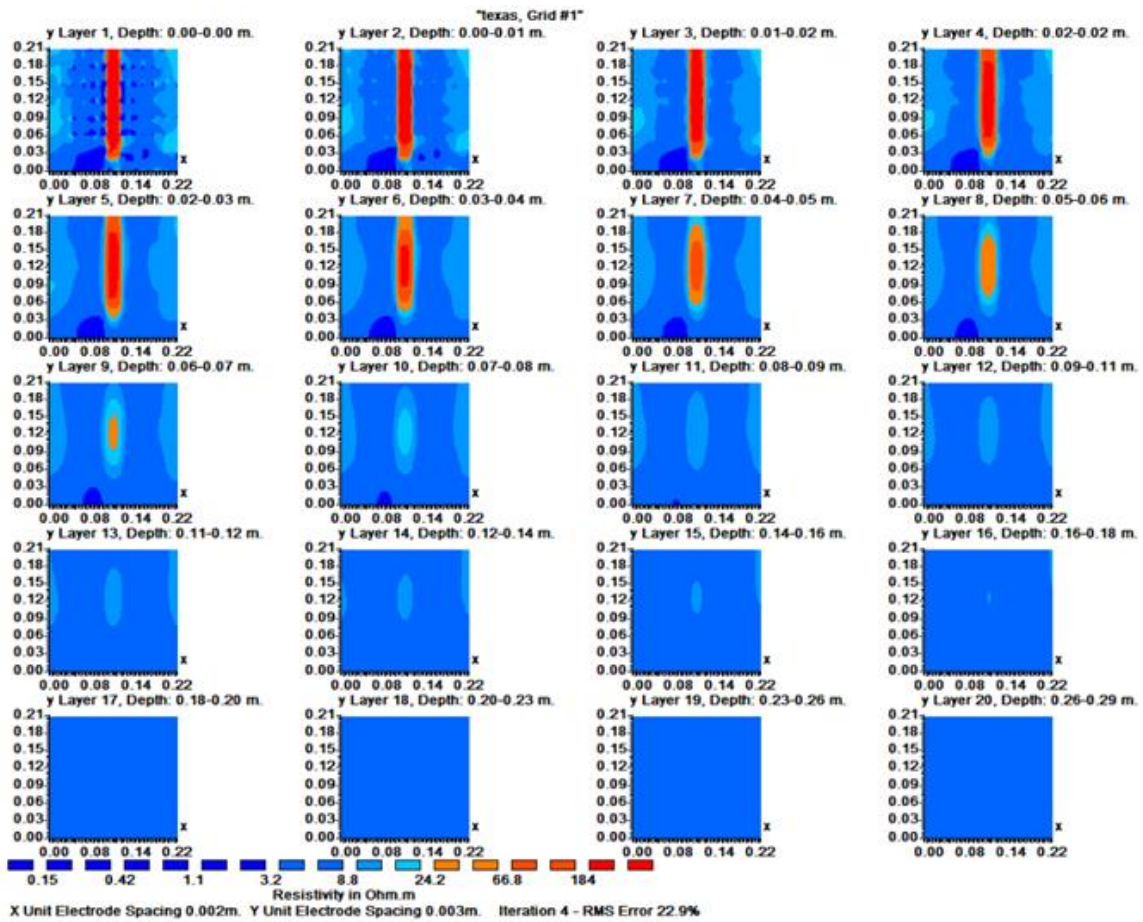
As shown in this figure, there was underestimation of the depth of the structure, but this problem is caused by the limitation of the contour values in the previous investigation. The width of the block was detected accurately, but the shape with vertical depth was not precise. To figure out the shape of the block precisely, three-dimensional visualization was processed using VOXLER 3D program with modified contour value profile.



**Figure V-12 Stereoscopic view for the result of Schlumberger array (d=10cm)**

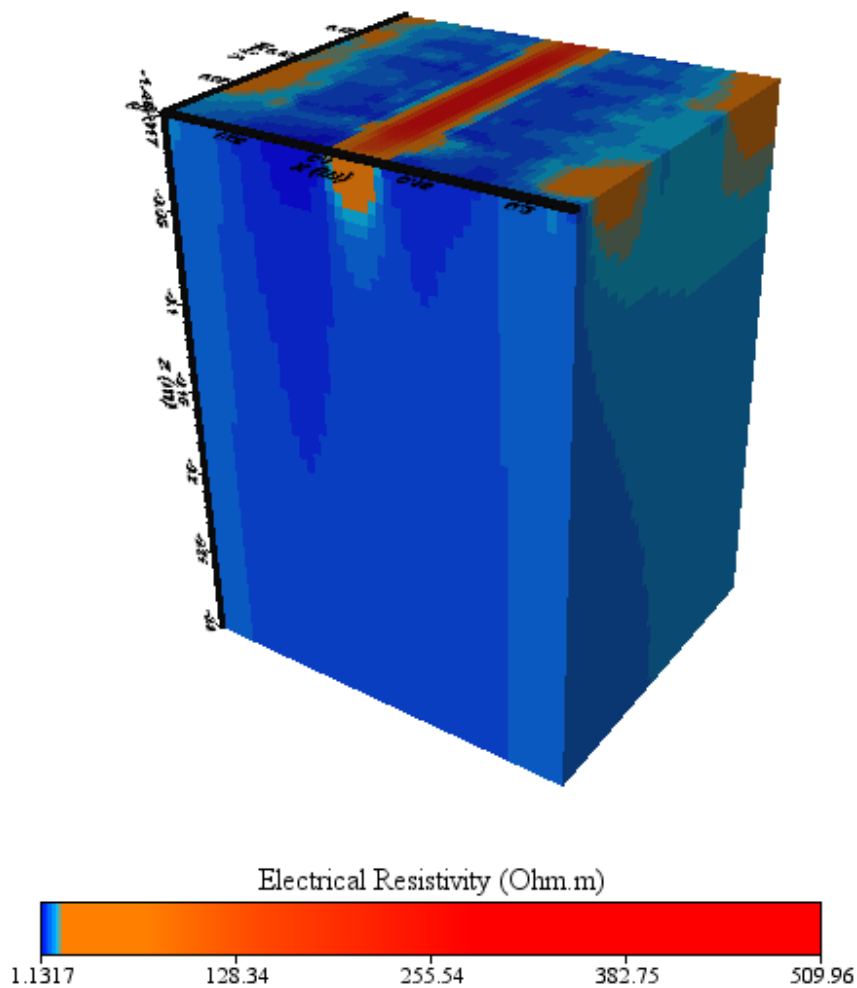
As shown in figure V-12, the depth of Styrofoam block was drawn corresponding to the real depth of this structure as 10cm. The width of block was decreased slightly with depth, but the entire shape was almost corresponded to the real shape of Styrofoam block.

The Dipole-Dipole array detected the vertical depth to 7cm as same with previous cases (Figure V-13).



**Figure V-13 Dipole-Dipole array results for the clay with one block structure (d=10cm)**

In all cases of preliminary ERT measurements, the Dipole-Dipole array could not detect entire depth of Styrofoam block structure. This array method showed relatively high sensitivity on horizontal profile at the surface. Three-dimensional images was also processed (Figure V-14).



**Figure V-14 Stereoscopic view for the result of Dipole-Dipole array (d=10cm)**

## **Discussion of the preliminary ERT measurement results**

According to the series of results from the preliminary ERT measurements, the Schlumberger array method is much more sensitive to vertical profile of electrical resistivity comparing to Dipole-Dipole array. Dipole-Dipole array is relatively more sensitive to detect horizontal mapping at the surface, but the coverage for the vertical profile was very poor. For the miniature array test of laboratory scale desiccation soil container, the Schlumberger array is appropriate method for detection of the fissure network within subsurface area.

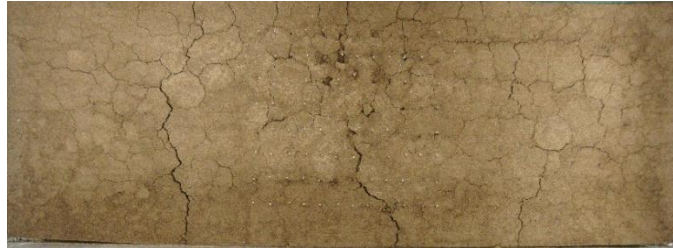
### **Desiccation soil container setup for the natural soil**

The acrylic rectangular container ( $0.63\text{m} \times 0.44\text{m} \times 0.32\text{m}$ ) was created for the desiccation of natural soil. There were two sections with ideally same dimension, so two types of test setup were applied with different initial water contents. The experiment using the natural soil was allowed to desiccate naturally with the surface left exposed. Electrical resistivity measurements were conducted at regular intervals over the three areas at each sections with the Schlumberger arrays. Measurements were stopped after 28 days of drying, when no additional cracking was investigated. After fully dried, the each section was completely saturated with the permeability test and allowed to dry again. Electrical resistivity measurements repeated with three cycle of drying and wetting. Electrical Resistivity Tomography (ERT) results for each sections were analyzed on following parts.

### **ERT results: Section A**

The natural soil on section A was prepared with water content of 10% which is corresponding to the dry side moisture content for 90% of relative compaction. Figure V-15 shows the evolution of the natural soil surface with drying-wetting cycle. As shown in this figure, the crack was generated initially at the surface and developed with horizontal directions. Repetition of drying-wetting cycle caused the propagation of the crack which was generated at the previous phase. The propagation in horizontal directions were monitored by surface exploration, but the propagation in depth could not be figured out with eye observation.

Electrical Resistivity Tomography (ERT) measurements were conducted to monitor the desiccation crack network within subsurface area of the soil. Three area were determined for the investigation considering the crack patterns at the surface, the results from the phase 3 and phase 4 analyzed.



(a) Phase 1: completely dried after initial setup



(b) Phase 2: completely dried after 1<sup>st</sup> re-saturation process



(c) Phase 3: completely dried after 2<sup>nd</sup> re-saturation process



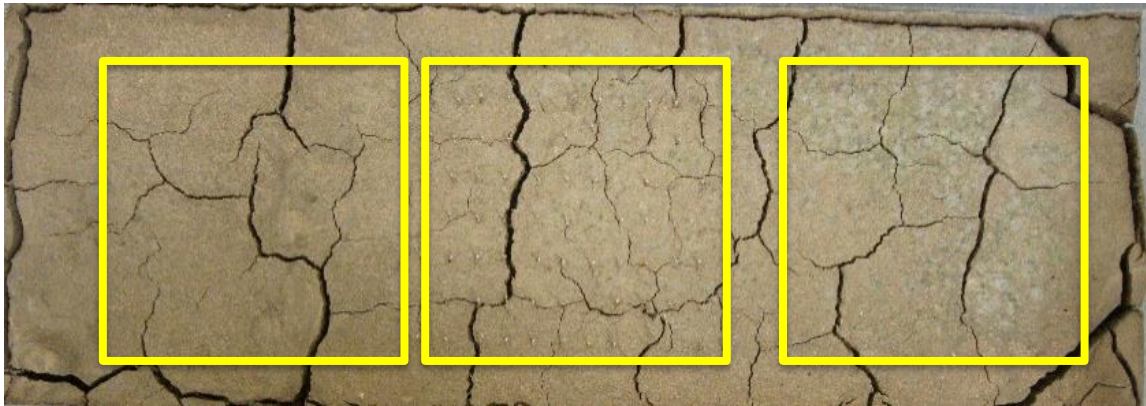
(d) Phase 4: completely dried after 3<sup>rd</sup> re-saturation process

**Figure V-15 Desiccation crack propagation with drying-wetting cycle on section A**



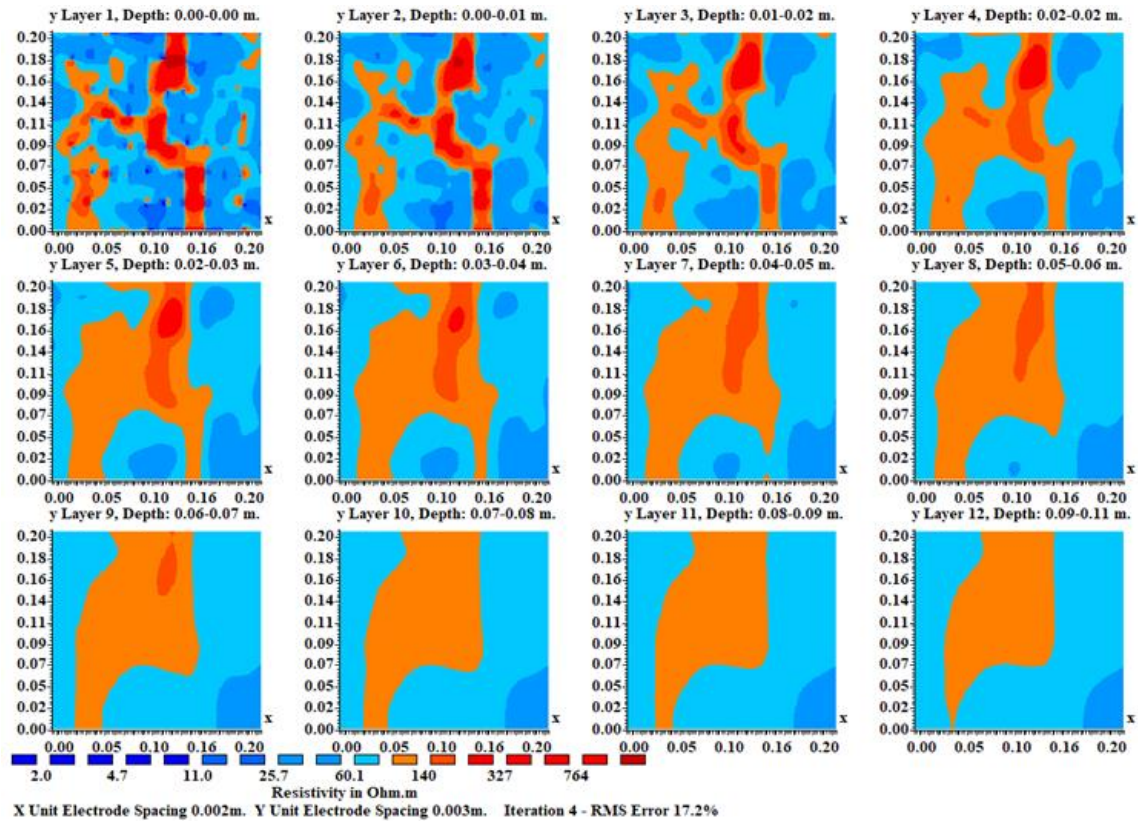
*Phase 3: Completely dried state after 2<sup>nd</sup> re-saturation process*

As shown in figure V-15(c), the complex crack patterns were developed from the surface of the soil by repetition of drying-wetting process. The ERT measurements were investigated at three different area of the surface. The planned area is represented in figure V-16. Electrical resistivity was measured using the Schlumberger array for each area with same formation of electrode.



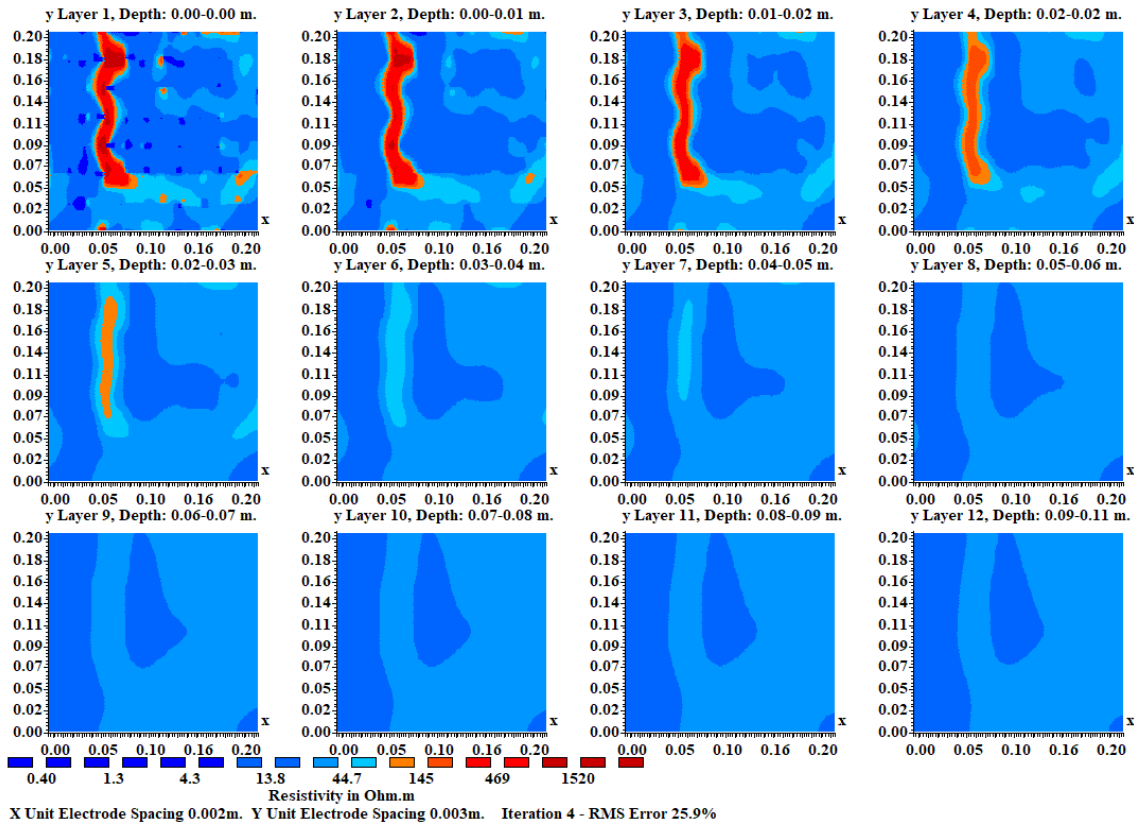
**Figure V-16 Three area selection for the ERT measurements (Section A, phase 3)**

Figure V-17 shows the ERT results from first area. The electrical resistivity greater than  $100 \text{ ohm} \cdot \text{m}$  was considered as cracked area. The width of the crack was overestimated by ERT measurements, but the crack network at the shallow depth was matching well with real fissuring.



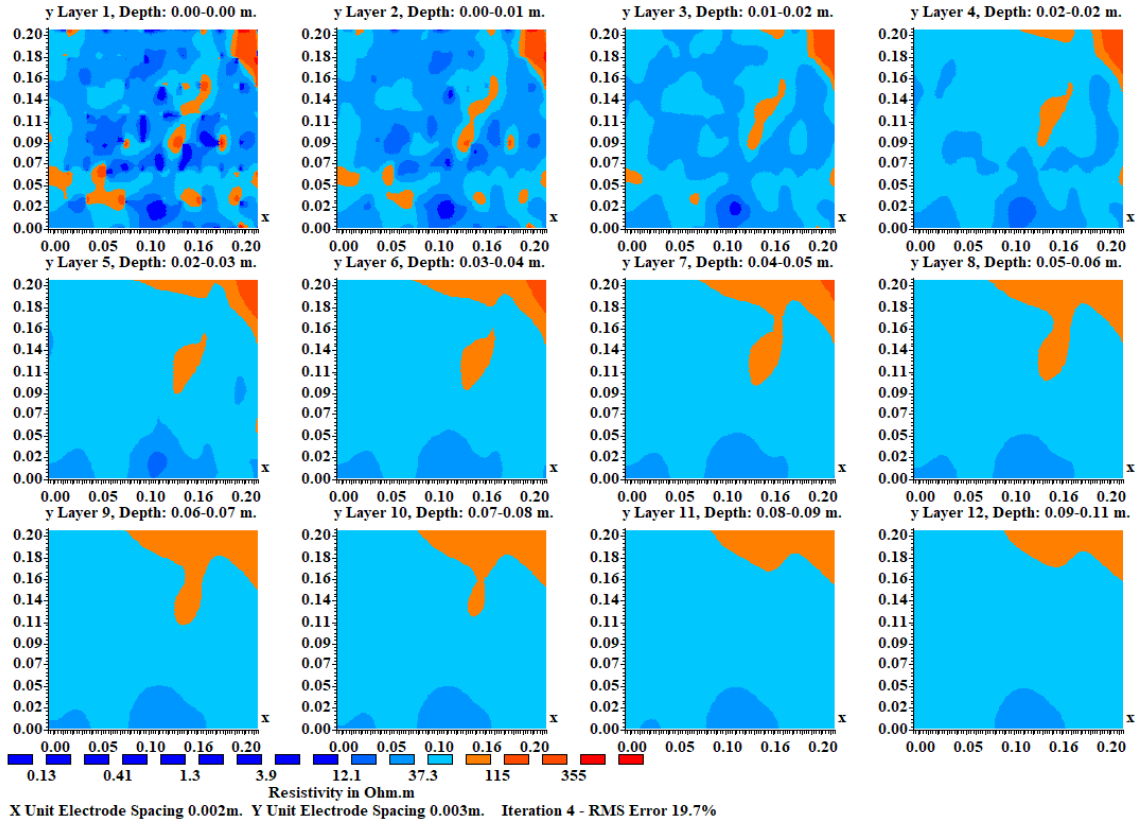
**Figure V-17 ERT result (A1, phase 3)**

Figure V-18 shows the ERT results from second area. There was a significant crack which was propagated from the top boundary of the soil container. As shown in this figure, the crack was developed to 6~7cm depth from the surface. Some tiny defects were also investigated at the surface with relatively high electrical resistivity.



**Figure V-18 ERT result (A2, phase 3)**

Figure V-19 shows the ERT results from third area. As shown in figure V-16, the width of the cracks were smaller than the cracks at the other two areas. Actually, there was interference of the crack network during the installation of the electrode at the surface, so the crack network could not be detected as observed at the surface. Meanwhile, larger cracks developed at the top right corner was observed properly with vertical dimension.



**Figure V-19 ERT result (A3, phase 3)**

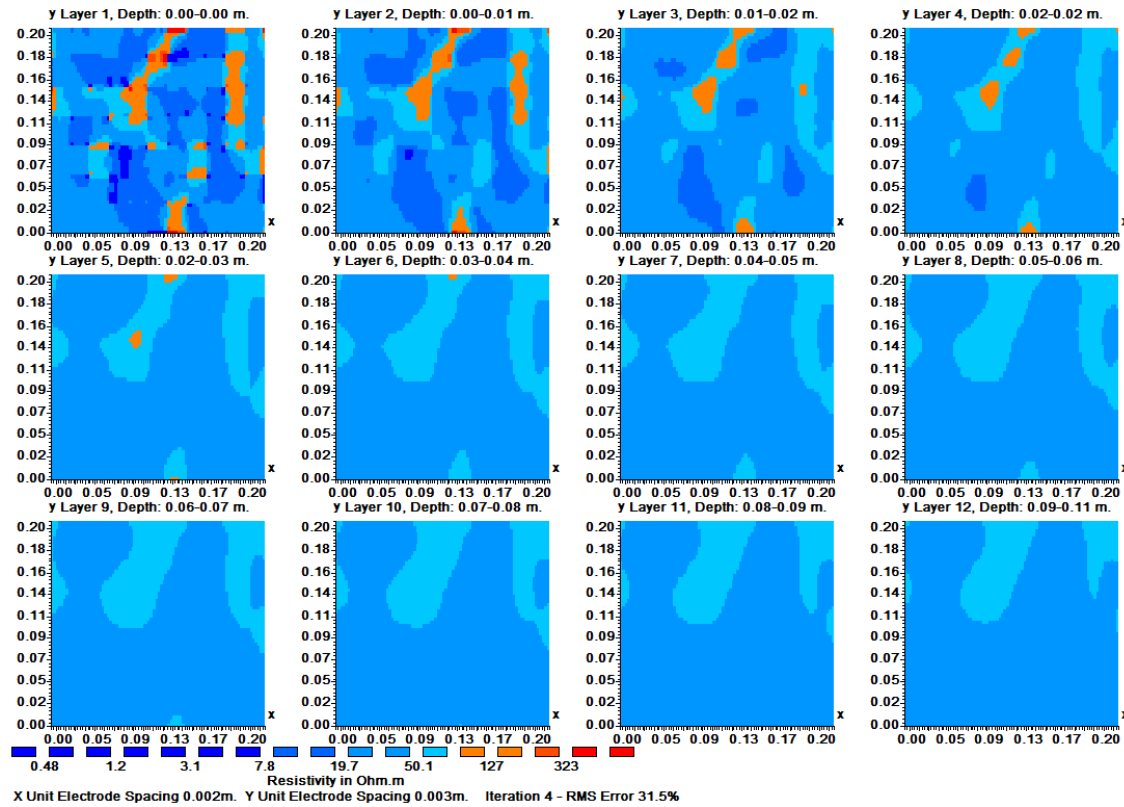
*Phase 4: Completely dried state after 3<sup>rd</sup> re-saturation process*

As shown in figure V-15(d), some of crack networks were remained from the previous phase and propagated as more complex network of cracks and there was newly generated cracks from the surface. The ERT measurements were also explored at almost same area of the surface corresponding to previous phase. Figure V-20 shows the target area of ERT measurements. Electrical resistivity measurement was conducted using the Schlumberger array with the same formation of electrode.



**Figure V-20 Three area selection for the ERT measurements (Section A, phase 4)**

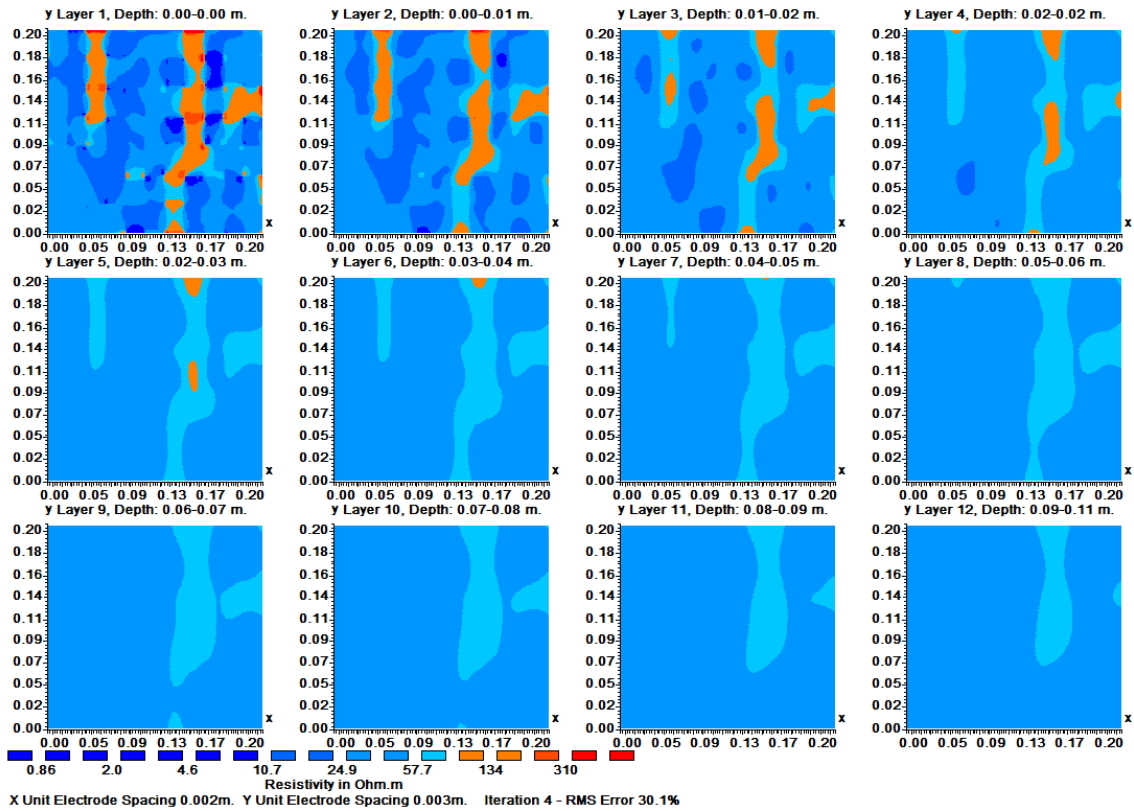
Figure V-21 shows the ERT results from first area. The crack patterns were more complicated comparing to the previous phase. The newly propagated crack network was generated at the right top of the area which was tiny crack before the wetting. ERT measurement figured out the crack network properly with pattern and depth, but the value of the electrical resistivity was relatively lower than previous phase result, because the electrical resistivity measurement was conducted before the soil was completely dried. The existence of the water within subsurface area enhanced the electrical conductivity. As discussed in the previous chapter, the soil and clay mixture with some amount of water content has higher electrical conductivity than completely dried material, because the moisture in the void area reduce the electrical resistivity, whereas the air in the void increase it.



**Figure V-21 ERT result (A1, phase 4)**

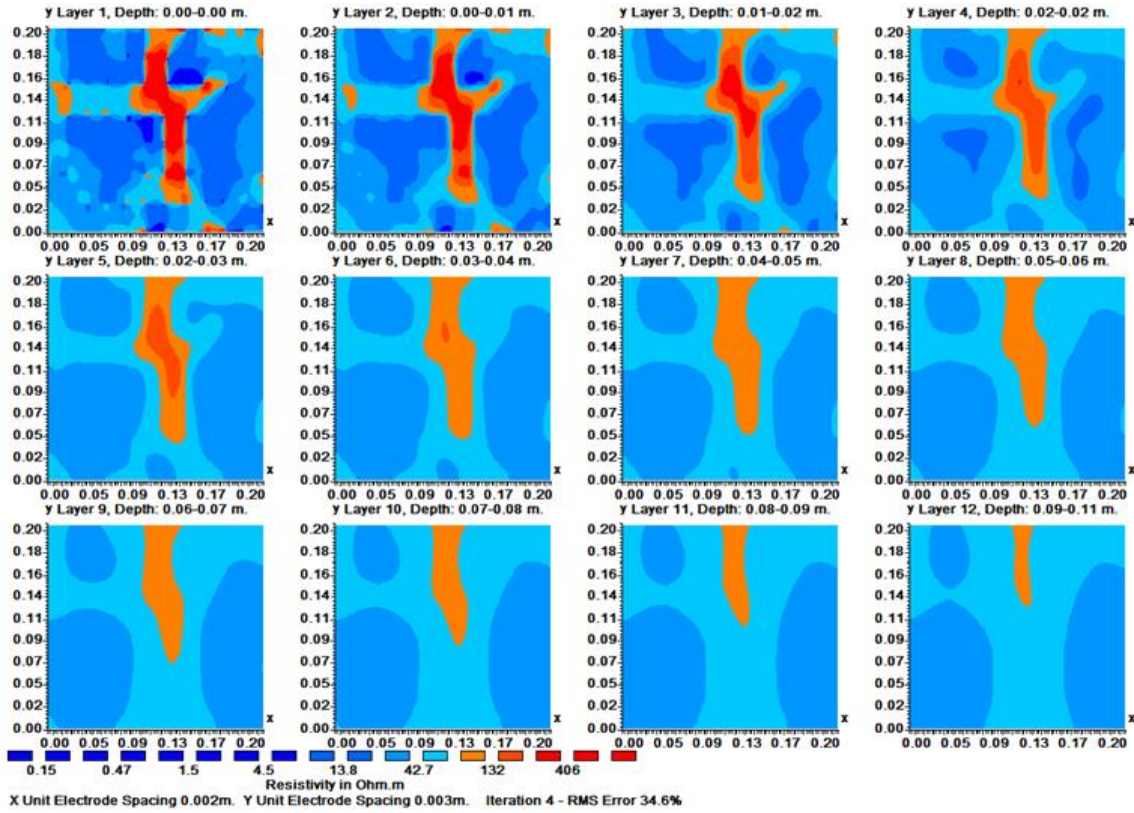
Figure V-22 shows the ERT results from second area. At the previous phase, there was small crack generated from the right top of the area, and it propagated as complex fissure network by wetting-drying process. This network was connected the other crack propagated from the bottom of the area, and it created more complicated network of cracks. As shown in figure V-22, the electrical resistivity measurements figured out the detailed crack networks propagated from the surface area, and it was also relatively lower than previous phase results. In addition, the cracks were developed with vertical direction which was reached to the bottom of the natural soil layer.





**Figure V-22 ERT result (A2, phase 4)**

The width of the crack was increased and propagated to connect with adjacent small cracks at the third area. Figure V-23 shows the ERT results from this area. As shown in this figure, the crack network at the central area was developed with both horizontal and vertical directions. Also, the electrical resistivity values were relatively lower than the previous phase with higher water content environment of the soil.



**Figure V-23 ERT result (A3, phase 4)**

#### *Discussion of the test results from section A*

The Electrical Resistivity Tomography (ERT) measurements were conducted to the selected area at the section A to investigate the crack network and propagation with repetition of drying-wetting process. The crack networks developed from the surface were detected properly with ERT measurements, but the relatively small (less than 2mm) width of crack was not monitored at all. Also, the crack network was developed both horizontally and vertically with accumulation of drying-wetting cycle and the fissure networks tended to connect with adjacent small cracks. The existence of the moisture within the soil reduces the average value of the electrical resistivity of the soil.



### **ERT results: section B**

The natural soil on section B was prepared as slurry state with water content of 60% which is corresponding to 150% of liquid limit of the natural soil. The soil on section B is relatively loose state because of the larger value of the water content. Figure V-24 shows the evolution of the natural soil surface with repetition of drying-wetting process. The crack was generated at the initial state on the surface and propagated with both horizontal and vertical directions. The crack dimension was much greater than that of section A because of the relatively low density of the soil. Generally, repeat of the drying-wetting cycle caused the development of the crack which was created initially at the surface and propagated with horizontal and vertical directions. In addition, some crack networks were filled with adjacent soils but the trace was remained at the surface. There was more complicated networks than dense soil at the section A.

The development of the fissure networks were monitored by the electrical resistivity measurements and the results were analyzed with the inversion program RES3DINV. In addition, three-dimensional visualization using VOXLER 3D was processed to develop the stereoscopic image of subsurface area with complicated crack patterns. For the section B, the ERT measurements were analyzed from phase 1 to phase 3. The further phases were investigated in the next chapter with the application of the clay mixture as filling material.



(a) Phase 1: completely dried after initial setup



(b) Phase 2: completely dried after 1<sup>st</sup> re-saturation process



(c) Phase 3: completely dried after 2<sup>nd</sup> re-saturation process

**Figure V-24 Desiccation crack propagation with drying-wetting cycle on section B**

*Phase 1: Completely dried after initial setup*

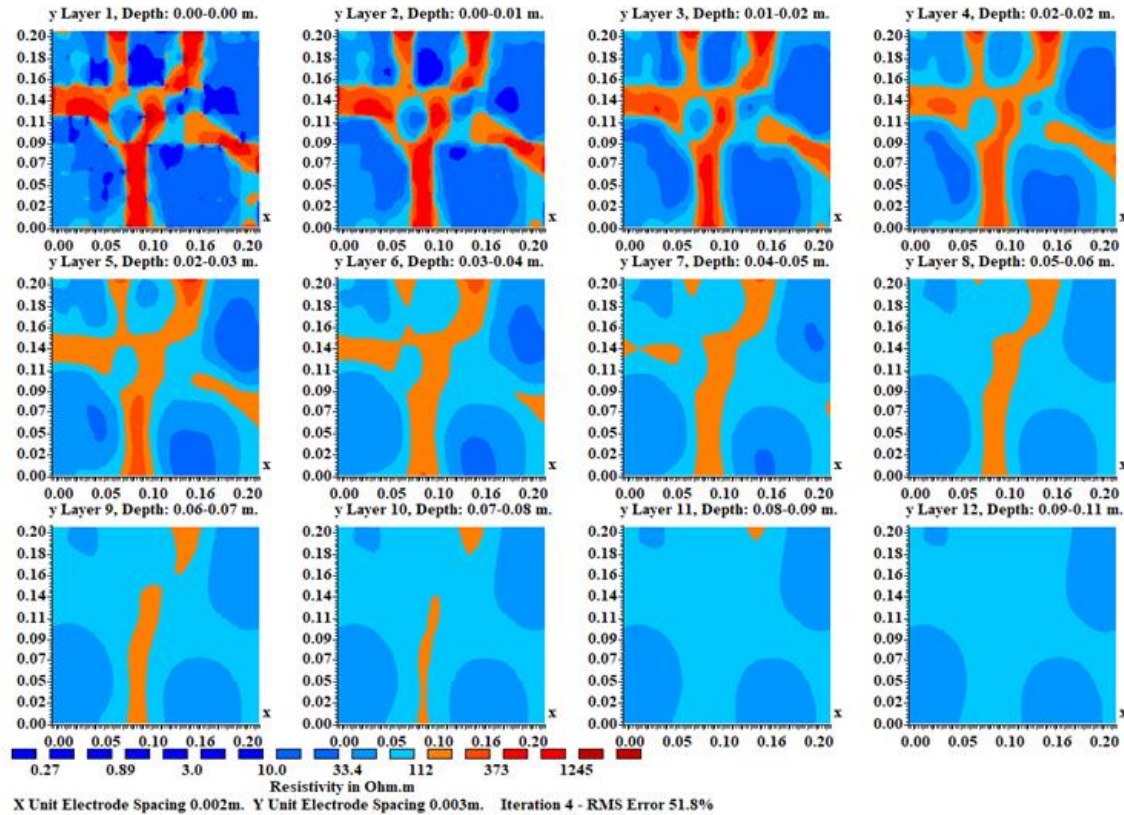
Figure V-25 shows the soil which was fully dried after initial wetting. Several crack networks were developed from the surface of the natural soil. The width of the crack was much larger than dense soil on section A, and the range of value was 0.5~1.0cm. The selected area for the ERT measurement is also shown in figure V-25. Electrical resistivity was measured using the Schlumberger array method for the selected area with the same formation of electrode on section A.



**Figure V-25 Area selection for the ERT measurement (Section B, phase 1)**

As shown in figure V-26, the complex crack network was mapped as two-dimensional plane figures with various depth. The electrical resistivity greater than 100 ohm · m was considered as cracked area. The crack networks were figured out properly with the ERT measurements. The crack at the center line was propagated to the depth of 8cm from the surface. The width of the crack was relatively overestimated compared to the real measured dimension of the fissure networks. The cracks with smaller width (less than 2mm) were expressed as low electrical resistivity zone compared to larger crack

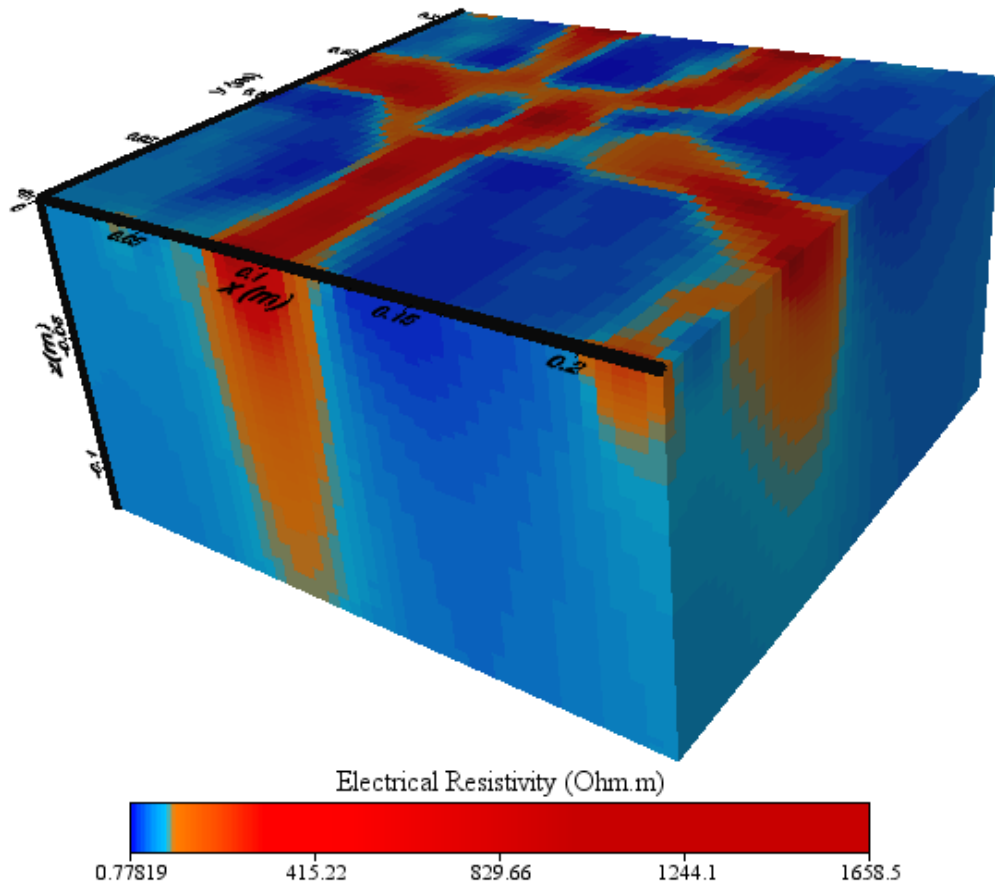
networks. Following the results from the inversion process using RES3DINV program, it was easy to figure out two-dimensional plane view with certain depths, but it was hard to figure out the three-dimensional shape of the crack network within subsurface area.



**Figure V-26 ERT result (B3, phase 1)**

The electrical resistivity data with x-, y-, and z- coordinate values were extracted from RES3DINV program, and this data was processed as three-dimensional image by VOXLER 3D. Figure V-27 shows the stereoscopic visualization of the subsurface area with crack networks. As discussed in the preliminary ERT measurements using Styrofoam blocks, the contour values were standardized for the consistency of the

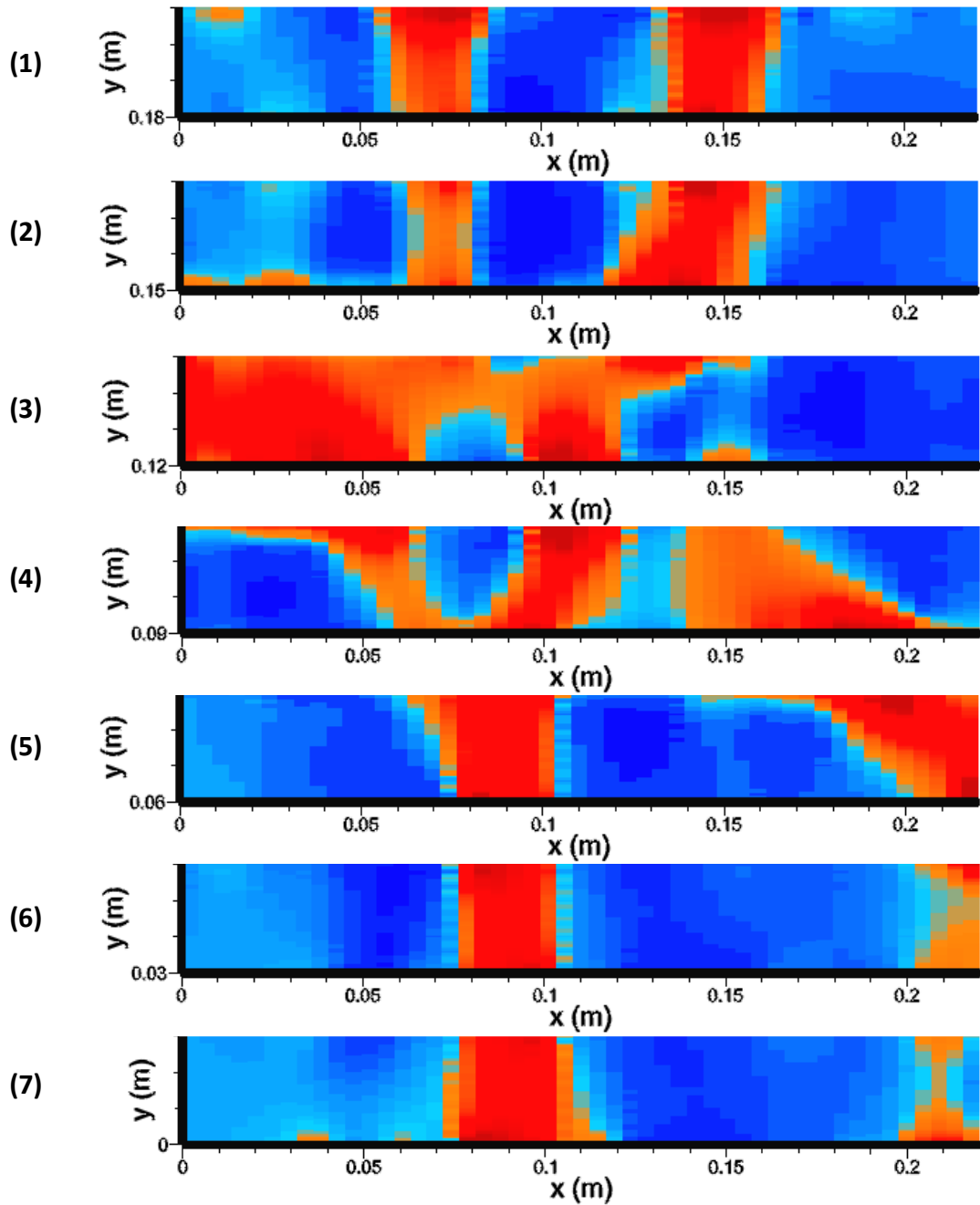
analysis. By the modification of the contour values, the crack patterns were matched more precisely with real crack networks.



**Figure V-27 3-D image of the ERT measured subsurface area (B3, phase 1)**

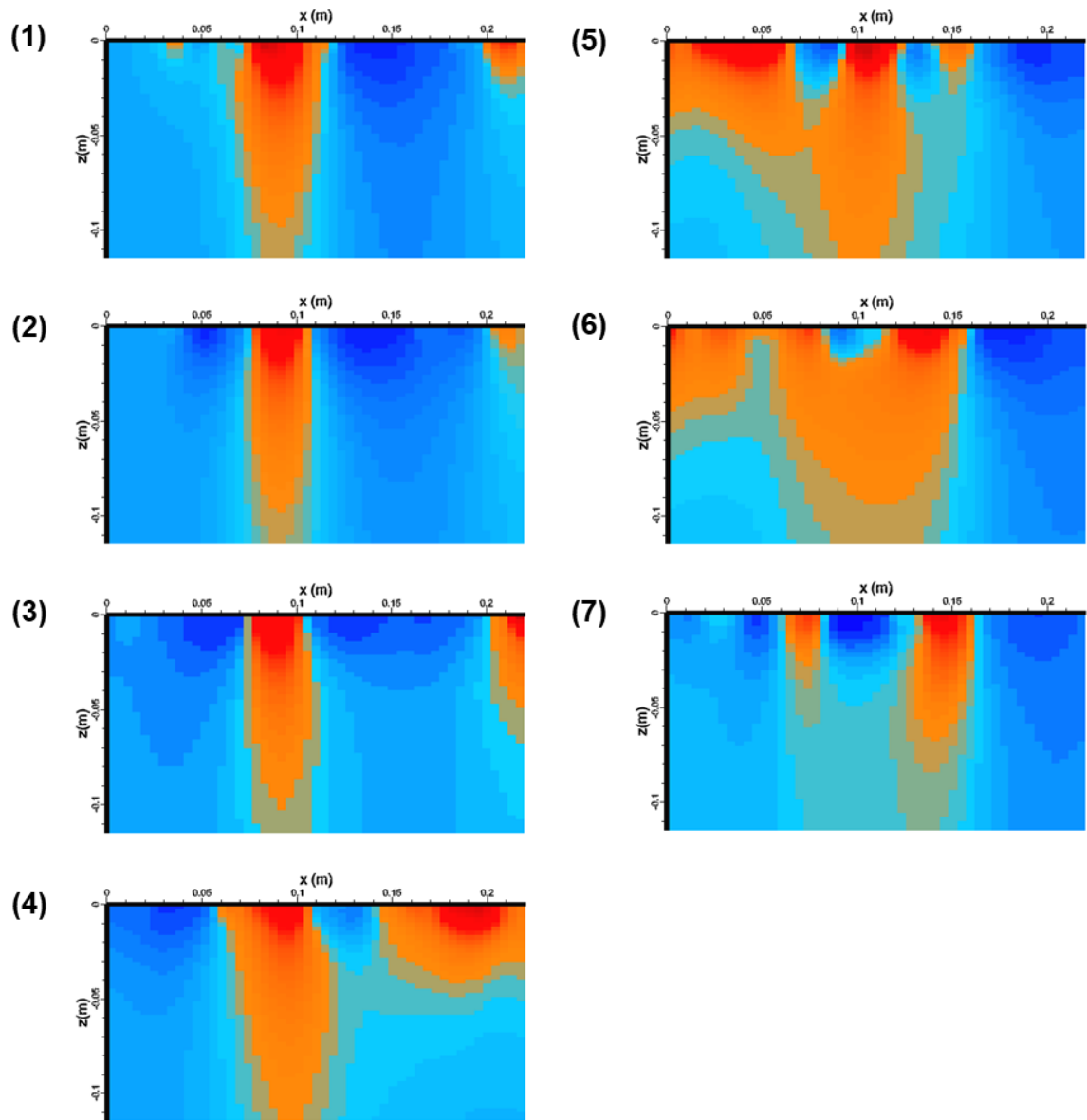
To figure out the crack networks within subsurface area, three-dimensional image can be sliced into several parts with determined dimension. Figure V-28 shows the horizontally sliced parts with vertical length of 3cm. By this procedure, the dimension of specified crack network can be analyzed and calculated directly. Also, it

can be visualized as front view and three-dimensional blocks (Figure V-29 and Figure V-30).

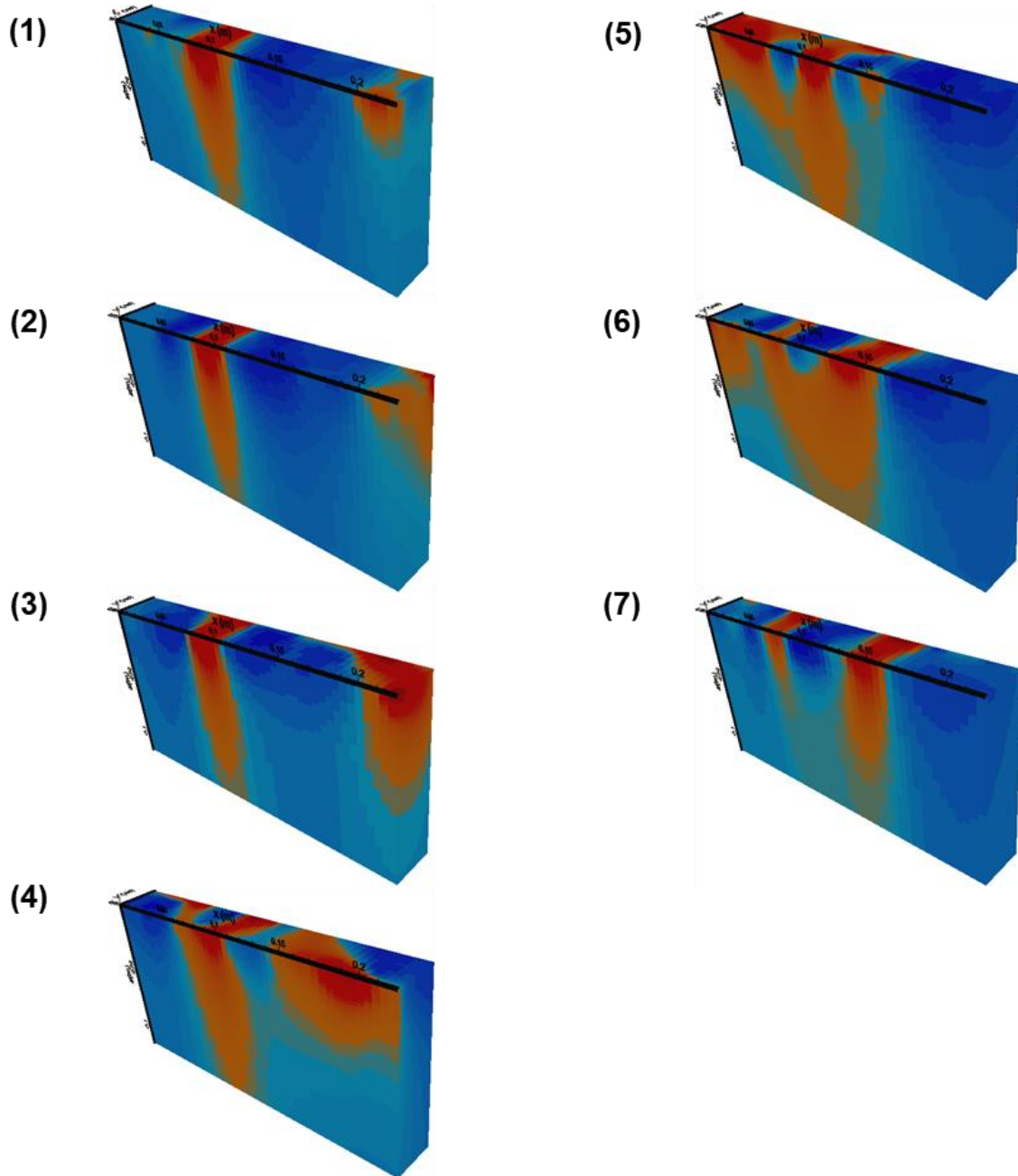


**Figure V-28 Horizontal sliced cut of ERT measured subsurface area (Top view, B3, phase 1)**





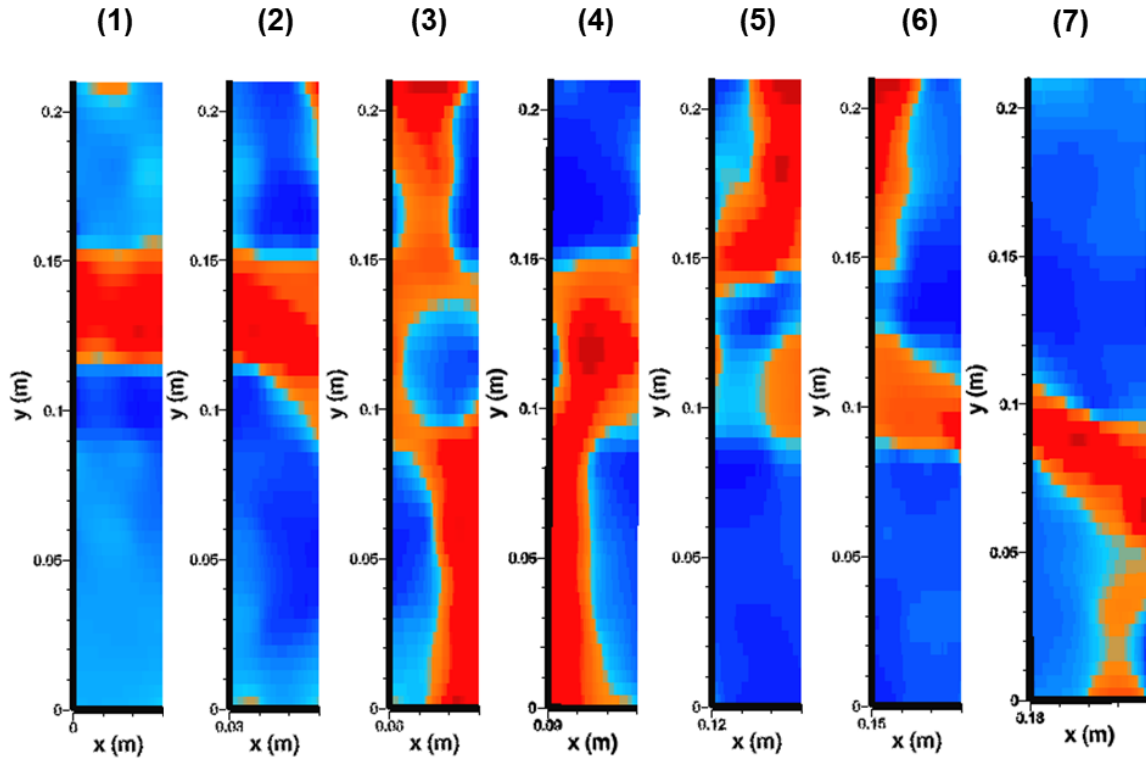
**Figure V-29 Horizontal sliced cut of ERT measured subsurface area (Front view, B3, phase 1)**



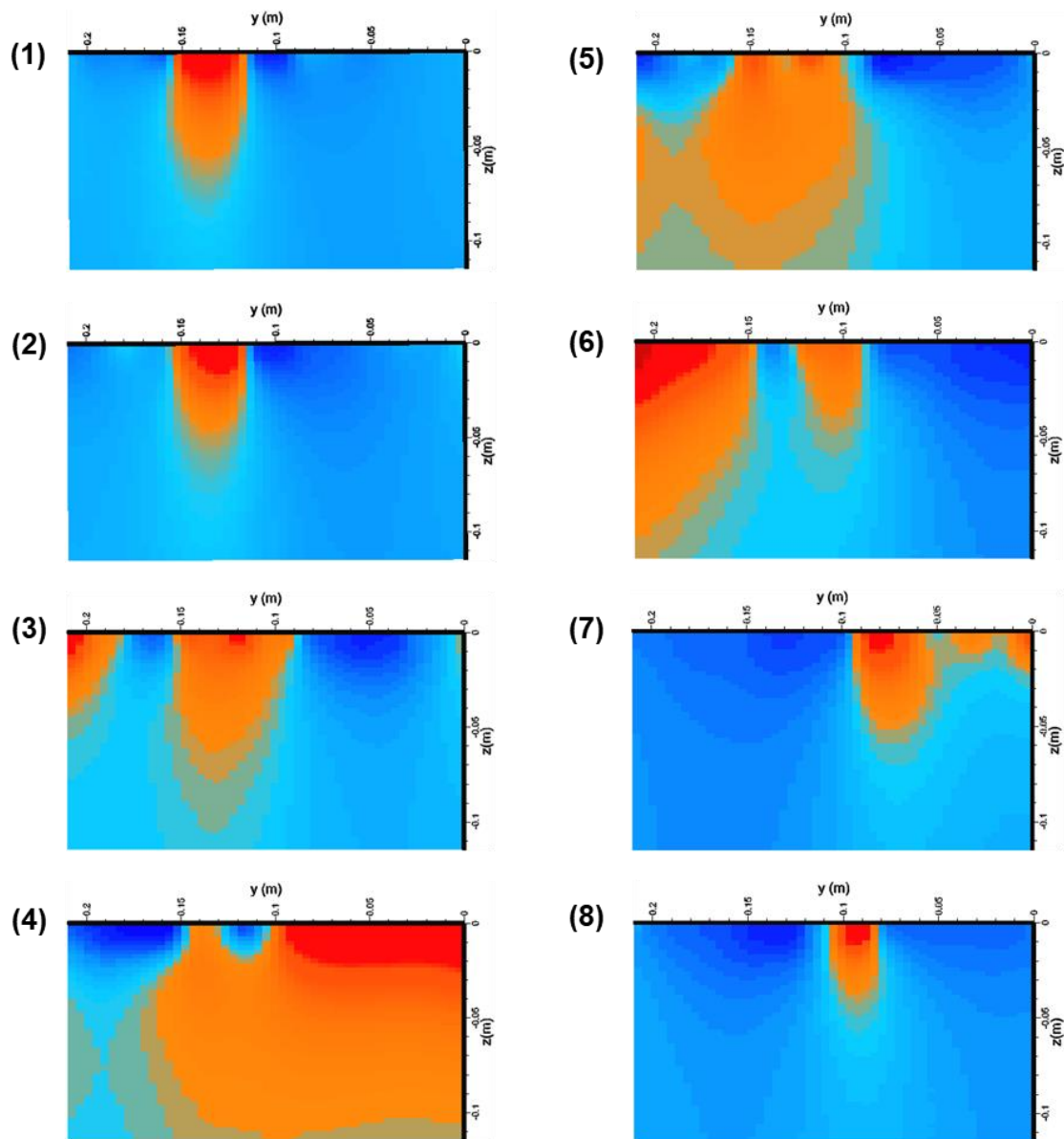
**Figure V-30 Horizontal sliced cut of ERT measured subsurface area (3-D view, B3, phase 1)**



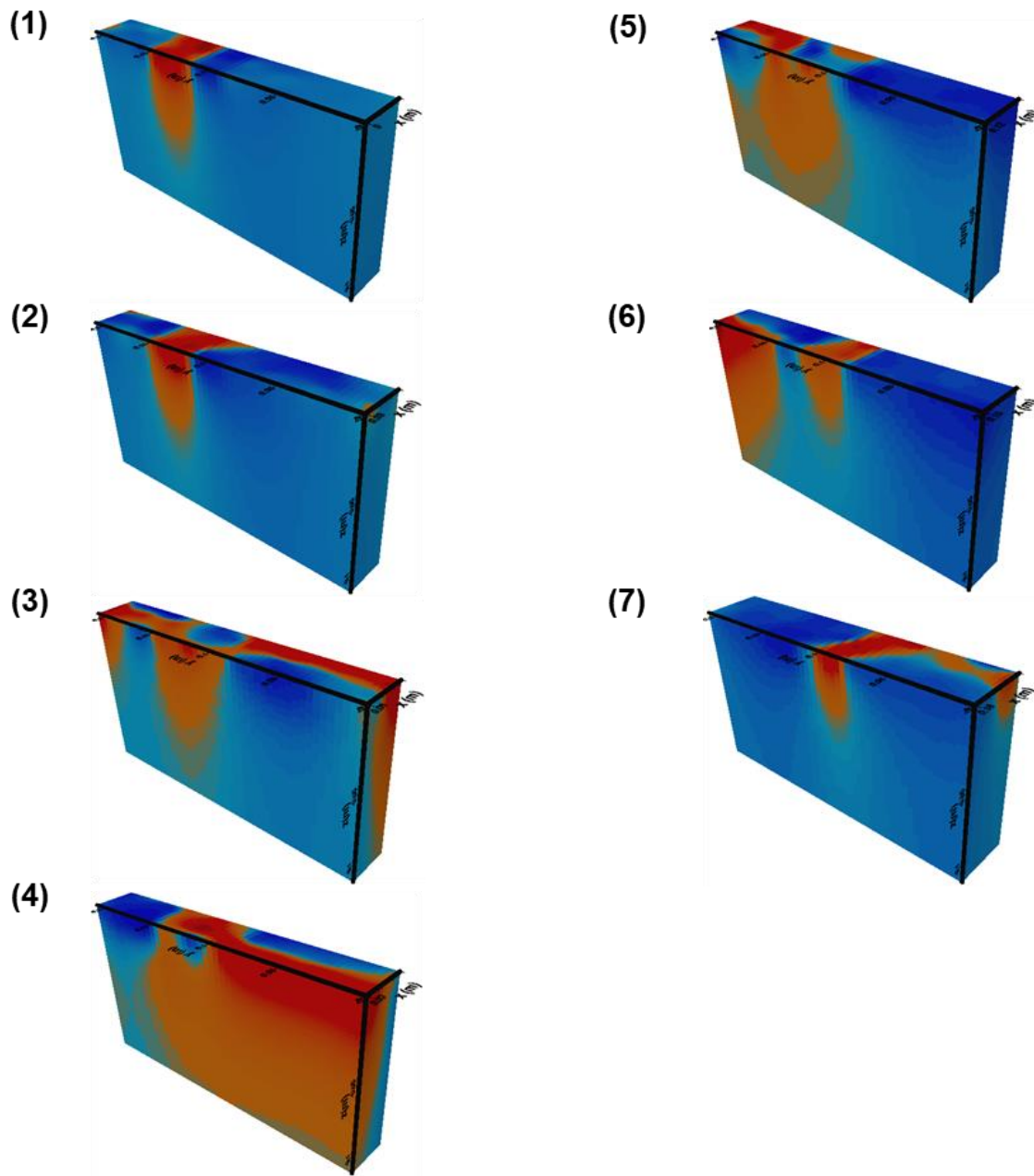
In addition, stereoscopic image can be also sliced into vertical direction. Figure V-31 ~ V-33 shows the various view of the vertical sliced cut. With this procedure, it is available to visualize the selected area of the measurement as two-dimensional or three-dimensional images. The dimensions are shown in every sliced or stereoscopic images of the parts, so it is available to validate the dimension of the crack networks directly within certain area.



**Figure V-31 Vertical sliced cut of ERT measured subsurface area (Top view, B3, phase 1)**



**Figure V-32 Vertical sliced cut of ERT measured subsurface area (Side view, B3, phase 1)**



**Figure V-33 Vertical sliced cut of ERT measured subsurface area (3-D view, B3, phase 1)**

*Phase 2: Completely dried after 1<sup>st</sup> re-saturation*

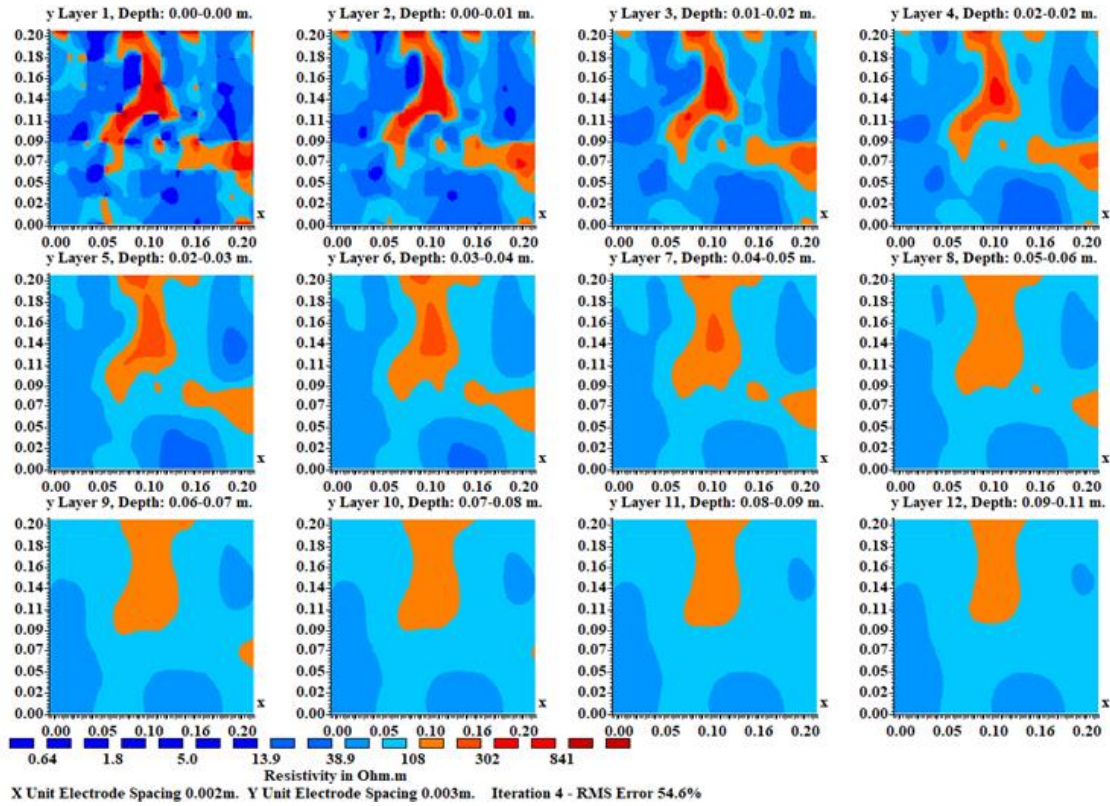
As shown in figure V-34, the crack networks in the selected area were changed significantly after 1<sup>st</sup> re-saturation process with permeability test. The main crack network at the center was filled with surrounded soil during the saturation, but the trace was remained from the surface. The new crack network was generated at the top of the trace, and it propagated to connect with adjacent cracks. The crack width was decreased compared to the previous phase.



**Figure V-34 Area selection for the ERT measurement (Section B, phase 2)**

The electrical resistivity measurement were mapped as two-dimensional figures with various depth in figure V-35. The crack networks were monitored appropriately with the measurements, and the trace of the former cracks were expressed as relatively lower value of resistivity. The newly generated crack at the center line was propagated to the depth of 12cm from the surface. The width of the crack was slightly overestimated. The three-dimensional coordinates from this measurement was also extracted from

RES3DINV program and processed using three-dimensional visualization program. The detailed figures are shown in APPENDIX A.

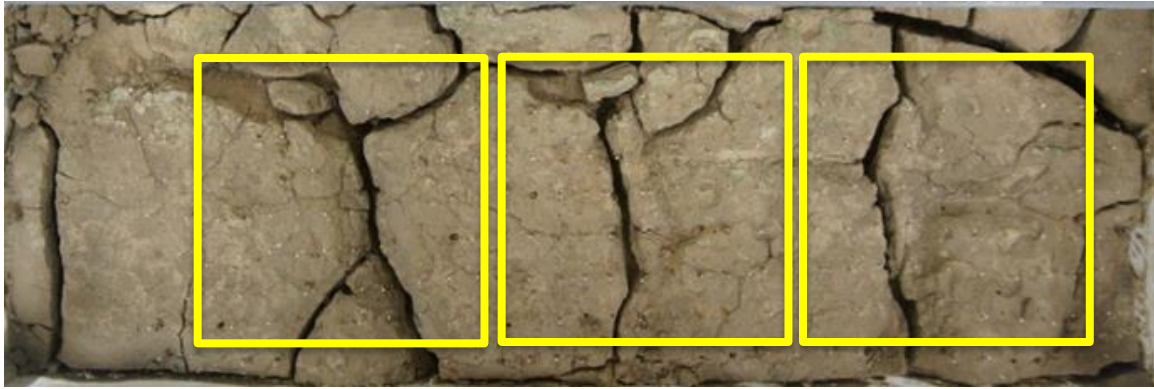


**Figure V-35 ERT result (B3, phase 2)**

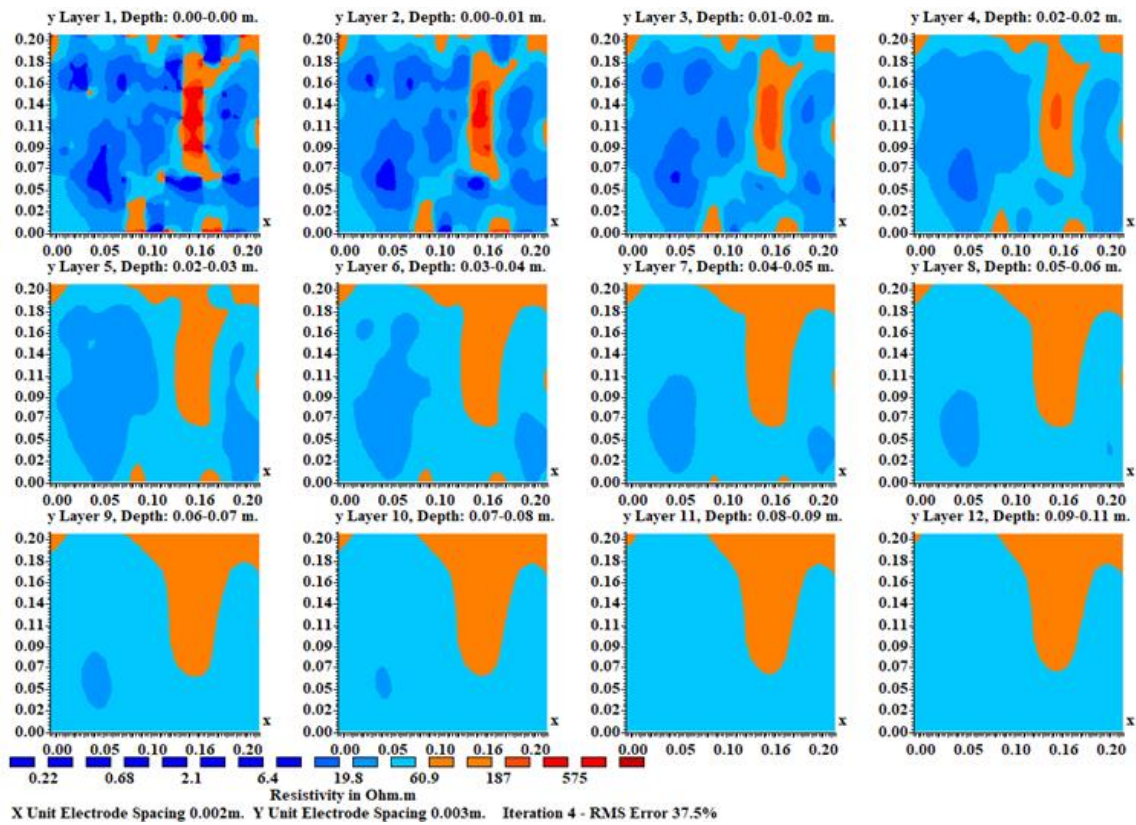
*Phase 3: Completely dried after 2<sup>nd</sup> re-saturation*

As shown in figure V-36, some crack networks were maintained and there was newly created fissure network with combination of developed crack and trace of the previous phase crack. In this phase, three areas were selected to measure the Electrical Resistivity Tomography. These results was compared to the soil structure with the filling material within desiccation crack area.



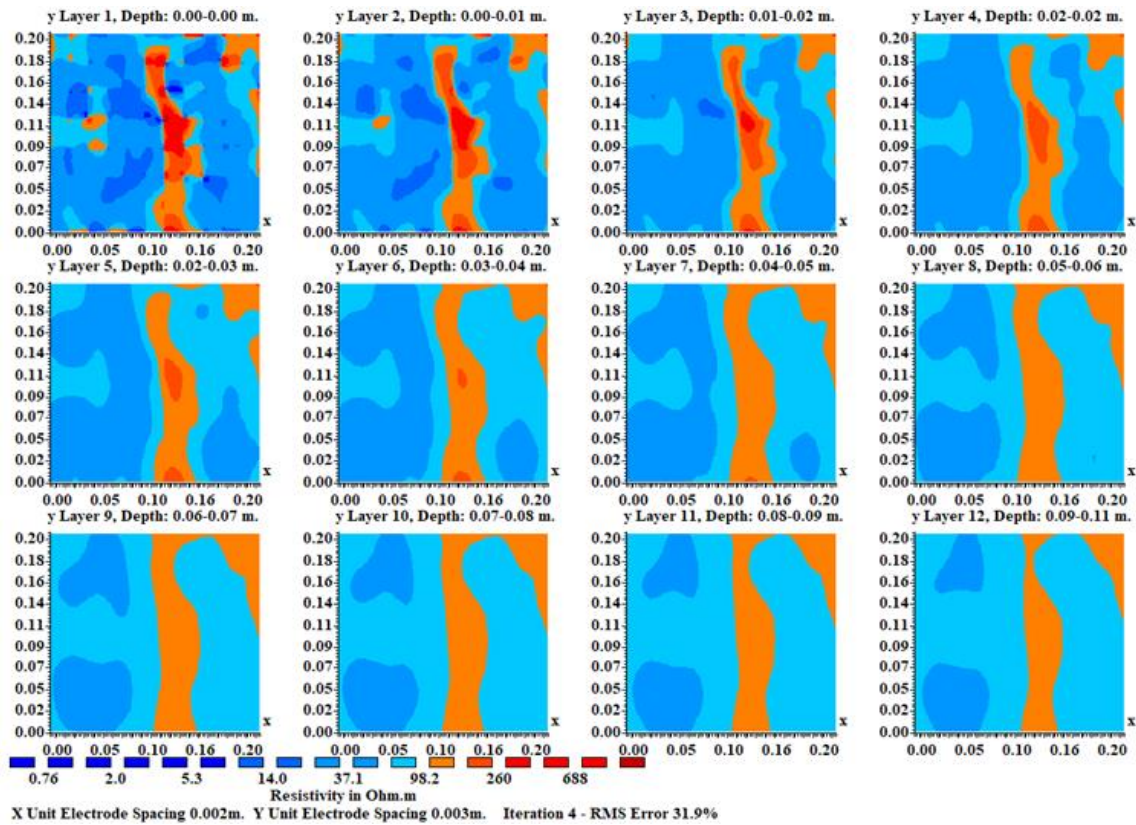


**Figure V-36 Three area selection for the ERT measurements (Section B, phase 3)**



**Figure V-37 ERT result (B1, phase 3)**

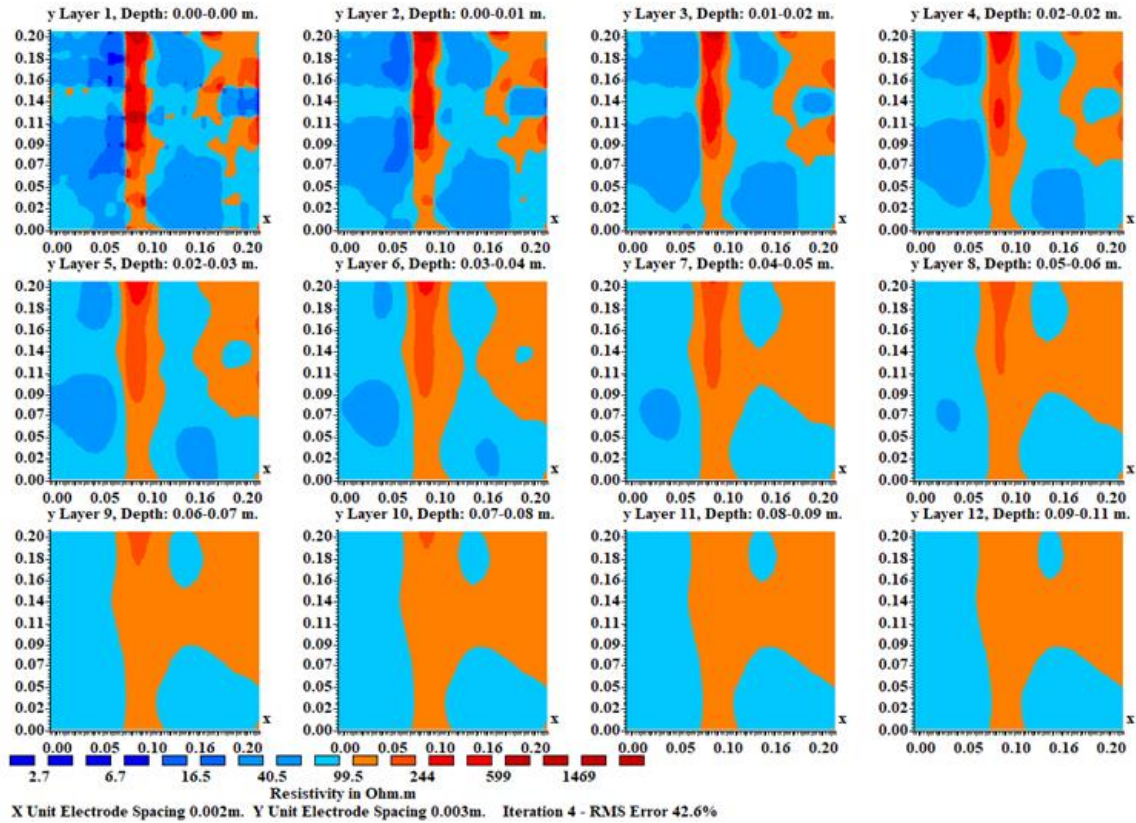
Figure V-37 shows the electrical resistivity measurements of the first area of section B. The crack network with relatively larger width (larger than 5mm) was well-monitored with electrical resistivity. The width of the crack was also slightly overestimated as same with other cases.



**Figure V-38 ERT result (B2, phase 3)**

Figure V-38 shows the results from second area of section B. The width of the central crack was overestimated which is corresponding to the summation of the crack and trace of the previously generated cracks. This area was evaluated as combined defected area with higher electrical resistivity compared to adjacent soil. The cracks

were propagated to the bottom of the natural soil with depth of 12cm, and the width of crack was increased with depth. Figure V-39 shows the electrical resistivity measurements of third area of section B. This area was continuously monitored with every phase, and the changes on crack pattern was very significant. The trace of crack generated in phase 1 and the crack propagated in phase 2 were combined as one fissure network vertically crossing the center. In addition, the traces were maintained and expanded as expressed the resistivity value between 50 and 100 ohm · m.



**Figure V-39 ERT result (B3, phase 3)**



### *Discussion of the test results from section B*

The Electrical Resistivity Tomography (ERT) measurements were conducted to the selected area at the section B to monitor the fissure network and propagation with repetition of drying-wetting cycle. The crack networks were more complicated developed compared to the dense state soil. The width of the crack was relatively larger than that of section A, the cracks were propagated both horizontally and vertically. In addition, some cracks were closed by filtration of surrounded soil under saturation, and the trace was remained as low resistivity area. To investigate with detailed stereoscopic view of the subsurface area, three-dimensional visualization using VOXLER 3D was developed and processed to produce multiple two-dimensional and three-dimensional images following the purposes. The standardization of the contour values allows the consistency of the electrical resistivity analysis.

### **Summary and conclusions**

In this chapter, a series of the Electrical Resistivity Tomography (ERT) measurements were performed to monitor the subsurface area with desiccation crack network under various circumstances. Preliminary ERT measurements using Styrofoam and electrical resistivity measurements for the natural soil subjected to drying were conducted, and the following results were obtained.

1. The preliminary ERT measurements were conducted using Styrofoam blocks structure to examine the Schlumberger array and the Dipole-Dipole array method for the miniature test. The Schlumberger array method is much more

sensitive to vertical profile of electrical resistivity comparing to the Dipole-Dipole array. The Dipole-Dipole array is relatively more sensitive to detect horizontal mapping at the surface area, but the coverage for the vertical depth was quite poor. For the miniature array test of laboratory scale desiccation soil container, the Schlumberger array is appropriate method for the detection of the desiccation crack network of subsurface area.

2. The Electrical Resistivity Tomography (ERT) measurements were conducted to the selected area at the section A to investigate the crack network and propagation with repetition of drying-wetting process. The crack networks developed from the surface were detected properly with ERT measurements, but the relatively small (less than 2mm) width of crack was not monitored at all. Also, the crack network was developed both horizontally and vertically with accumulation of drying-wetting cycle and the fissure networks tended to connect with adjacent small cracks. The existence of the moisture within the soil reduces the average value of the electrical resistivity of the soil.
3. The Electrical Resistivity Tomography (ERT) measurements were conducted to the selected area at the section B to monitor the fissure network and propagation with repetition of drying-wetting cycle. The crack networks were more complicated developed compared to the dense state soil. The width of the crack was relatively larger than that of section A, the cracks were propagated both horizontally and vertically. In addition, some cracks were closed by filtration of surrounded soil under saturation, and the trace was

remained as low resistivity area. To investigate with detailed stereoscopic view of the subsurface area, three-dimensional visualization using VOXLER 3D was developed and processed to produce multiple two-dimensional and three-dimensional images following the purposes. The standardization of the contour values allows the consistency of the electrical resistivity analysis.

## CHAPTER VI

### APPLICATION OF THE CLAY MIXTURE AS FILLING MATERIAL FOR SUBSURFACE CRACKING AREA

#### **Introduction**

The aim of this research is to examine the applicability of the clay mixture as filling material which was investigated and suggested in the chapter IV. Preliminary injection was carried out to investigate washing out of the clay mixture under saturation, because the injected material should not be extracted or solvent in water. Also, permeability test was conducted to figure out the hydraulic conductivity evolution with drying-wetting cycle and the effect of clay mixture as reducing agent of the permeability.

In addition, Electrical Resistivity Tomography (ERT) measurements were conducted for the natural soil with clay mixture filled into the desiccation crack area. This process allows to check the clay mixture filtration through the fissure networks. Direct shear test was conducted to compare the shear strength of the natural soil and soil-clay mixture structure in the aspect of strengthening effect by mixture injection.

Finally, the dismantlement of the natural soil with injected clay mixture was carried out for direct vision exploration of soil-clay mixture structure within subsurface area. This procedure allows to validate the mixture injection technique for the defected area.

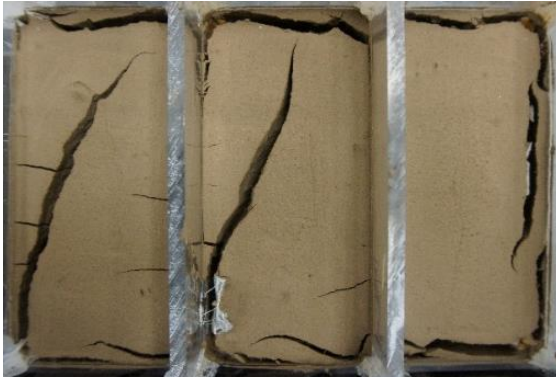
### **Preliminary injection test using small-scale container**

The preliminary injection test was conducted using small-scale acrylic container. The shape of the container was same proportion with the dimension of the desiccation soil container as rectangular shape. The natural soil with same water content of section B ( $w=90\%$ ) was mixed and poured into the three sections of the container. These specimens were completely dried and some cracks were propagated to allow the mixture injection within area.

**Table VI-1 The clay mixture description for preliminary injection test**

No.	Label	Main components (%)			Additives (%)		
		Kaolinite	Graphite	Cement	$\beta$ -glucan	Xanthan gum	SP
1	B	70.00	30.00	-	1.50	-	1.50
2	X	70.00	30.00	-	-	1.50	1.50
3	C	50.00	30.00	20.00	-	-	1.50

Three types of clay mixture were selected for the preliminary injection. Table VI-1 shows the detailed profile of each clay mixtures. The purpose of this test is to examine the durability of the biopolymers ( $\beta$ -glucan and xanthan gum) and cement components under saturation. Cement mixture composition is identically same with the previous research by Kim to compare with other mixtures without cement proportion. Each clay mixture was mixed with same water content of 90% and injected at the different sections and air dried.



(a) Completely dried state after casting



(b) Clay mixture injected within cracking area ( $\beta$ -glucan / Xanthan gum / Cement)



(c) After saturation from the surface  
( $\beta$ -glucan / Xanthan gum / Cement)



(d) Completely dried state after saturation  
( $\beta$ -glucan / Xanthan gum / Cement)

**Figure VI-1 Preliminary injection test procedure**

Figure VI-1 shows the procedure for the preliminary injection test. After fully dried, the clay mixtures were casted into the cracking area at each containers and air dried. As shown in figure VI-1(b), some cracks were generated at the surface of the clay mixtures. Three of soil containers were saturated again from the surface. There was a hole at the bottom of the container to allow drainage through the soil media. After saturation, the soil containers were air dried until moisture does not exist within the soil. Figure VI-1(d) shows the final state of the preliminary injection.

As shown in this figure, at the first container (left), the clay mixture with  $\beta$ -glucan was completely lost its structure within cracking area. This mixture was totally dissolved in water and spread out on the surface of the soil. This mixture was dried out with crack generation at the entire surface area of the soil media. Meanwhile, the clay mixture with xanthan gum was not washed out and maintained own structure as it was casted. Some tiny cracks were generated at the surface of the mixture, but they did not propagated to vertical direction. In addition, the clay mixture with cement proportion was not washed out either, but there was some parts were popped out from the structure because they were contacted to acrylic surface not the natural soil. Consequently, the clay mixture with xanthan gum or cement were not washed out and lost its own structure during the saturation, but the mixture with  $\beta$ -glucan was dissolved and spread out through the soil surface. Thus,  $\beta$ -glucan is not appropriate additives as filling material within fissure areas.

## **Electrical Resistivity Tomography (ERT) measurements for the mixture injected area**

### *The clay mixture injection within desiccation cracking area*

The clay mixture profile was determined following the preliminary injection test result and evaluation of properties of clay mixture investigated in the chapter 4.

Compare to the injection mixture which was applied in the previous research by Kim, the proportion of cement is decreased from 20% to 10% and fine-grained soil portion is increased as amount of cement ratio reduction. The water content value is also decreased dramatically by application of superplasticizer. This value is decreased from 120~150% to 90%. It is also expected to prevent excessive shrinkage. In addition, Xanthan gum biopolymer is also included to reinforce the strength of clay mixture, to prevent washing out of the mixture, and to minimize the crack propagation. Table VI-2 shows the detailed proportion of each components and additives for the clay mixture.

**Table VI-2 The clay mixture component and additive composition**

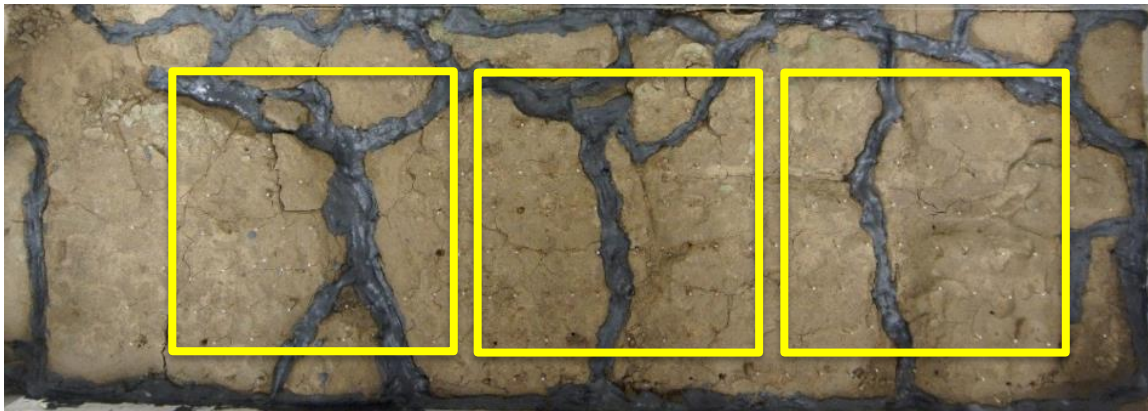
Main components (%)			Additives (%)			W/C (%)
Kaolinite	Graphite	Cement	$\beta$ -glucan	Xanthan-gum	SP	
60.00	30.00	10.00		0.3	1.50	90.00

### *ERT result of the soil with clay mixture injection within crack networks*

The clay mixture was mixed following the ingredient profile and casted into the desiccation cracking area of section B. As discussed in the Chapter V, the initial state of section B was slurry state with high water content and low density. The cracking potential was much higher than compacted soil of section A and complex crack networks



were propagated as expected. To explore whether the clay mixture is injected effectively and to compare permeability reduction effect, the mixture was only applied for the section B. The clay mixture was injected within crack networks from the surface using a disposable syringe.

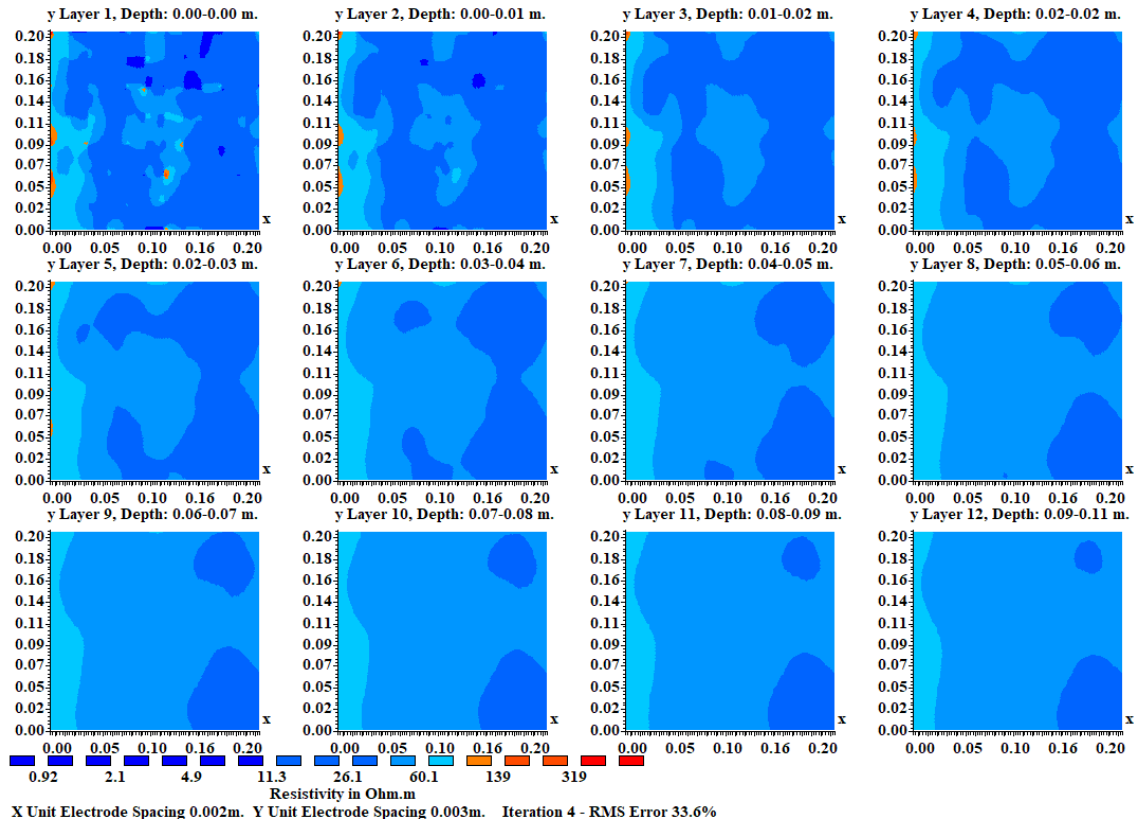


**Figure VI-2 Surface image of section B after the clay mixture injection and area selection**

Figure VI-2 shows the top view of section B after the clay mixture injection. The clay mixture was filled into the syringe and casted within the crack networks. The mixture color is dark gray because the graphite is black-colored material and control the base color of the clay mixture. The clay mixture was allowed to air drying until fully dehydrated. The electrodes were installed at the surface of the soil corresponding to the selected areas which were measured on the previous stage (phase 3).

Electrical Resistivity Tomography (ERT) measurements were conducted for selected areas. Figure VI-3 shows the ERT results from first area of section B. As shown in this figure, the electrical resistivity values of crack networks were decreased

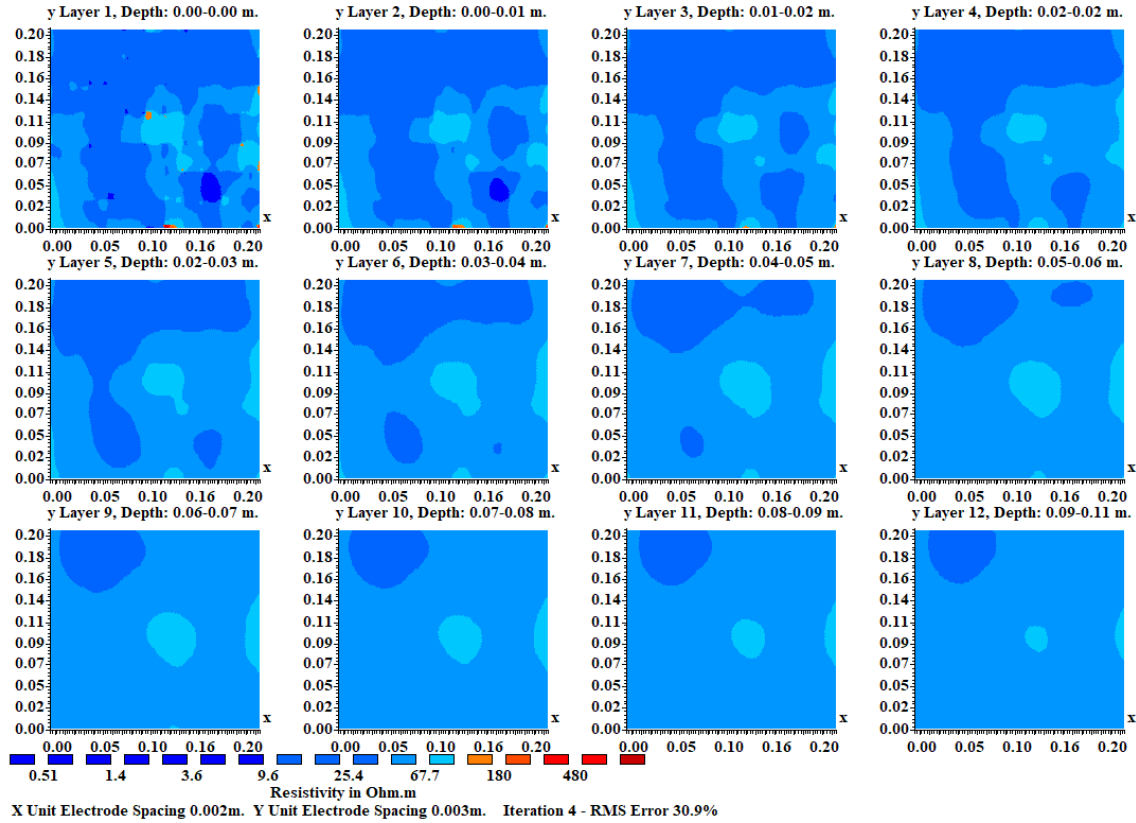
drastically. It implies that the clay mixture was penetrated within cracking area successfully. The electrical resistivity value of treated area is relatively lower than that of the natural soil territory. The average electrical resistivity value was decreased corresponding to filling of the crack with the clay mixture.



**Figure VI-3 ERT result of mixture injected area (B1)**

Figure VI-4 shows the ERT results from second area of section B. As analyzed on the chapter V, there was a linear crack network at the center of this area and some traces remained surround it. As shown in figure VI-4, the crack networks were completely filled with high conductivity materials and the remained trace of old crack

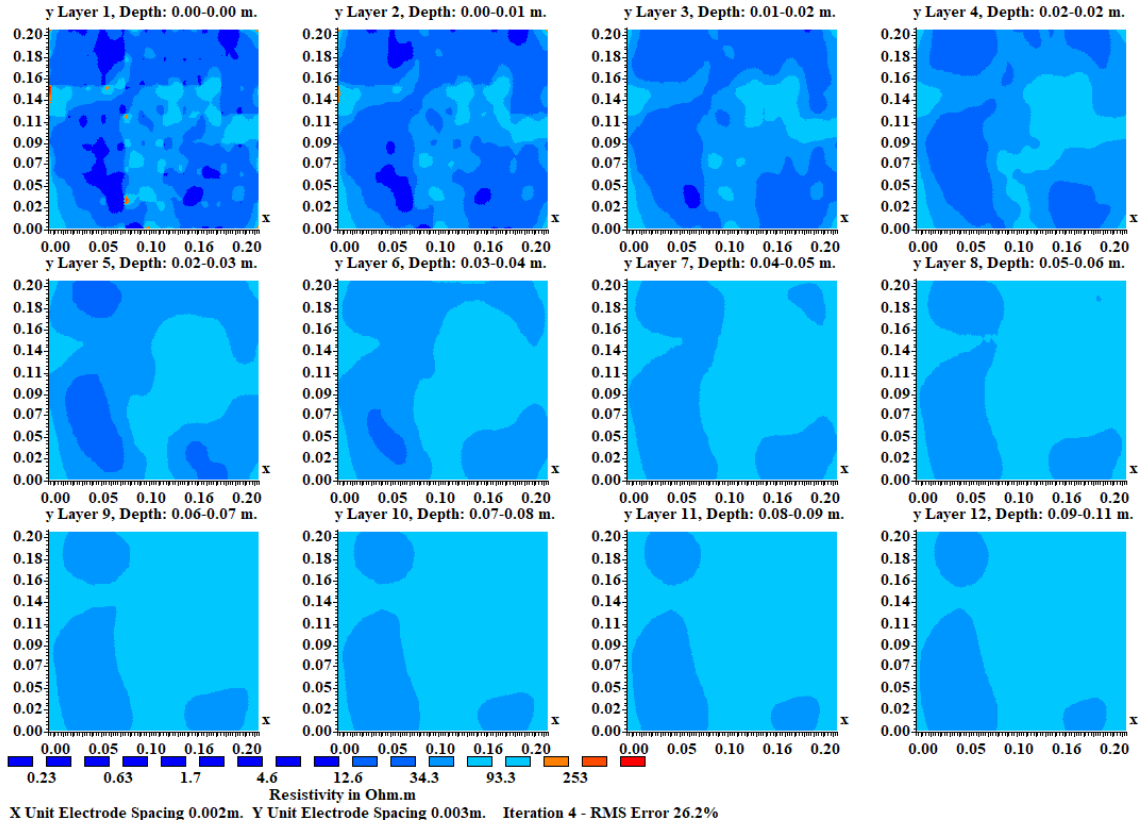
was expressed as relatively higher values. The clay mixture was successfully applied also in this area.



**Figure VI-4 ERT result of mixture injected area (B2)**

Third area of section B was monitored continuously from the beginning of this research. The crack networks are more complex than the other territories and this network was changed significantly at each stage of wetting-drying process. This area was the most defected area compared to the other territories. As shown in figure VI-5, the entire crack network was filled with the clay mixture successfully. The trace of old crack were still remained at the surface of this area, so this domain was expressed with

relatively high electrical resistivity values. As a result, the clay mixture was completely injected into the desiccation crack networks on section B as monitored with ERT measurements.

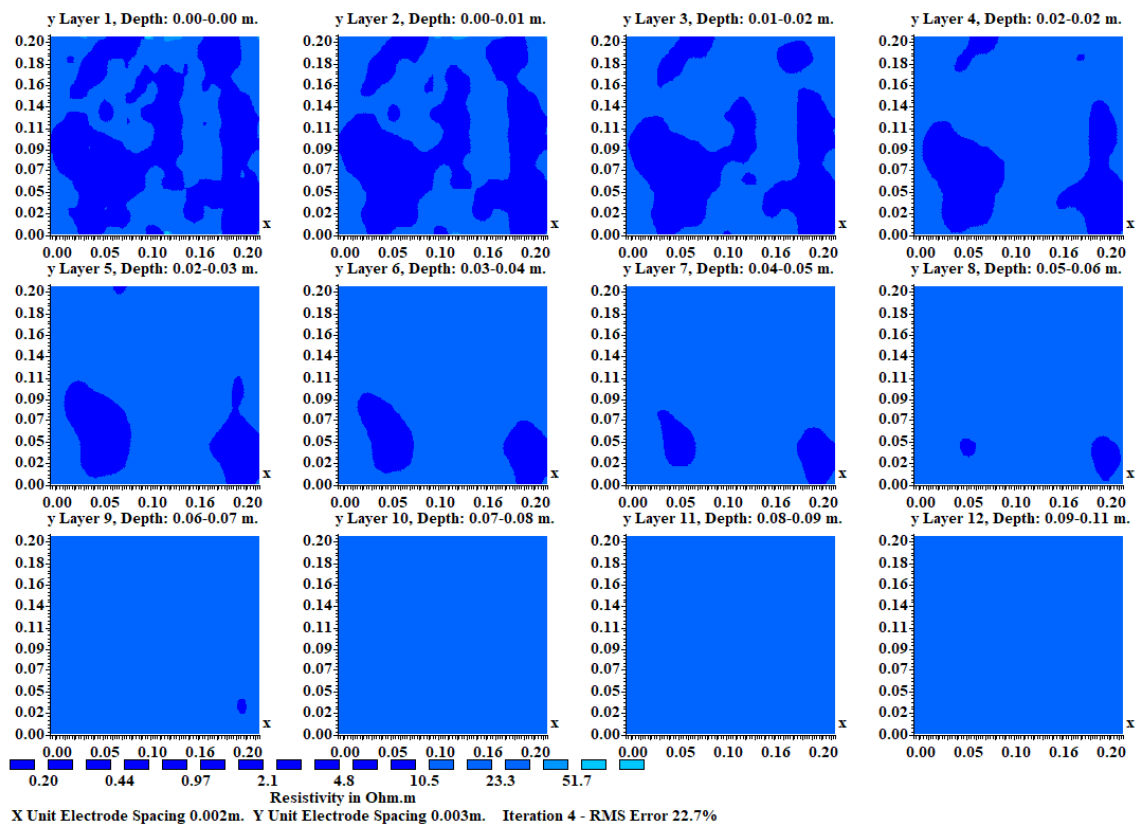


After ERT measurements, all of electrodes were extracted from the soil surface and the natural soil was saturated from the surface. There was a two purpose for this saturation. The permeability test was conducted to validate the hydraulic conductivity decrease effect of the clay mixture injection. Also, washing out of the clay mixture after saturation was monitored by surface observation. Figure VI-6 shows the surface image of section B right after saturation. As shown in this figure, the most of clay mixture

structure was remained at the injected area. The clay mixture was not washed out or dissolved. Some area was covered with the natural soil of surrounding domains.

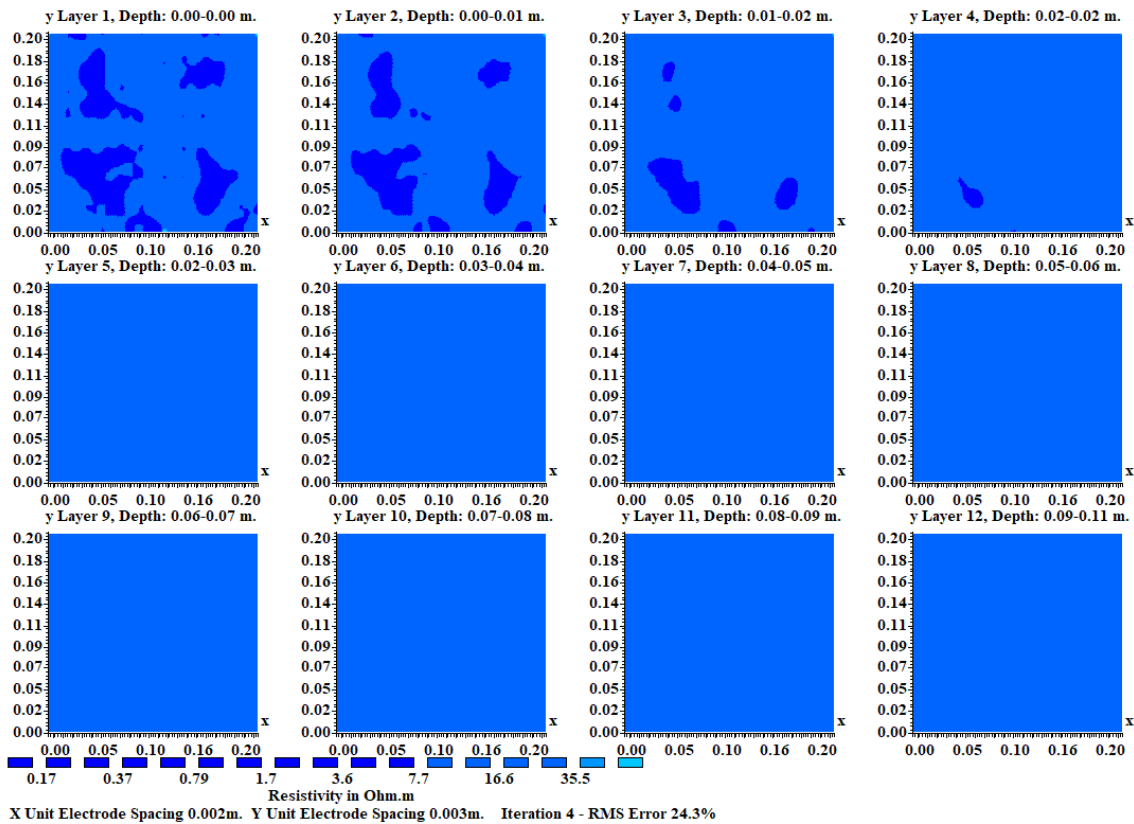


**Figure VI-6 Surface image of section B after permeability test**



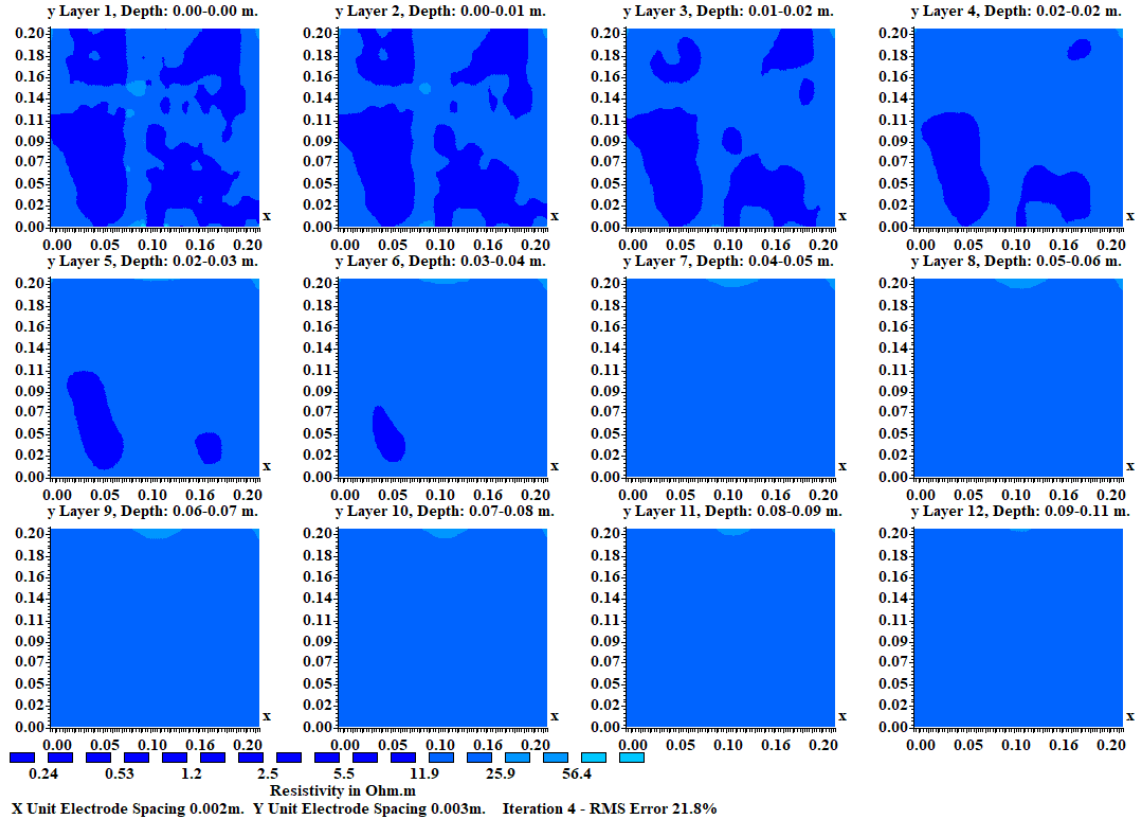
**Figure VI-7 ERT result of mixture injected area after saturation (B1)**

The ERT measurements were carried out after the stabilization of the soil surface. This measurements were conducted on almost same target area which is corresponding to former investigations. The first area was monitored as shown in figure VI-7. The clay mixture injected area was expressed as very low electrical resistivity less than 10 ohm · m. The electrical resistivity value of the natural soil was also low (less than 30), but this value is higher than the clay mixtures. As discussed before in the chapter of 5, the electrical resistivity value range was decreased compared to the dry state because of the existence of moisture within the void area of soil and clay mixtures.



**Figure VI-8 ERT result of mixture injected area after saturation (B2)**

Figure VI-8 shows the ERT result from second area. This area was also monitored with very low value of the electrical resistivity. The contrast between the clay mixture and the natural soil is not obvious, but both of them was low enough.



**Figure VI-9 ERT result of mixture injected area after saturation (B3)**

As shown in figure VI-9, third area of section B was also monitored with low value of the electrical resistivity. Especially on low depth area (0~2cm), relatively high range of the electrical resistivity value is corresponded to the trace of old cracks. These cracks were remained during several wetting-drying process and it forms some kind of valley domains. At the beginning of this research, the initial state of the natural soil

surface was flat because this condition was intended. Repetition of wetting-drying cycle caused significant change in the crack networks and remained trace of old cracks created some kind of topography with different elevation to surrounded domains. However, in this research with ERT measurements, the elevation of surface ground could not be considered and just expressed with relatively higher value of the electrical resistivity compared to surrounded area. To overcome this limitation, the further research with the ERT measurement could be better if this investigation is collaborated with geography data.

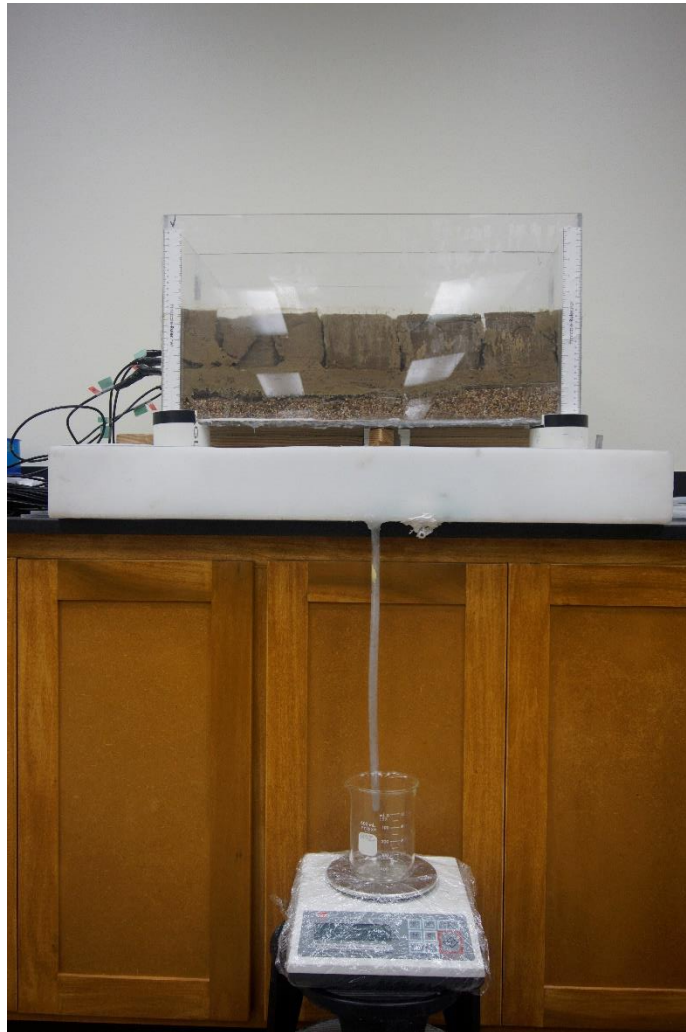
### **Permeability test with the phase of drying-wetting cycle**

#### *Permeability test setup and procedure*

Permeability test was conducted for the natural soil in the desiccation container at each phase of wetting process. At the initial stage, the natural soil was intact, so low range of permeability was expected. Considering this circumstance, the falling head test was applied for initial condition of the natural soils. On the other hand, further phases of the soil condition was damaged by repetition of drying-wetting cycle. The constant head test was examined for the natural soil at these phases. Several holes with regular spacing were drilled at the bottom of the desiccation soil container to allow the drainage through the soil media. The soil container was supported by four columns at each edge of the rectangular box. Drainage tank was located below the columns and this tank covered entire area of the desiccation soil container. The drainage hole was at the tank was connected to the silicon tube and the drained water was collected at the end of the tube



by bicker on the balance. Figure VI-10 shows the constant head test setup for the desiccation soil container.







**Figure VI-10 Constant head test setup**

*Permeability test result of section A*

The natural soil of section A was prepared to realize the condition of compacted soil with 90% of relative compaction. This soil was relatively dense with intact surface,

so the falling head test was conducted at the initial phase. The soil container was filled with water and the top of the acrylic box was completely sealed to prevent dehydration at the surface of water. Table VI-2 shows detailed measurements and the permeability calculated. The permeability was evaluated as  $4.63 \times 10^{-6} \text{ cm/s}$  and this value is very low value. The soil was categorized as silt or silty clay with permeability.

**Table VI-3 Permeability test for section A at the initial phase (Falling head test)**

				
<b>Date &amp; Time</b>	3/29 14:30	3/30 14:30	3/31 14:30	4/1 14:30
<b>h (cm)</b>	1.85	1.45	1.05	0.65
<b><math>\Delta h</math> (cm)</b>		0.4	0.4	0.4
<b><math>\Delta t</math> (sec)</b>		86400	86400	86400
<b>k (cm/sec)</b>		$4.63 \times 10^{-6}$	$4.63 \times 10^{-6}$	$4.63 \times 10^{-6}$

The natural soil on section A was under drying-wetting process within the phase of 2 and 3, and additional permeability test was conducted at the beginning of the phase 4 (3<sup>rd</sup> re-saturation). Desiccation cracks on soil were propagated and the constant head test was conducted for this section because the increase of permeability was expected compared to the intact state. Table VI-3 shows the permeability test result. Compare to the intact soil, the permeability was increased significantly in the degree of  $10^2$ . As shown in table VI-3, permeability value was decreased with time, and it implies that the desiccation crack network within subsurface area was closed during the saturation and it affected to the hydraulic conductivity of soil.

**Table VI-4 Permeability test result for section A at the phase 4 (Constant head test)**

<b>t (sec)</b>	<b>Q (ml)</b>	<b>Q (cm<sup>3</sup>)</b>	<b>L (cm)</b>	<b>h (cm)</b>	<b>A (cm<sup>2</sup>)</b>	<b>k (cm/sec)</b>
3492	500	500	12.7	2.54	1386	5.165E-04
3523	500	500	12.7	2.54	1386	5.120E-04
3540	500	500	12.7	2.54	1386	5.095E-04
					<b>Average k</b>	5.127E-04

The average value of permeability is  $5.127 \times 10^{-4}$  cm/sec. With this value, the soil was categorized silty soil with low permeability. As a result, the desiccation cracking increased the permeability of the soil media and caused the soil to weaken in terms of density with hydraulic conductivity.

*Permeability test result of section B*

The natural soil of section B was slurry state at initial state with 60% of water contents. This value is corresponding to the 150% of liquid limit of the natural soil. The falling head test was conducted also on this section, the soil container was filled with water and top of the acrylic container was entirely covered to prevent evaporation of water from the surface.

**Table VI-5 Permeability test for section B at the initial phase (Falling head test)**


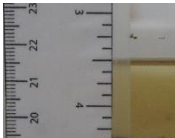


				
<b>Date &amp; Time</b>	3/21 14:06	3/22 15:22	3/23 09:33	3/26 09:41
<b>h (cm)</b>	22.22	21.60	21.10	19.60
<b>Δh (cm)</b>		0.6	0.5	1.5
<b>Δt (sec)</b>		90960	65460	259680
<b>k (cm/sec)</b>		$6.60 \times 10^{-6}$	$7.64 \times 10^{-6}$	$5.78 \times 10^{-6}$

Table VI-4 shows the measured values from the permeability test. The permeability was calculated as  $6.67 \times 10^{-6}$  cm/sec, and this value is slightly higher than

compacted soil on section A. This soil also categorized as silt or silty clay in terms of permeability.

The natural soil on section B was also under drying-wetting process within phase of 2 and 3, and additional permeability test was conducted at the beginning of each phase. (1<sup>st</sup> and 2<sup>nd</sup> re-saturation). A complicated fissure networks were developed within subsurface area on section B, so the permeability was expected as increased significantly compared to the intact condition. Table VI-5 shows the permeability test result. Because of the fissure networks propagated to the entire depth of the natural soil, the permeability was increased drastically in the degree of  $10^4$ . This test was conducted at the early stage of saturation process and the crack networks closed gradually with time duration of saturation, but the further test was not conducted. The permeability of the natural soil after crack closed would be much lower than the permeability at the early period of saturation.

**Table VI-6 Permeability test result for section B at the phase 2 (Constant head test)**

<b>t (sec)</b>	<b>Q (ml)</b>	<b>Q (cm<sup>3</sup>)</b>	<b>L (cm)</b>	<b>h (cm)</b>	<b>A (cm<sup>2</sup>)</b>	<b>k (cm/sec)</b>
155	500	500	12.7	2.54	1386	1.164E-02
157	500	500	12.7	2.54	1386	1.149E-02
160	500	500	12.7	2.54	1386	1.127E-02
					<b>Average k</b>	1.147E-02

The permeability test was conducted again during 2<sup>nd</sup> re-saturation process (phase 3). In this case, preliminary saturation was carried out until the surface crack was closed. Table VI-6 shows the permeability test of section B in the phase 3. Permeability

was decreased compared to the phase 2, because this test was conducted after the closure of the surface cracks. However, this value is also higher than that of intact condition soil, because the fissure network within subsurface area allows the infiltration of water easily. As shown in table VI-7, permeability was decreased gradually with test execution, it implies that the crack network within subsurface area was closed under saturated condition and it decreased the permeability directly.

**Table VI-7 Permeability test result for section B at the phase 3 (Constant head test)**

<b>t (sec)</b>	<b>Q (ml)</b>	<b>Q (cm<sup>3</sup>)</b>	<b>L (cm)</b>	<b>h (cm)</b>	<b>A (cm<sup>2</sup>)</b>	<b>k (cm/sec)</b>
273	500	500	12.7	2.54	1386	6.607E-03
320	500	500	12.7	2.54	1386	5.637E-03
352	500	500	12.7	2.54	1386	5.124E-03
					<b>Average k</b>	5.789E-03

The clay mixture was injected within fissure network area of section B, and the permeability test was conducted after the clay mixture was completely dried. As expected, due to the clay mixture injection within cracking area, the permeability was decreased significantly compared to former phases. The permeability was decreased in the degree of 10 with the clay mixture injection. Table VI-8 shows the results from the permeability test. Permeability was decreased with time, because the closure of the crack which was not developed at the surface (the clay mixture was not injected). Thus, the clay mixture injection is effective to reduce the permeability of soil with closing of void area and densification of adjacent soil.

**Table VI-8 Permeability test result for section B after injection (Constant head test)**

<b>t (sec)</b>	<b>Q (ml)</b>	<b>Q (cm<sup>3</sup>)</b>	<b>L (cm)</b>	<b>h (cm)</b>	<b>A (cm<sup>2</sup>)</b>	<b>k (cm/sec)</b>
3202	500	500	12.7	2.54	1386	5.633E-04
3234	500	500	12.7	2.54	1386	5.577E-04
3256	500	500	12.7	2.54	1386	5.540E-04
					<b>Average k</b>	5.583E-04

*Discussion of the permeability test results*

The several cases of the permeability test were conducted for the natural soil on both section A and B. The results from the tests is shown in table VI-9. In both cases, the permeability was increased significantly by desiccation cracking, especially it was remarkable on the section B with more complex fissure networks. At the early stage of saturation, the permeability value was much higher which could be regarded as sand layer. As time passed during the saturation, the crack networks started to be closed from the surface, and the permeability was decreased with this phenomenon. The clay mixture injection was applied to the section B, and the permeability values was decreased dramatically with this treatment. Fissure networks were closed and adjacent soil was densified by injection of filling materials. As a results, the clay mixture injection within the desiccation cracking area can be effective to decrease the hydraulic conductivity of soil media.

**Table VI-9 Overall permeability test results**

<b>Section A</b>	<b>k (cm/sec)</b>	<b>Section B</b>	<b>k (cm/sec)</b>
<b>Phase 1 (Initial)</b>	$4.63 \times 10^{-6}$	<b>Phase 1 (Initial)</b>	$6.67 \times 10^{-6}$
<b>Phase 4</b>	$5.13 \times 10^{-4}$	<b>Phase 2</b>	$1.15 \times 10^{-2}$
		<b>Phase 3</b>	$5.79 \times 10^{-3}$
		<b>Phase 4 (Injected)</b>	$5.58 \times 10^{-4}$

### **Direct shear test for soil-clay mixture structure**

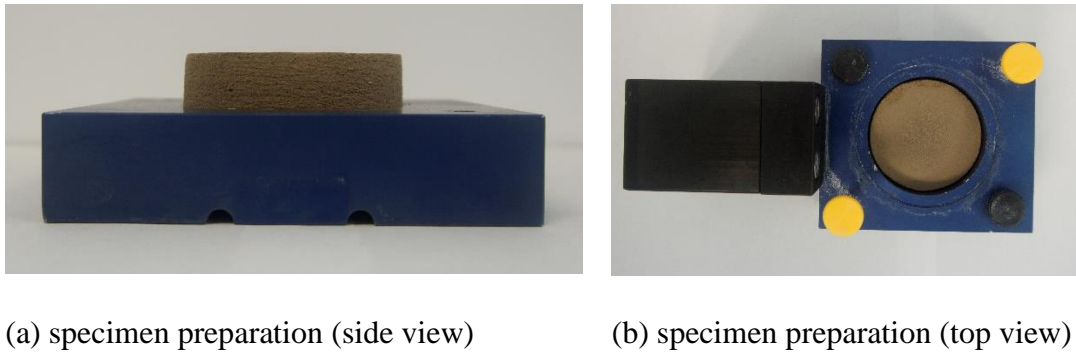
#### *Test setup and procedure*

For the direct shear test, the samples were prepared using PVC circular container. To prepare the free shrunk circular specimen for the direct shear test, one of the circular plate was treated with Vaseline at the inside perimeter. Another one was prepared under friction condition, so desiccation crack was generated and treated with the clay mixture injection. Two types of specimen represents the natural soil only structure and the natural soil with clay mixture injection, respectively. The aim of this condition, the strengthening effect of the clay mixture injection can be evaluated by this experiment. The prepared samples were fully dried and trimmed using the consolidation mold with the specified dimensions ( $d = 2.5\text{in.}$ ,  $h = 1\text{in.}$ ). Figure VI-11 shows the test specimen in the direct shear mold.

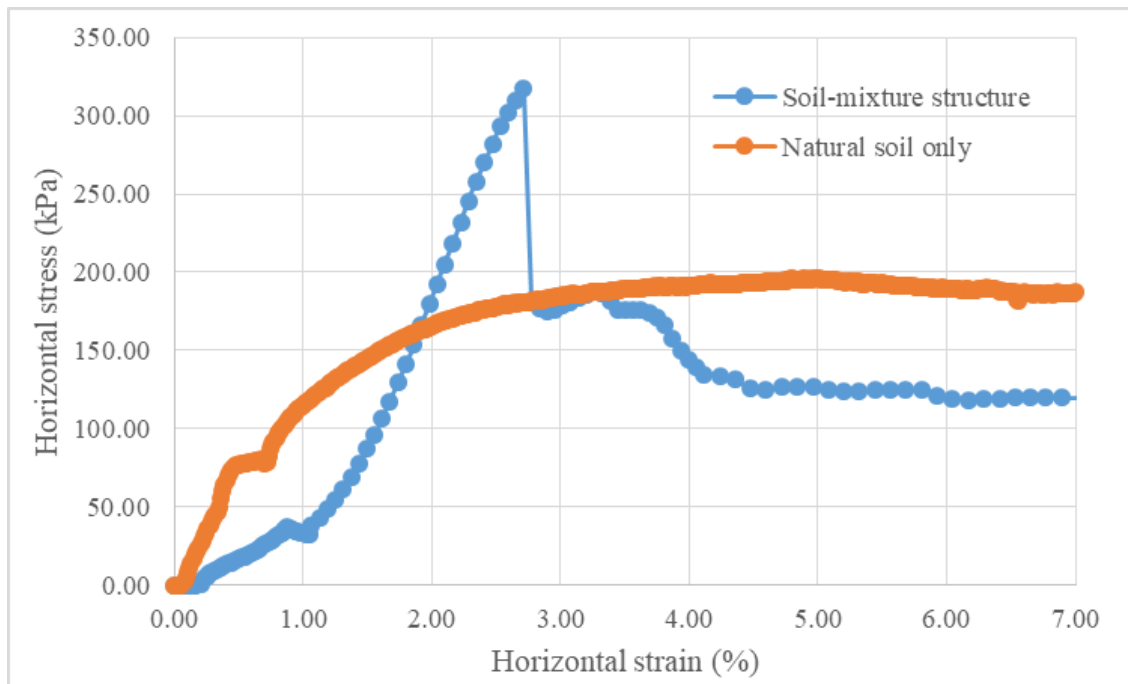


### *Direct shear test results*

Direct shear test was conducted using GEOTAC instruments in RELLIS campus. Two tests were conducted for each specimen and the confining vertical stress was 250 kPa for both cases. Figure VI-12 shows the result from direct shear tests.



**Figure VI-11 Test specimen preparation for the direct shear test**



**Figure VI-12 Direct shear test results**

As shown in this figure, the horizontal stress of the soil-mixture structure was much higher than that of the natural soil. The horizontal strength of soil-mixture structure was 317.07 kPa at 2.71% of peak strain, and the horizontal strength of the natural soil was 196.39 kPa at 5.00% of peak strain. According to the test results, the soil-mixture structure has larger shear strength than the natural soil, but residual stress was lower than that after failure.

### **Soil structure exploration with dismantlement**

The desiccation soil container was air dried after the permeability test at the phase 4. Especially on the section B, the surface area was monitored until completely dried to explore the change of soil surface with injected clay mixture. Figure VI-13 shows the surface of section B which is completely dried state. As shown in this figure, there were several tiny cracks generated from the surface. Some cracks were developed at the boundary of soil and mixture, and there were some fissures propagated within the natural soil territories and the trace of old cracks.



**Figure VI-13 Surface image of section B after completely dried**

The width of these cracks were less than 1mm. For the investigation of subsurface area with injected clay mixture, the desiccation soil container was dismantled from the surface.



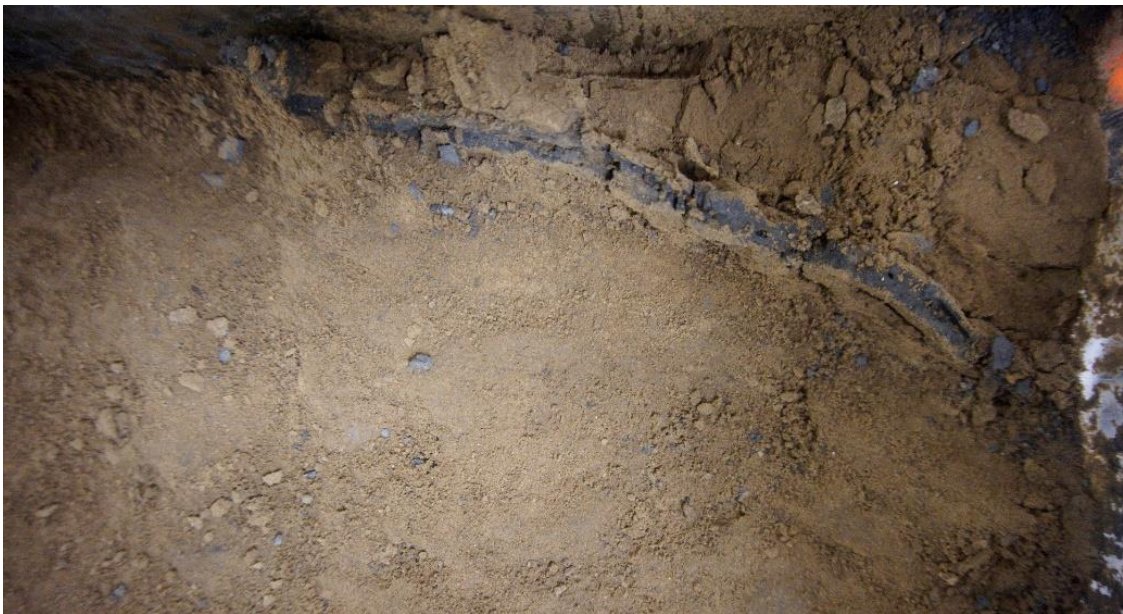
**Figure VI-14 Boundary of the natural soil and the clay mixture (B2)**

The soil structure was sliced vertically and dismantled from surface area to explore the contact area between the natural soil and injected clay mixture. Figure VI-14 and 6.15 show the contact surface of two structures. As shown in these figures, the clay mixture was successfully penetrated into the crack networks and maintained its own structure with surrounding soils. Especially on the right edge of the section B (Figure VI-15), deep and large scale desiccation crack was monitored and filled with the clay mixtures monitored by Electrical Resistivity Tomography (ERT) measurements.





**Figure VI-15 Boundary of the natural soil and the clay mixture (B3)**



**Figure VI-16 Injected clay mixture structure (B3)**

As shown in figure VI-16, the clay mixture was injected properly in vertical direction and retained own structure even though the surrounded soils were excavated. As a result, the clay mixture was injected well through the fissure networks and it maintained own structure without failure. Thus, the clay mixture injection could be a practical solution for the damaged soil structure by desiccation cracking or fissure networks.

### **Summary and conclusions**

In this chapter, several types of experiments were conducted to examine the applicability of the clay mixture as filling material within desiccation cracking area. Preliminary injection, ERT measurements for the soil with clay mixture injection, series of permeability test, direct shear test, and observation of the clay mixture with dismantlement were performed, and the following results were obtained.

1. The clay mixture with xanthan gum or cement were not washed out and lost its own structure during the saturation, but the mixture with  $\beta$ -glucan was dissolved and spread out through the soil surface. Thus,  $\beta$ -glucan is not appropriate additives as filling material within fissure areas. Following these results, filling material profile was designed with specific proportion of each components. Main components are kaolinite (60%), graphite (30%), and cement (10%) with water content of 90%. In addition, xanthan gum biopolymer (0.3%) and superplasticizer (1.5%) were applied as additives.

The clay mixture was mixed following these specification and injected to desiccation crack area in the soil container to assess the applicability.

2. ERT measurements were conducted to compare the electrical resistivity change with the clay mixture injection. The clay mixture was injected completely and it was monitored as significant reduction of the electrical resistivity within fissure networks. After the saturation, it was investigated by ERT measurements that the clay mixture within cracking area was not washed out and maintained its structure.
3. In both cases, the permeability was increased significantly by desiccation cracking, especially it was remarkable on the section B with more complex fissure networks. At the early stage of saturation, the permeability value was much higher which could be regarded as sand layer. As time passed during the saturation, the crack networks started to be closed from the surface, and the permeability was decreased with this phenomenon. The clay mixture injection was applied to the section B, and the permeability values was decreased dramatically with this treatment. Fissure networks were closed and adjacent soil was densified by injection of filling materials. As a results, the clay mixture injection within the desiccation cracking area can be effective to decrease the hydraulic conductivity of soil media.
4. Direct shear test was conducted for the natural soil only specimen and the soil with clay mixture structure. The shear strength of the soil-clay mixture was larger than that of the natural soil, but the residual stress was relatively lower.

The clay mixture injection could be an acceptable choice in the aspect of strengthening.

5. As the final procedure, the desiccation soil container was dismantled for the visual observation of the natural soil and the clay mixture structure below the surface. The soil structure was sliced vertically with certain depth, and dismantled from the surface to the bottom of the container. According to the visual observation of the soil, the clay mixture was successfully injected within cracking area and maintained its own structure. Also, it was observed the well-bonded contact surface between the natural soil and the clay mixture.

## CHAPTER VII

### CONCLUSIONS

This dissertation has investigated how to enhance the Electrical Resistivity Tomography (ERT) technique for the exploration of the soil subsurface with a crack network triggered by a drying process and has also study the use of clay mixtures as potential remedial solution for improving cracked soils properties. With this aim, preliminary ERT measurements using kaolinite and Styrofoam block structure was conducted to compare two kinds of miniature arrays. Also, desiccation soil container was prepared with water content probe and drainage system setup to investigate desiccation crack network evolution with drying-wetting cycle. Two types of soil container were prepared with different initial condition, compacted and slurry state, respectively. ERT measurements data was analyzed by inversion process and visualized as three-dimensional images using VOXLER 3D program.

The mechanical and geophysical properties of clay mixture was examined to figure out the characteristics of each components. With this aim, unconfined compression, free shrinkage, flow table tests were carried out to evaluate the physical properties of mixture with various proportion. Also, the four-electrode methods was conducted to measure the electrical conductivity (or resistivity) of the untreated and treated soils. The clay mixture profile was suggested based on these results and applied as filling material within desiccated cracked soil mass. To verify the applicability of clay mixture, preliminary injection using small scale container was conducted to check the



occurrence of washing out, and permeability test and direct shear experiments were carried out to assess the reduction of hydraulic conductivity and strength increment of treated soils.

### **Evaluation of mechanical and geophysical properties of clay mixture as filling material**

The objective of this chapter is the evaluation of mechanical and geophysical properties of clay mixture as remedial solution for desiccation crack area. In the previous research conducted by Kim, clay mixture with carbon black and graphite were washed out by saturation of soil, and the cement was added to prevent this problem. Based on this previous research, the research on the filling material was concentrated (1) reduce the portion of the cement without decrease of strength, (2) reduce the water content to prevent shrinkage and crack occurrence, and (3) enhance the workability and prevent washing out problem. The following conclusions were obtained.

1. Unconfined compression tests were performed to evaluate uniaxial strength, peak strain, and the elastic modulus of different clay mixtures. All components and additives are effective to enhance the compressive strength of the clay mixture, especially Xanthan gum biopolymer is highly efficient (even at small amounts). Xanthan gum biopolymer can be applied as a material to compensate the decrease in cement content from 20% to 10%.
2. Flow table test were conducted to evaluate the workability of the clay mixture. A superplasticizer was chosen for the enhancement of the fluidity of the mixture

and it is proved that this additive is very effective when interacting with cement. Thus, cement is required to apply the superplasticizer and maximize the workability. Biopolymers and graphite decreased the workability of the mixture, but it can be overcoming by application of cement and superplasticizer. To satisfy the workability criteria, Xanthan gum biopolymer percentage is suggested to be 0.3% in mass, which implied an improvement of 110% of flow.

3. Free shrinkage test was carried out to evaluate the volumetric strain with various component of the clay mixture. All of components and additives are effective on reducing the volumetric shrinkage, but the cement is the most critical to minimize the shrinkage. Biopolymers are also working as a shrinkage reducing agent, especially  $\beta$ -glucan is slightly better than Xanthan gum when evaluating volumetric shrinkage.
4. Four-electrode method was applied to evaluate the electrical resistivity (or conductivity) of the clay mixture considering different mixture percentages. The electrical resistivity values changed with the state of the mixture related to water content. Initial, minimum, and the final values are analyzed from the different type of the clay mixtures. Graphite is the highly electrically conductive material and it is the most effective in reducing the electrical resistivity of the clay mixture. Cement and biopolymers are also efficient to enhance the electrical conductivity of the clay mixture with chemical interaction between polymers and clay particles, but this is not enough comparing to graphite. Thus, to trace the

clay mixture within desiccation cracking area, graphite is the key component in relation to electrical conductivity.

### **Electrical Resistivity Tomography (ERT) technique for mapping of desiccation crack network within subsurface crack area**

In this study, a series of the Electrical Resistivity Tomography (ERT) measurements were performed to monitor the subsurface area with desiccation crack network under various circumstances. Preliminary ERT measurements using Styrofoam and electrical resistivity measurements for the natural soil subjected to drying were conducted, and the following results were obtained.

1. The preliminary ERT measurements were conducted using Styrofoam blocks structure to examine two methods for the miniature test, namely, Schlumberger and Dipole-Dipole arrays. The Schlumberger array method is much more sensitive to vertical profile of electrical resistivity comparing to the Dipole-Dipole one. The Dipole-Dipole array is relatively more sensitive to detect horizontal mapping at the surface area, but the coverage for the vertical depth was quite poor. For the miniature array test at laboratory scale desiccation soil container, it was concluded that the Schlumberger array is a more appropriate method for the detection of the desiccation crack network of subsurface area.
2. The Electrical Resistivity Tomography (ERT) measurements were conducted in the selected area at the section A to investigate the crack network and propagation with repetition of drying-wetting process. The crack networks

developed from the surface were detected properly with ERT measurements, but the relatively small width cracks (i.e. less than 2mm) were not detected. Also, the crack network was developed in both directions, horizontal and vertical during successive drying-wetting cycles and the fissure networks tended to connect with adjacent small cracks. The existence of the moisture within the soil reduces the average value of the electrical resistivity of the soil.

3. The Electrical Resistivity Tomography (ERT) measurements were conducted in the selected area of section B (i.e. slurry soil) to monitor the fissure network and propagation with repetition of drying-wetting cycles. The crack networks were more complex compared to the compacted soil. The width of the crack was relatively larger than that of section A (i.e. compacted soil), the cracks were propagated both horizontally and vertically. In addition, cracks closed during water in filtration and wetting of the surrounded soil. The trace remained as a low resistivity area. To investigate with detailed stereoscopic view of the subsurface area, a three-dimensional visualization tool was developed using the software VOXLER 3D. This tool was used to process and to produce multiple two-dimensional and three-dimensional images that enables a better analysis of the problem. The standardization of the contour values allows the consistency of the electrical resistivity analysis.

### **Applicability of the clay mixture as filling material for subsurface crack area**

Several types of experiments were conducted to examine the applicability of the clay mixture as a filling material within desiccation crack volume. Preliminary injection, ERT measurements for the soil with clay mixture injection, series of permeability test, direct shear test, and observation of the clay mixture during dismantling were conducted. The following results were obtained.

1. The clay mixture with xanthan gum or cement were not washed out during soaking and they didn't lose their structure during the saturation, but the mixture with  $\beta$ -glucan was dissolved and spread out through the soil surface. Thus,  $\beta$ -glucan is not an appropriate additive to be used as filling material within fissure areas. Based on these results, the filling material was designed with an optimized contribution from each ingredient. The main components adopted are: kaolinite (60%), graphite (30%), and cement (10%) with water content of 90%. In addition, xanthan gum biopolymer (0.3%) and superplasticizer (1.5%) were included as additives. The clay mixture was mixed following these specifications and injected to desiccation crack area in the soil container to assess their applicability.
2. ERT measurements were conducted to compare the electrical resistivity change by the clay mixture injection. The clay mixture was injected attempting to fill-in all the crack. The ERT monitoring shows a significant reduction of the electrical resistivity within fissure networks. After the saturation, the ERT measurements

show that the clay mixture within the cracking area was not washed out and maintained its structure.

3. In both cases, the permeability was increased significantly by desiccation cracking, especially it was remarkable on the section B with more complex fissure networks. At the early stage of saturation, the permeability value was much higher (i.e. close to a sandy soil). As time passed by during the saturation, the crack networks started to close out from the surface, and consequently the permeability decreased because of this phenomenon. The clay mixture injection was applied to the section B, and the permeability values was decreased dramatically with this treatment. Fissure networks were closed and adjacent soil was densified by injection of filling materials. As a result, the clay mixture injection within the desiccation cracking area can be considered as an effective treatment to decrease the hydraulic conductivity of a cracked soil mass.
4. Direct shear tests were conducted for the natural soil only specimen and the soil with clay mixture structure. The shear strength of the soil-clay mixture was larger than that of the natural soil, but the residual stress was relatively lower. The bonding between filling mixture and natural soil can be considered excellent and the injection increased the strength of the treated soil.
5. Finally, the desiccated treated soil container was dismantled for the visual observation of the natural soil and the clay mixture structure below the surface. The soil structure was sliced vertically at pre-established depth intervals, and dismantled from the surface to the bottom of the container. According to the

visual observation of the soil, the clay mixture was successfully injected within cracking area and maintained the initial mixture structure. Also, it was observed an excellent bonding at the contact between the natural soil and the clay mixture.

### **Future works**

1. Enhancement of the clay mixtures as possible remedial solutions with several kind of biopolymers considering environmental aspects and cost
2. Verification of applicability of the clay mixture injection within cracked area in the field (e.g. water embankment and tunnel)
3. Economic evaluation of the clay mixture associated with the field applicability and carbon reduction by using the eco-friendly materials
4. Enhancement of the Electrical Resistivity Tomography (ERT) technique to investigate the desiccation cracks network in soils more precisely in the aspects of dimension

## REFERENCES

- Albrecht, B. A., & Benson, C. H. (2001). Effect of desiccation on compacted natural clays. *Journal of Geotechnical & Geoenvironmental Engineering*, 127(1), 67-75.
- Albright, W. H., Benson, C. H., Gee, G. W., Abichou, T., McDonald, E. V., Tyler, S. W., & Rock, S. A. (2006). Field performance of a compacted clay landfill final cover at a humid site. *Journal of Geotechnical & Geoenvironmental Engineering*, 132(11), 1393-1403.
- Alonso, S., & Palomo, A. (2001). Alkaline activation of metakaolin and calcium hydroxide mixtures: influence of temperature, activator concentration and solids ratio. *Materials Letters*, 47(1), 55-62.
- Atique, A., Sanchez, M., & Romero, E. (2009). Investigation of crack desiccation in soil from a flood protection embankment. *CRC Press*, 413-418.
- Barker, R.D., 1979. Signal contribution sections and their use in resistivity studies. *Geophysics* 59 (1), 123–129.
- Cardimona, S. (2002). Electrical resistivity techniques for subsurface investigation. Paper presented at the Geophysics 2002 conference, Los Angeles, California, USA.
- Casas, J. A., Santos, V. E., & García-Ochoa, F. (2000). Xanthan gum production under several operational conditions: molecular structure and rheological properties☆. *Enzyme and Microbial Technology*, 26(2), 282-291.



- Chang, I., & Cho, G. C. (2014). Geotechnical behavior of a beta-1, 3/1, 6-glucan biopolymer-treated residual soil. *Geomechanics and Engineering*, 7(6), 633-647.
- Chang, I., Im, J., Prasidhi, A. K., & Cho, G. C. (2015). Effects of Xanthan gum biopolymer on soil strengthening. *Construction and Building Materials*, 74, 65-72.
- Comba, S., & Sethi, R. (2009). Stabilization of highly concentrated suspensions of iron nanoparticles using shear-thinning gels of xanthan gum. *Water Research*, 43(15), 3717-3726.
- Costa, S., & Kodikara, J. (2008). Modelling of Desiccation Crack Development in Clay Soils. Paper presented at the The 12th International Conference of IACMAG, Goa, India.
- Costa, S., Kodikara, J., & Thusyanthan, N. I. (2008). Study of desiccation crack evolution using image analysis. Paper presented at the First European Conference on Unsaturated Soils.
- Daniel, D. E. W., Y-K. (1993). Compacted clay liners and covers for arid sites. *Journal of Geotechnical Engineering*, 119(2), 223-237.
- Davidovits, J. (2008). *Geopolymer. Chemistry and Applications*. Institute Geopolymere, Saint-Quentin, France.
- Davidson, R. L. (1980). *Handbook of water-soluble gums and resins*.
- Depountis, N., Harris, C., & Davies, M. C. R. (1999). The application of miniaturised electrical imaging in scaled centrifuge modelling of pollution plume migration.

- Paper presented at the 2nd BGS international geoenvironment engineering conference, London.
- Dyer, M. R., Utili, S., & Zielinski, M. (2009). Field study into fine desiccation fissuring at Thorngumbald. Paper presented at the Water management (WM3).
- Fang, M., Wang, K., Lu, H., Yang, Y., & Nutt, S. (2009). Covalent polymer functionalization of graphene nanosheets and mechanical properties of composites. *Journal of Materials Chemistry*, 19(38), 7098-7105.
- Gachet, P., Klubertanz, G., Vulliet, L., & Laloui, L. (2003). Interfacial Behavior of Unsaturated Soil with Small-scale Models and Use of Image Processing Techniques. *Geotechnical Testing Journal*, 26(1), 12-21.
- Gallipoli, D., & Perlot, C. (2017). Mechanical properties of biopolymer-stabilised soil-based construction materials. *Géotechnique Letters*, 7(4), 1-18.
- Giannelis, E. P. (1996). Polymer Layered Silicated Nanocomposites. *Advanced Materials*, 8(1), 29-35.
- Gong, X., Liu, J., Baskaran, S., Voise, R. D., & Young, J. S. (2000). Surfactant-Assisted Processing of Carbon Nanotube/Polymer Composites. *Chemistry of Materials*, 12(4), 1049-1052.
- Horgan, G. (1998). Mathematical morphology for analysing soil structure from images. *European Journal of Soil Science*, 49(2), 161-173.
- Jones, G., Sentenac, P., & Zielinski, M. (2014). Desiccation cracking detection using 2-D and 3-D Electrical Resistivity Tomography: Validation on a flood embankment. *Journal of Applied Geophysics*, 106, 196-211.

- Jones, G., Zielinski, M., & Sentenac, P. (2012). Mapping desiccation fissures using 3-D electrical resistivity tomography. *Journal of Applied Geophysics*, 84, 39-51.
- Jones, G. M., Cassidy, N. J., Thomas, P. A., Plante, S., & Pringle, J. K. (2009). Imaging and monitoring tree-induced subsidence using electrical resistivity imaging. *Near Surface Geophysics*, 7(3), 191-206.
- Kanema, J. M., Eid, J., & Taibi, S. (2016). Shrinkage of earth concrete amended with recycled aggregates and superplasticizer: Impact on mechanical properties and cracks. *Materials & Design*, 109, 378-389.
- Krivenko, P. V., & Kovalchuk, G. Y. (2007). Directed synthesis of alkaline aluminosilicate minerals in a geocement matrix. *Journal of Materials Science*, 42(9), 2944-2952.
- Lakshmikantha, M. R., Prat, P. C., & Ledesma, A. (2009). Image Analysis for the Quantification of a Developing Crack Network on a Drying Soil. *Geotechnical Testing Journal*, 32(6), 505-515.
- Landi, B. J., Raffaele, R. P., Heben, M. J., Alleman, J. L., VanDerveer, W., & Gennett, T. (2002). Single Wall Carbon Nanotube–Nafion Composite Actuators. *Nano Letters*, 2(11), 1329-1332.
- Lecocq, N., & Vandewalle, N. (2003). Dynamics of crack opening in a one-dimensional desiccation experiment. *Physica. A*, 321(3-4), 431-441.
- Li, J. H., & Zhang, L. M. (2011). Study of desiccation crack initiation and development at ground surface. *Engineering Geology*, 123, 347-358.

- Liu, L., & Grunlan, J. C. (2007). Clay Assisted Dispersion of Carbon Nanotubes in Conductive Epoxy Nanocomposites. *Advanced Functional Materials*, 17(14), 2343-2348.
- Mann, S. (2006). Report on Nanotechnology and Construction. Institute of Nanotechnology, European Nanotechnology, Gateway.
- Marsland, A. (1957). The design and construction of earthen flood banks. *J. Inst. Water Eng*, 11(3), 236-258.
- Marsland, A. (1968). The shrinkage and fissuring of clay in flood banks. Building research establishment, Internal report No. 39/68.
- Melchior, S. (1997). In-situ studies on the performance of landfill caps. Paper presented at the International Containment Technical Conference.
- Michielsen, K., & De Raedt, H. (2001). Integral-Geometry Morphological Image Analysis. *Physics Reports*, 347, 461-538.
- Mitchell, J. K., & Santamarina, J. C. (2005). Biological Considerations in Geotechnical Engineering. *Journal of Geotechnical & Geoenvironmental Engineering*, 131(10), 1222-1233.
- Nahlawi, H., & Kodikara, J. (2002). Experimental observations on curling of desiccating clay. Paper presented at the Third International Conference on Unsaturated Soils, Recife, Brazil.
- Nahlawi, H., & Kodikara, J. K. (2006). Laboratory experiments on desiccation cracking of thin soil layers. *Geotechnical & geological Engineering*, 24(6), 1641-1664.

- Nataraja, M. C., & Nalanda, Y. (2008). Performance of industrial by-products in controlled low-strength materials (CLSM). *Waste Management*, 28(7), 1168-1181.
- Önal, O., Ören, A. H., Özden, G., & Kaya, A. (2008). Determination of Cylindrical Soil Specimen Dimensions by Imaging with Application to Volume Change of Bentonite-Sand Mixtures. *GEOTECHNICAL TESTING JOURNAL*, 31, 124-131.
- Orts, W. J., Roa-Espinosa, A., Sojka, R. E., Glenn, G. M., Imam, S. H., Erlacher, K., & Pedersen, J. S. (2007). Use of Synthetic Polymers and Biopolymers for Soil Stabilization in Agricultural, Construction, and Military Applications. *Journal of Materials in Civil Engineering*, 19(1), 58-66.
- Peron, H., Hueckel, T., Laloui, L., & Hu, L. B. (2009). Fundamentals of desiccation cracking of fine-grained soils: experimental characterisation and mechanisms identification. *Canadian Geotechnical Journal*, 46(10), 1177-1201.
- Perrot, A., D. Rangeard, D., Picandet, V., & Mélinge, Y. (2013). Hydro-mechanical properties of fresh cement pastes containing polycarboxylate superplasticizer. *Cement and Concrete Research*, 53.
- Philip, L. K., Shimell, H., Hewitt, P. J., & Ellard, H. T. (2002). A field-based test cell examining clay desiccation in landfill liners. *Quarterly Journal of Engineering Geology and Hydrogeology*, 35, 345-354.
- Plank, J. (2004). Applications of biopolymers and other biotechnological products in building materials. *Applied Microbiology and Biotechnology*, 66(1), 1-9.

- Pozdnyakova, L. (1999). Electrical Properties of Soils. (Ph.D.). University of Wyoming, Laramie, Wyoming, USA.
- Preston, S., Griffiths, B. S., & Young, I. M. (1997). An investigation into sources of soil crack heterogeneity using fractal geometry. *European Journal of Soil Science*, 48(1), 31-37.
- Puppala, A. J., Griffin, J. A., Hoyos, L. R., & Chomtid, S. (2004). Studies on Sulfate-Resistant Cement Stabilization Methods to Address Sulfate-Induced Soil Heave. *Journal of Geotechnical & Geoenvironmental Engineering*, 130(4), 391-402.
- Rayhani, M. H. T., Yanful, E. K., & Fakher, A. (2007). Desiccation-induced cracking and its effect on the hydraulic conductivity of clayey soils from Iran. *Canadian Geotechnical Journal*, 44(3), 276-283.
- Reynolds, J. M. (1997). An introduction to applied and environmental geophysics. New York, USA: John Wiley & Sons.
- Ringrose-Voase, A. J., & Sanidad, W. B. (1996). A method for measuring the development of surface cracks in soils - application to crack development after lowland rice. *Geoderma*, 71, 245-261.
- Robain, H. D., M; Ritz, M; Atangana, Q.Y. (1996). A multiscale electrical survey of a lateritic soil system in the rain forest of Cameroon. *Journal of Applied Geophysics*, 34, 237-253.
- Rodríguez, R., Sánchez, M., Ledesma, A., & Lloret, A. (2007). Experimental and numerical analysis of desiccation of a mining waste. *Canadian Geotechnical Journal*, 44(6), 644-658.

- Rosalam, S., & England, R. (2006). Review of xanthan gum production from unmodified starches by *Xanthomonas comprestris* sp. *Enzyme and Microbial Technology*, 39(2), 197-207.
- Rounsevell, M. D. A., Evans, S. P., & Bullock, P. (1999). Climate change and agricultural soils - Impacts and adaptation. *Climate Change*, 43, 683-709.
- Rounsevell, M. D. A., & Loveland, P. J. (1994). Soil responses to climate change. edited by Mark D.A. Rounsevell, Peter J. Loveland: Springer-Verlag.
- Samouëlian, A., Cousin, I., Richard, G., Tabbagh, A., & Bruand, A. (2003). Electrical Resistivity Imaging for Detecting Soil Cracking at the Centimetric Scale. *Soil Science Society of America Journal*, 67(5), 1319-1326.
- Samouëlian, A., Richard, G., Cousin, I., Guérin, R., Bruand, A., & Tabbagh, A. (2004). Three-dimensional crack monitoring by electrical resistivity measurement. *European Journal of Soil Science*, 55(4).
- Sanchez, M., Atique, A., Kim, S., Romero, E., & Zielinski, M. (2013). Exploring desiccation cracks in soils using a 2D profile laser device. *Acta Geotechnica*, 8(6), 583-596.
- Sarmah, A. K., Pillai-McGarry, U., & McGarry, D. (1996). Repair of the structure of a compacted Vertisol via wet/dry cycles. *Soil and Tillage Research*, 38(1), 17-33.
- Sentenac, P., Jones, G., Zielinski, M., & Tarantino, A. (2013). An approach for the geophysical assessment of fissuring of estuary and river flood embankments: validation against two case studies in England and Scotland. *Environmental Earth Sciences*, 69(6), 1939-1949.

- Sentenac, P., & Zielinski, M. (2009). Clay fine fissuring monitoring using miniature geo-electrical resistivity arrays. *Environmental Earth Sciences*, 59(1), 205-214.
- Shin, H., & Santamarina, J. C. (2011). Desiccation cracks in saturated fine-grained soils: particle-level phenomena and effective-stress analysis. *Geotechnique*, 61(11), 961-972.
- Siegel, R. W. (2006). *Nanotechnology*. Rensselaer Polytechnic Institute Publication, 1-8.
- Sofi, M., van Deventer, J. S. J., Mendis, P. A., & Lukey, G. C. (2007). Bond performance of reinforcing bars in inorganic polymer concrete (IPC). *Journal of Materials Science*, 42(9), 3107-3116.
- Southen, J. M., & Rowe, R. K. (2005). Laboratory investigation of geosynthetic clay liner desiccation in a composite liner subjected to thermal gradients. *Journal of Geotechnical & Geoenvironmental Engineering*, 131(7), 925-935.
- Sposito, G. (1989). *The Chemistry of soils*. New York, USA: Oxford University Press.
- Tay, Y. Y., Stewart, D. I., & Cousens, T. W. (2001). Shrinkage and desiccation cracking in bentonite-sand landfill liners. *Engineering Geology*, 60, 263-274.
- Thusyanthan, N. I., Take, W. A., Madabhushi, S. P. G., & Bolton, M. D. (2007). Crack initiation in clay observed in beam bending. *Geotechnique*, 57(7), 581-594.
- Tungittiplakorn, W., Lion, L. W., Cohen, C., & Kim, J.-Y. (2004). Engineered Polymeric Nanoparticles for Soil Remediation. *Environmental Science & Technology*, 38(5), 1605-1610.
- van Elsas, J. D., & Heijnen, C. E. (1990). Methods for the introduction of bacteria into soil: A review. *Biology and Fertility of Soils*, 10(2), 127-133.



- Velde, B. (2001). Surface cracking and aggregate formation observed in a Rendzina soil, La Touche (Vienne) France. *Geoderma*, 99, 261-276.
- Vogel, H. J., Hoffmann, H., & Roth, K. (2005). Studies of crack dynamics in clay soil. I. Experimental methods, results, and morphological quantification. *Geoderma*, 125, 203-211.
- Wang, S., Liang, Z., Liu, T., Wang, B., & Zhang, C. (2006). Effective amino-functionalization of carbon nanotubes for reinforcing epoxy polymer composites. *Nanotechnology*, 17(1551).
- Weinberger, R. (1999). Initiation and growth of cracks during desiccation of stratified muddy sediments. *Journal of Structural Geology*, 21, 379-386.
- White, D. J., W.A., T., & Bolton, M. D. (2003). Soil deformation measurement using particle image velocimetry (PIV) and photogrammetry. *Geotechnique*, 53(7), 619-631.
- Winograd, I. J. (1981). Radioactive Waste Disposal in Thick Unsaturated Zones. *Science*, 212(4502), 1457-1464.
- Xanthakos, P. P., Abramson, L. W., & D.A., B. (1994). Ground control and improvement. Chichester, New York, J. Wiley.
- Yassoglou, N., C.S., K., Moustakas, N., Tzianis, E., & Danalatos, N. G. (1994). Cracking in recent alluvial soils as related to easily determined soil properties. *Geoderma*, 63, 289-298.

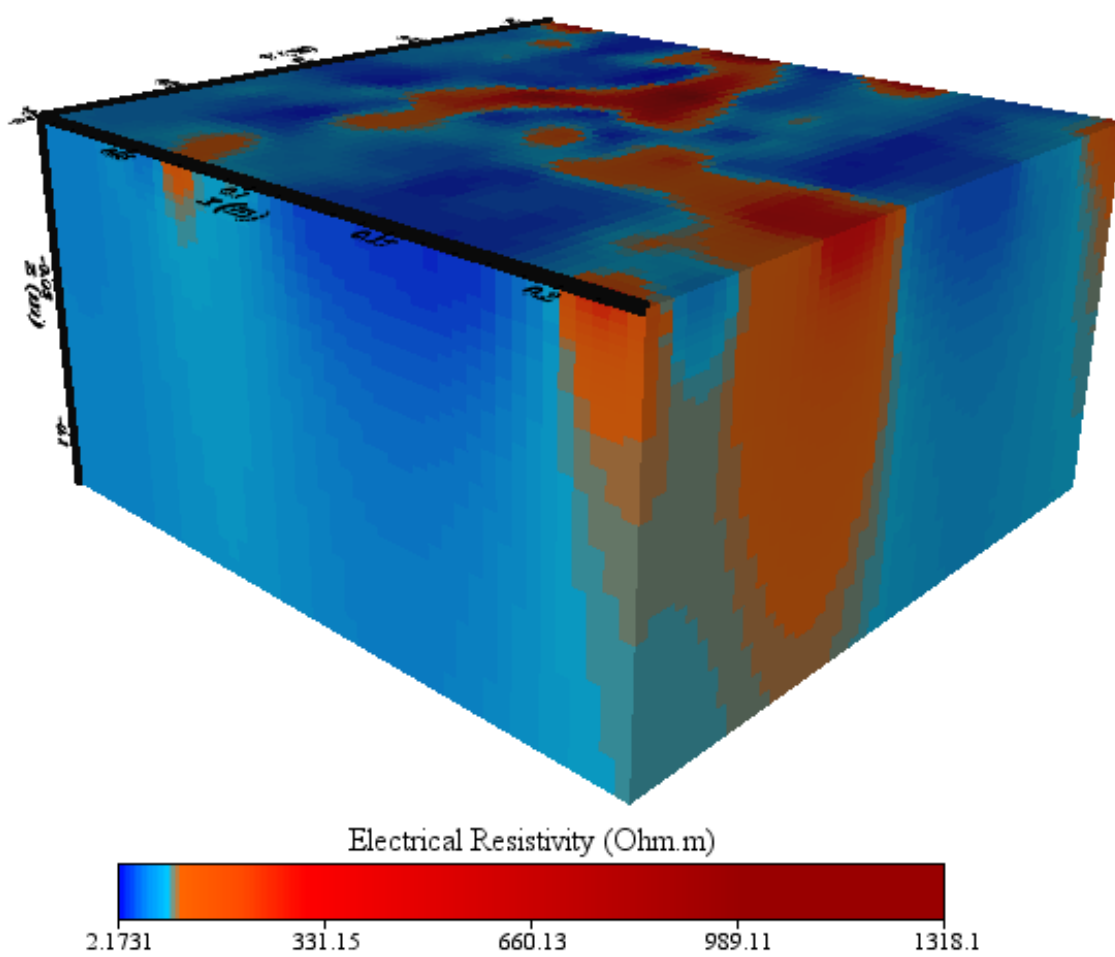
- Yesiller, N., Miller, C. J., Inci, G., & Yaldo, K. (2000). Desiccation and cracking behavior of three compacted landfill liner soils. *Engineering Geology*, 57, 105-121.
- Yoon, S., & Abu-Farsakh, M. (2009). Laboratory investigation on the strength characteristics of cement-sand as base material. *KSCE Journal of Civil Engineering*, 13(1), 15.

APPENDIX A

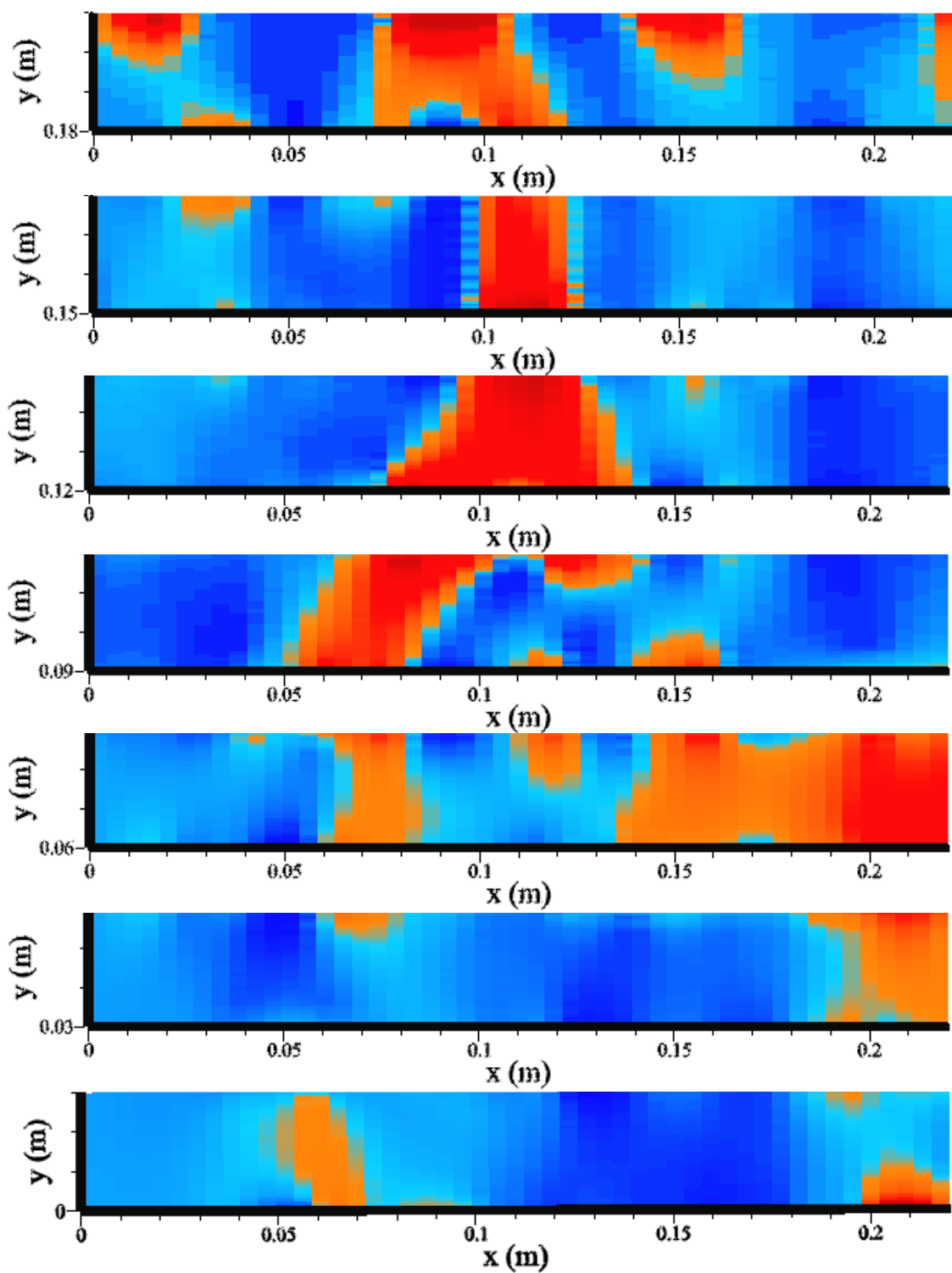
THREE DIMENSIONAL VISUALIZATION OF ERT RESULTS USING VOXLER

3D (SECTION B3)

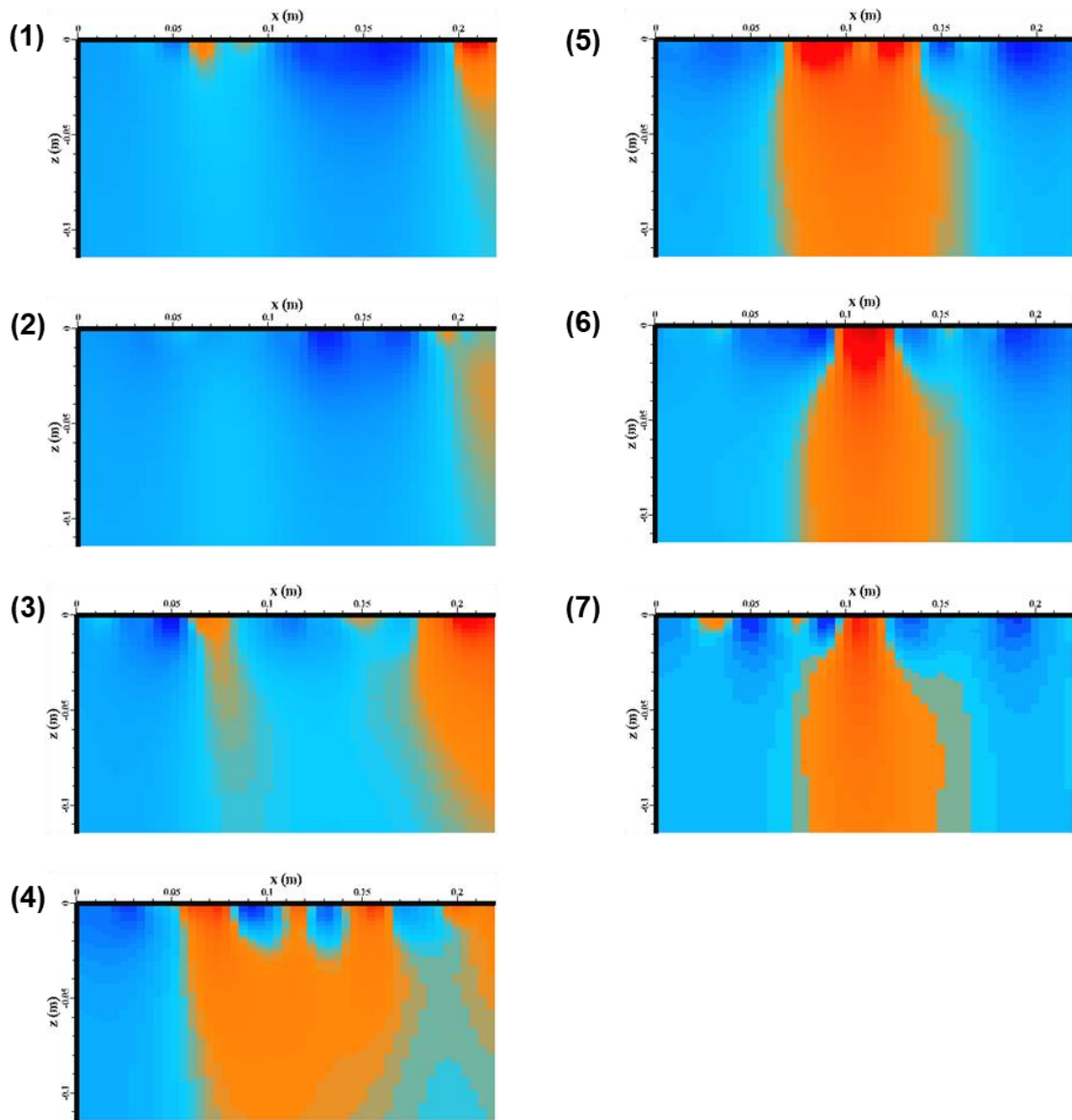
**A1. 3-D ERT results (section B3, phase 2)**



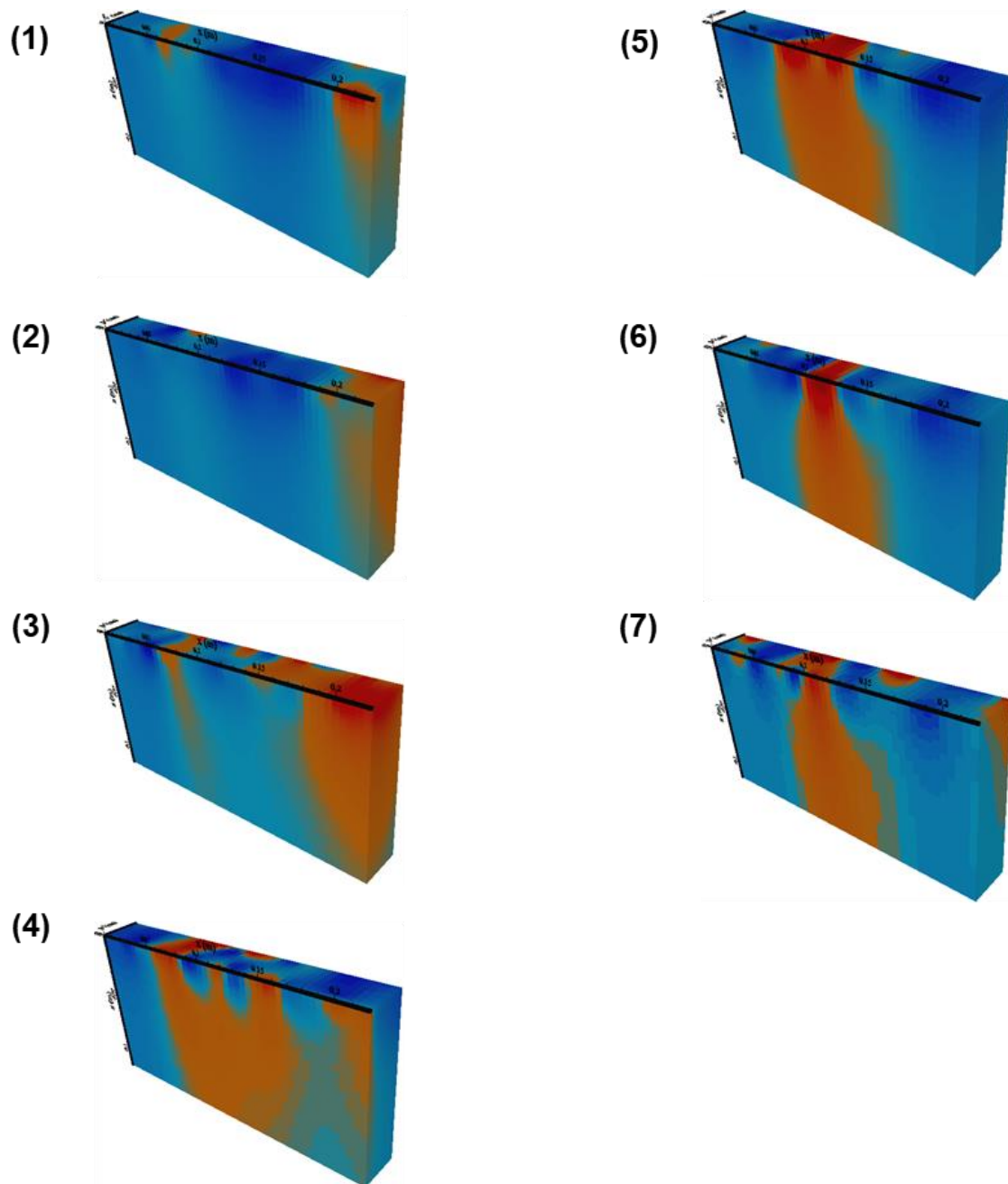
**Figure A-1 3-D image of the ERT measured subsurface area (B3, phase 2)**



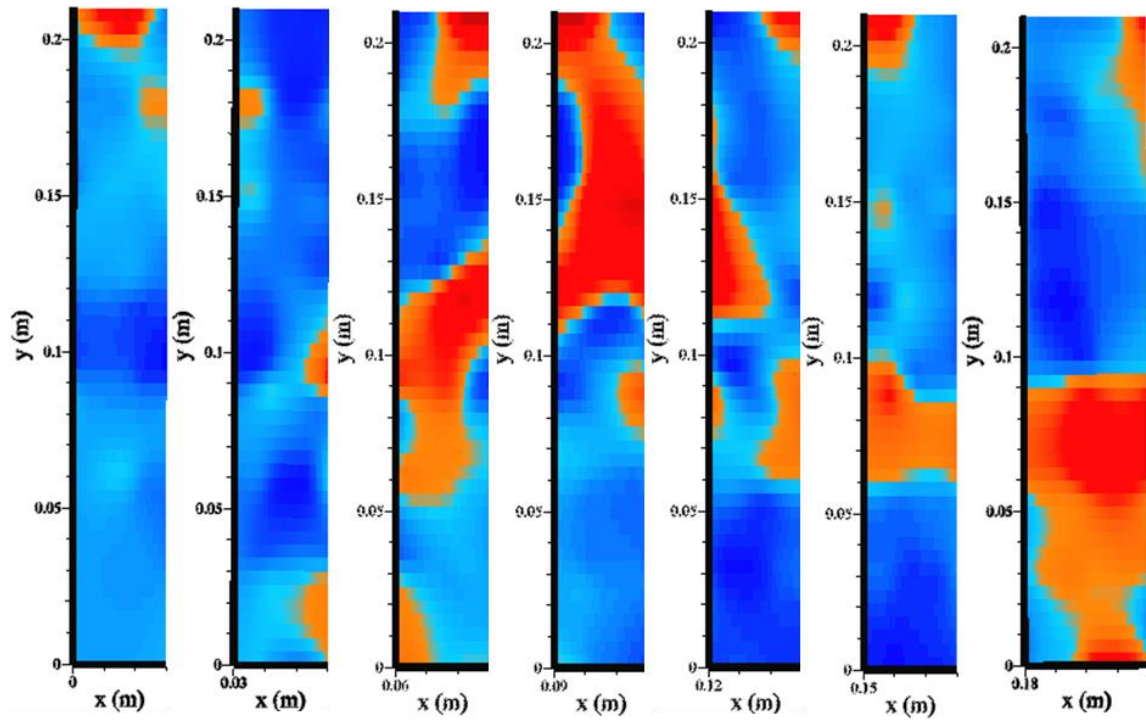
**Figure A-2 Horizontal sliced cut of ERT measured subsurface area (Top view, B3, phase 2)**



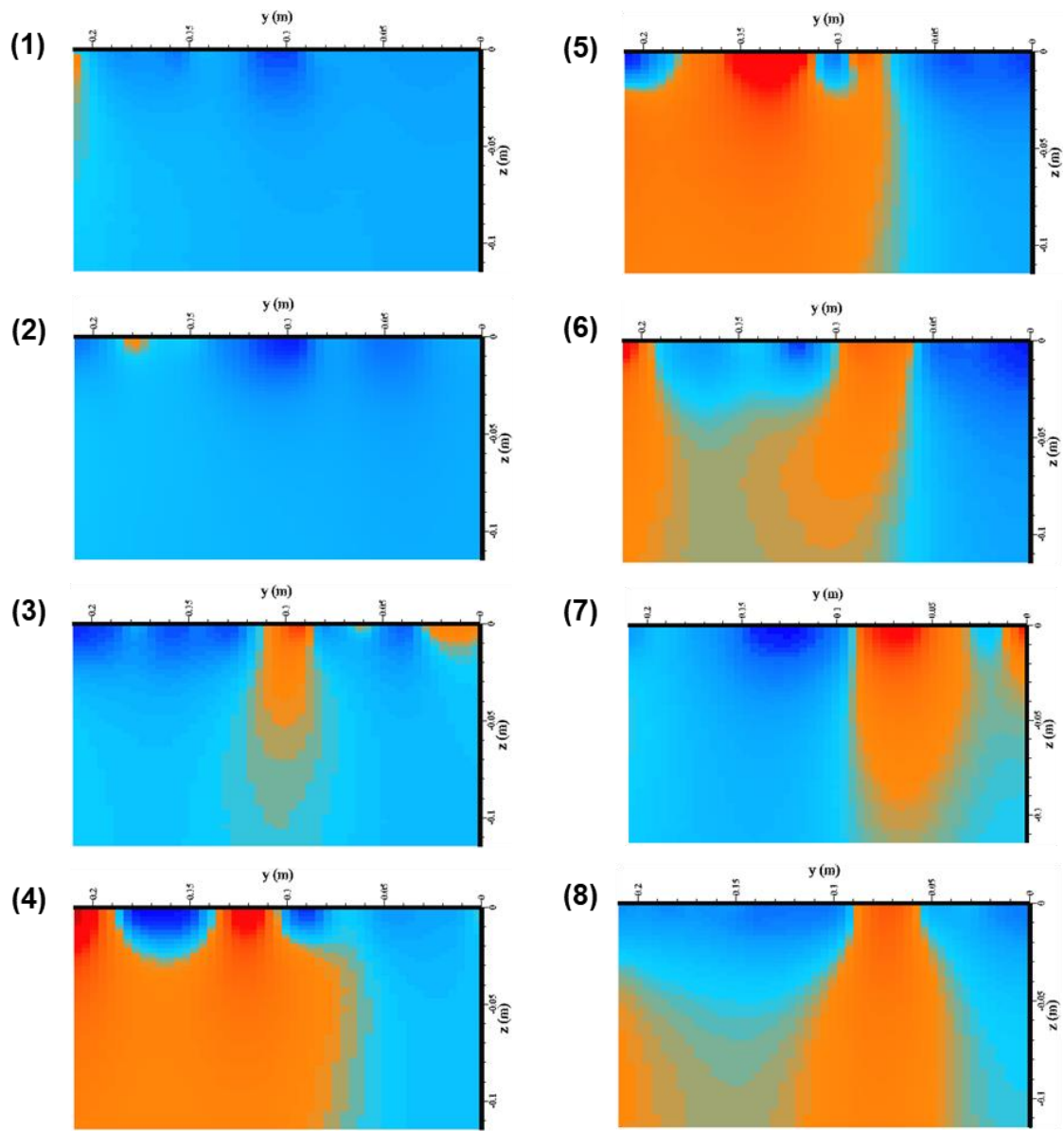
**Figure A-3 Horizontal sliced cut of ERT measured subsurface area (Front view, B3, phase 2)**



**Figure A-4 Horizontal sliced cut of ERT measured subsurface area (3-D view, B3, phase 2)**

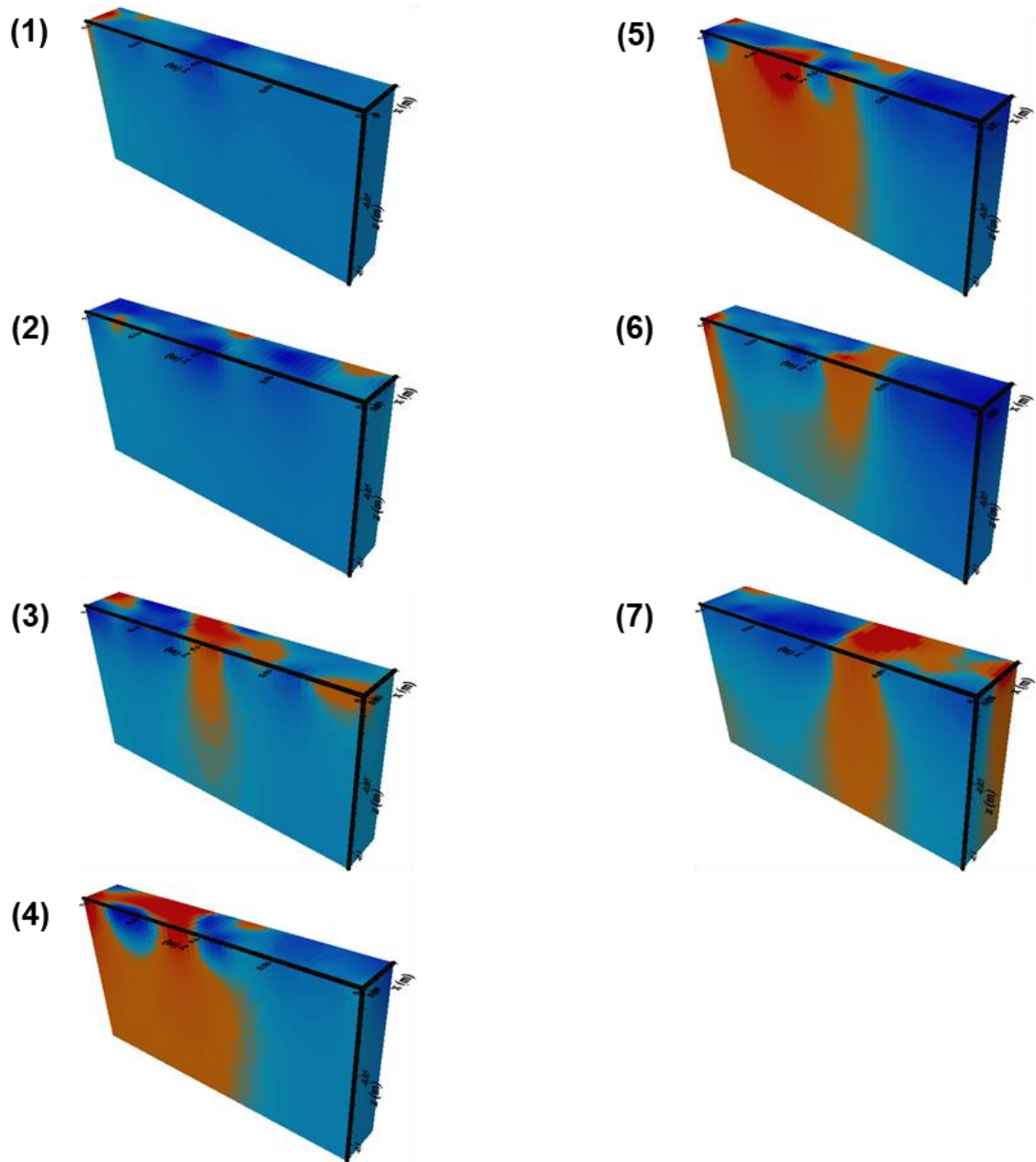


**Figure A-5 Vertical sliced cut of ERT measured subsurface area (Top view, B3, phase 2)**



**Figure A-6 Vertical sliced cut of ERT measured subsurface area (Side view, B3, phase 2)**





**Figure A-7 Vertical sliced cut of ERT measured subsurface area (3-D view, B3, phase 2)**

### A2. 3-D ERT results (section B3, phase 3)

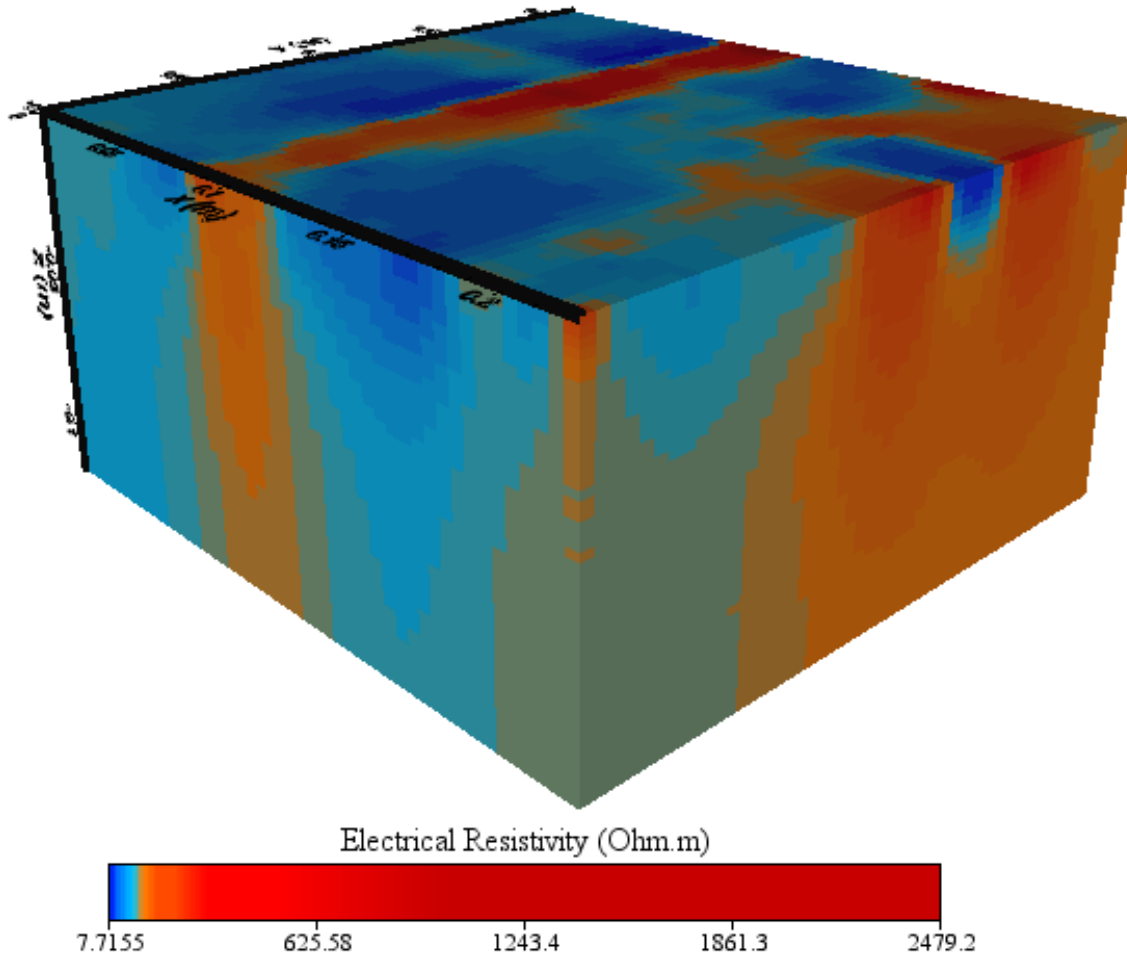


Figure A-8 3-D image of the ERT measured subsurface area (B3, phase 3)

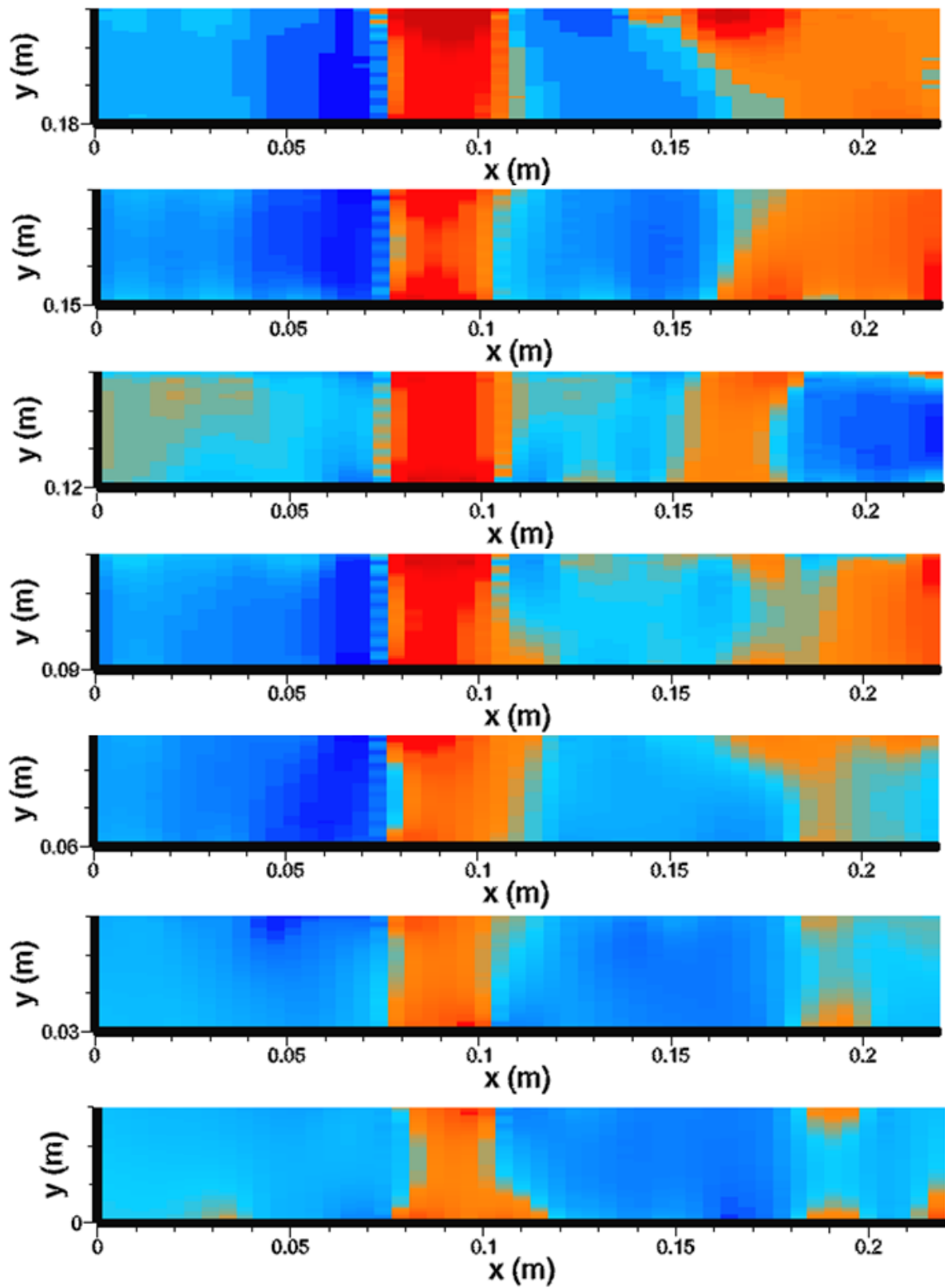
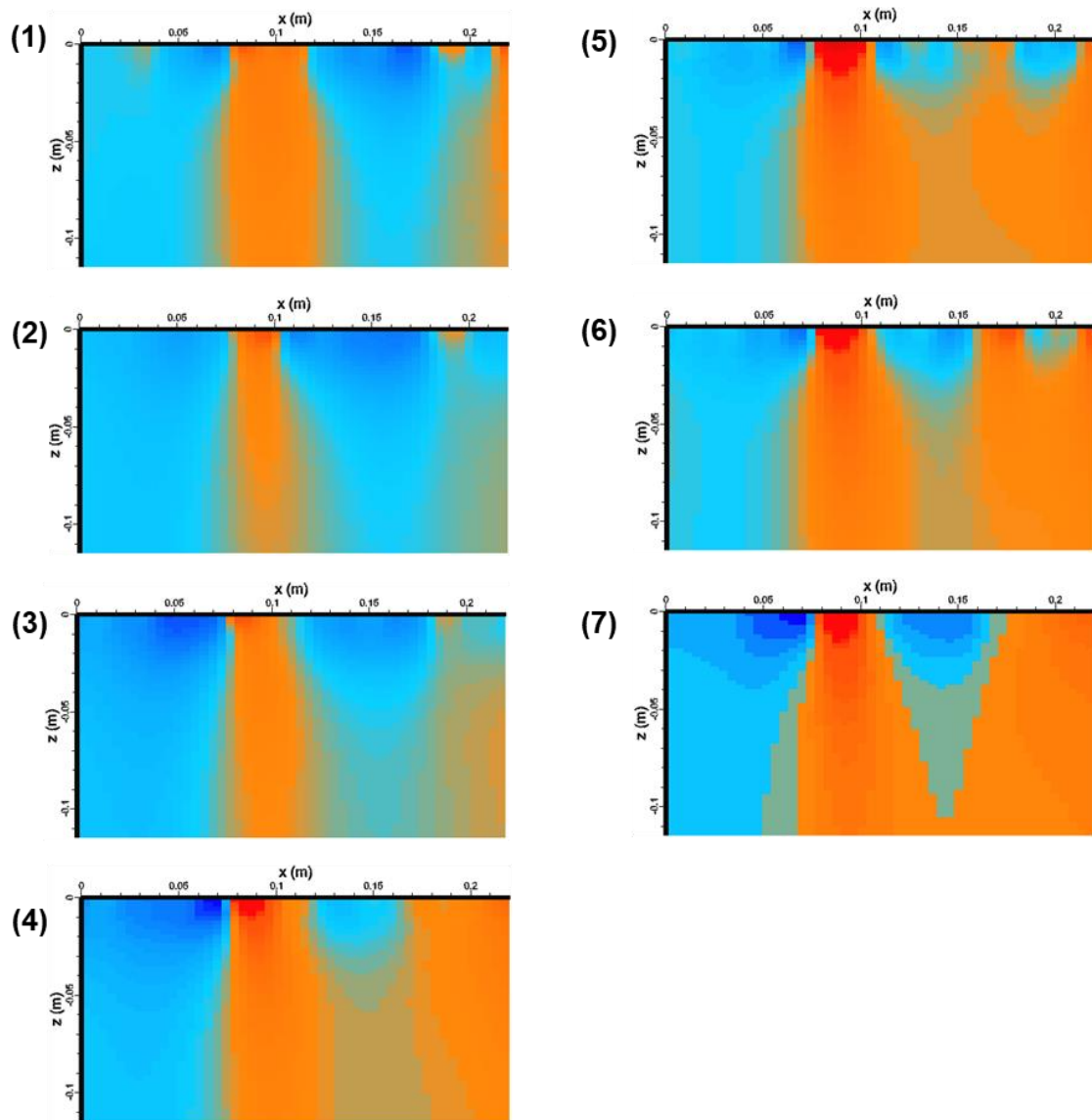
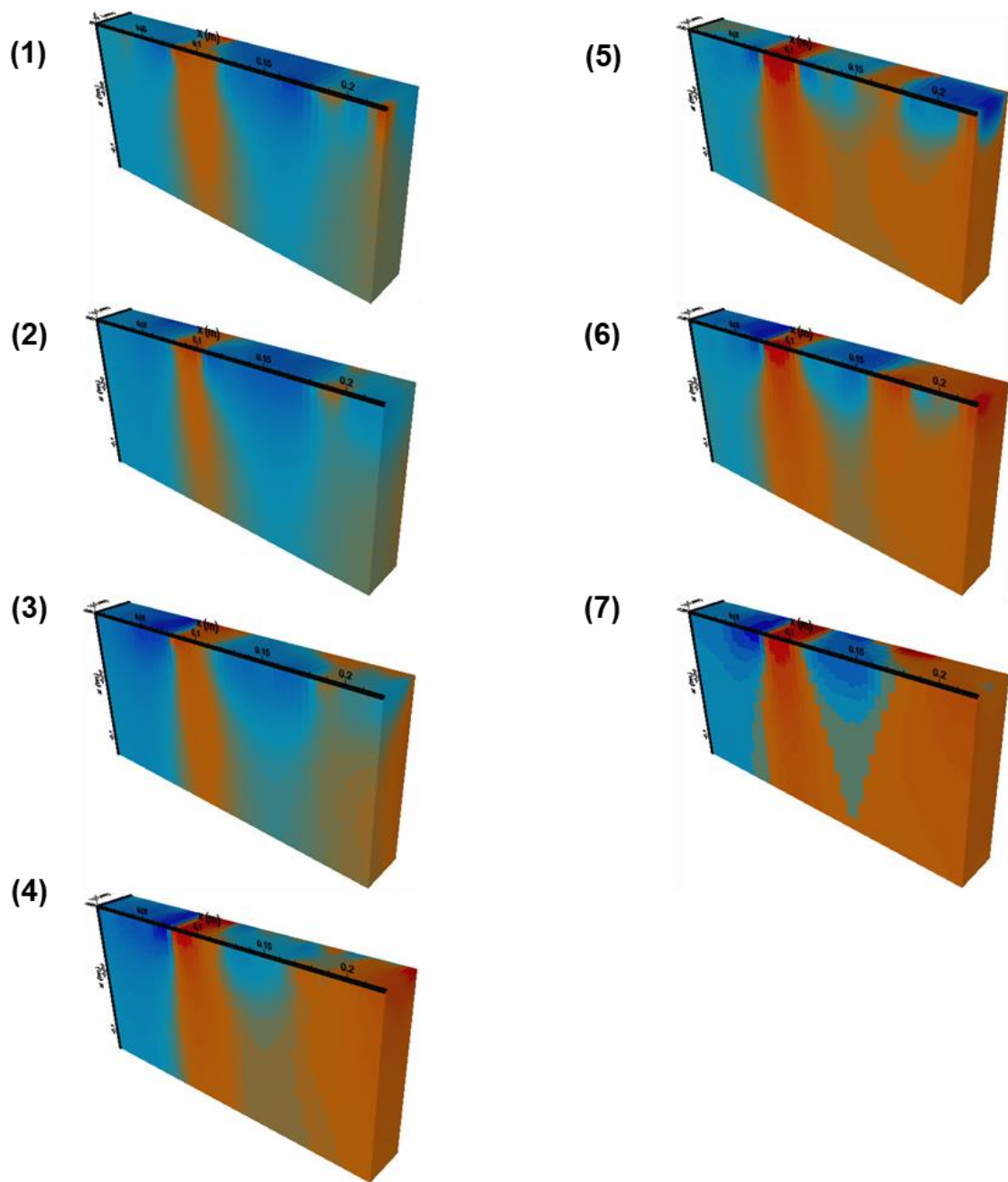


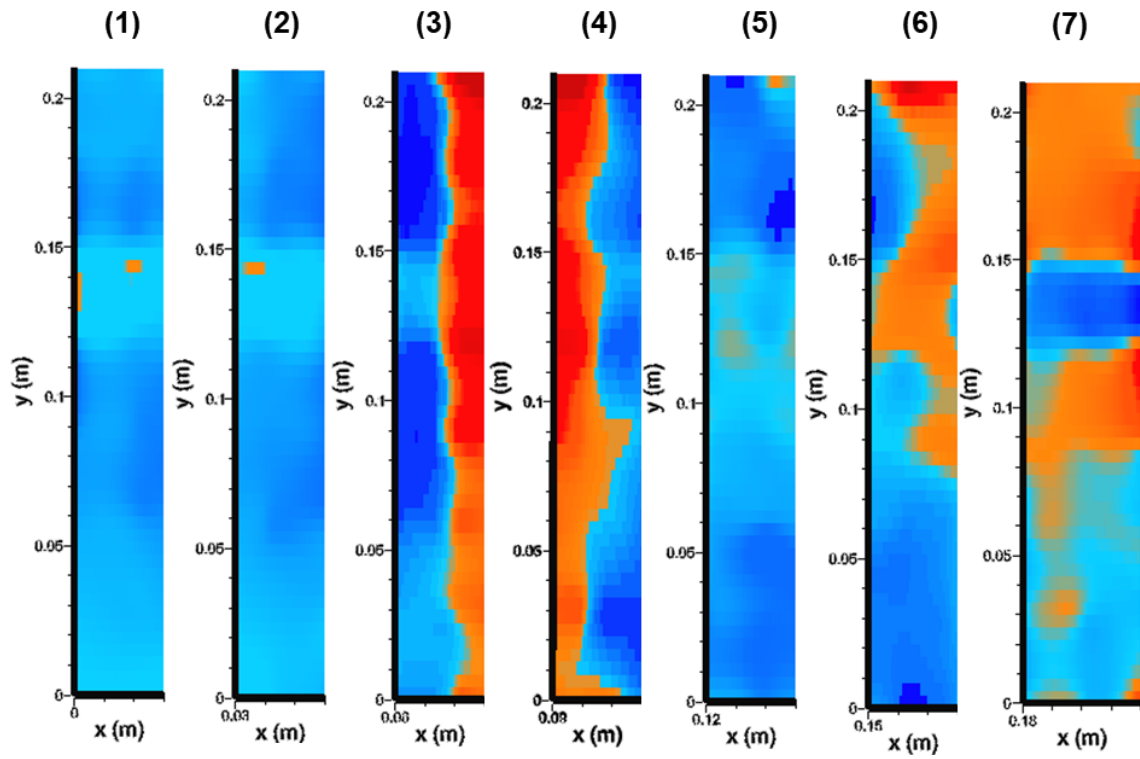
Figure A-9 Horizontal sliced cut of ERT measured subsurface area (Top view, B3, phase 3)



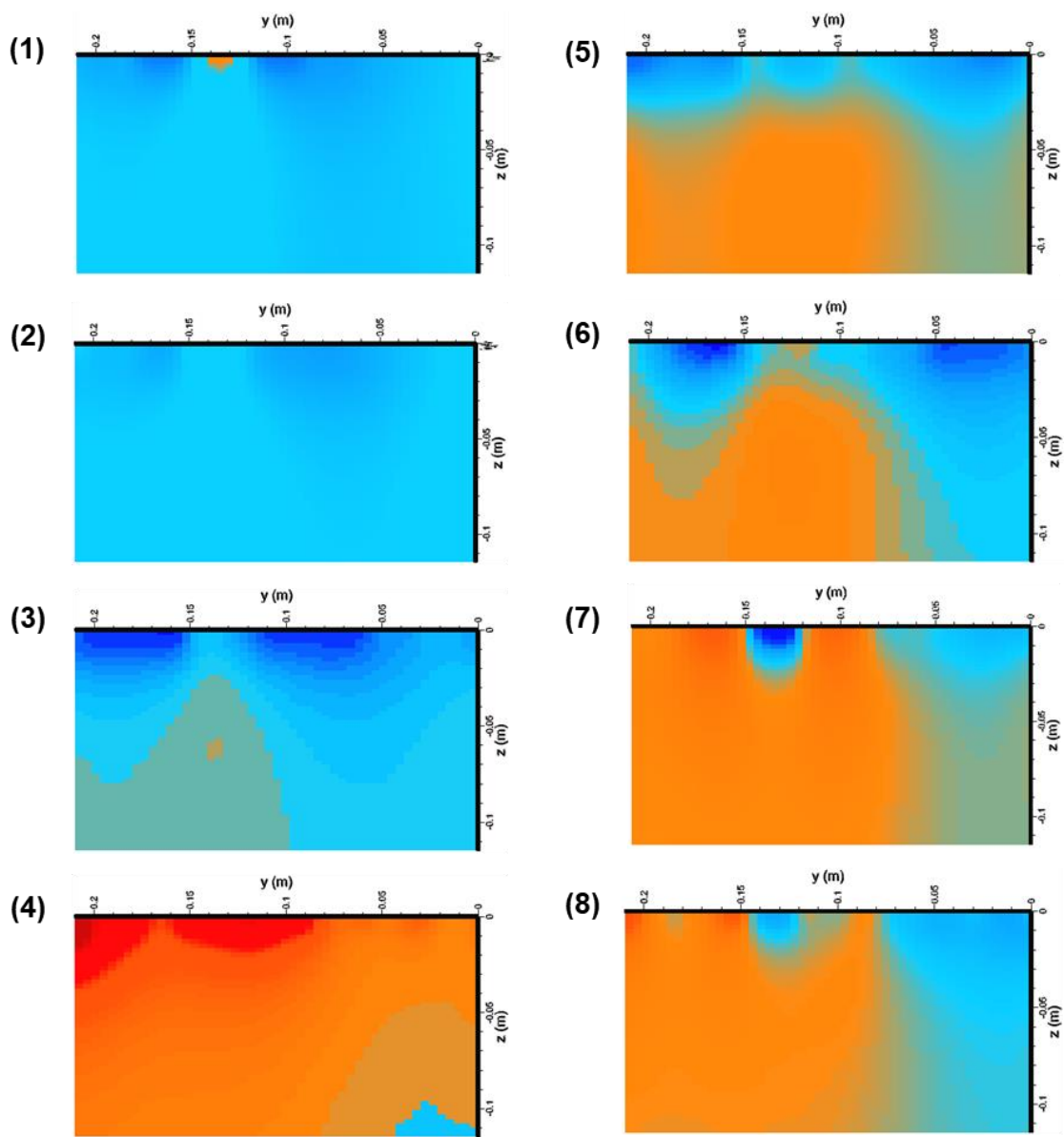
**Figure A-10 Horizontal sliced cut of ERT measured subsurface area (Front view, B3, phase 3)**



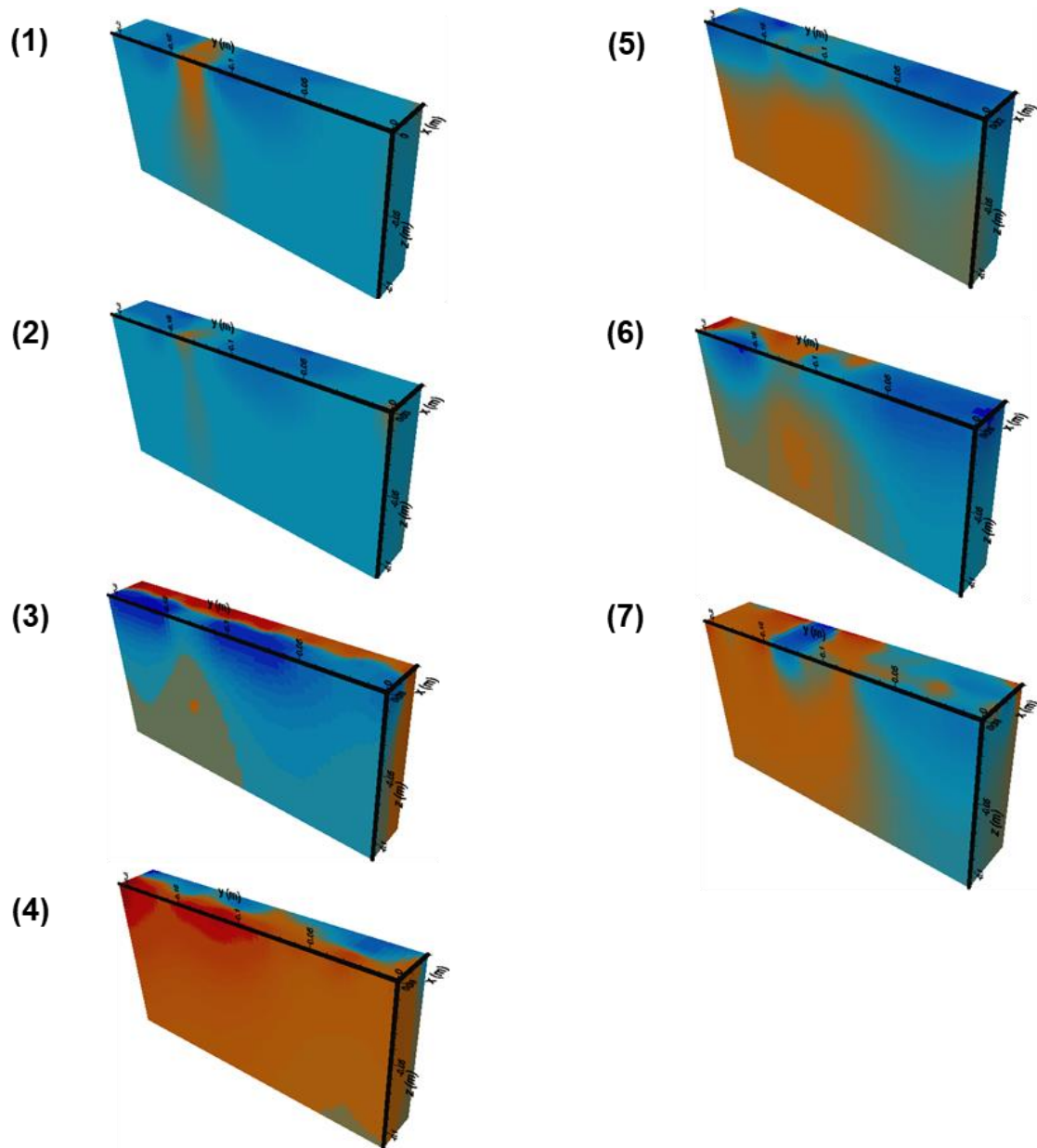
**Figure A-11 Horizontal sliced cut of ERT measured subsurface area (3-D view, B3, phase 3)**



**Figure A-12 Vertical sliced cut of ERT measured subsurface area (Top view, B3, phase 3)**



**Figure A-13 Vertical sliced cut of ERT measured subsurface area (Side view, B3, phase 3)**



**Figure A-14 Vertical sliced cut of ERT measured subsurface area (3-D view, B3, phase 3)**